AN OPTICAL SENSOR FOR IN-STREAM MONITORING OF SUSPENDED SEDIMENT
CONCENTRATION

by

YALI ZHANG

B.S., Qingdao Agricultural University, China, 1997

M.S., South China Agricultural University, China, 2000

AN ABSTRACT OF A DISSERTATION

submitted in partial fulfillment of the requirements for the degree

DOCTOR OF PHILOSOPHY

Department Of Biological and Agricultural Engineering

College of Engineering

KANSAS STATE UNIVERSITY

Manhattan, Kansas

2009

Abstract

Suspended sediment concentration (SSC) in water is one of the most important parameters to evaluate water quality. Monitoring SSC provides important information on determining sediment transport for soil erosion research and soil/water conservation practices. Sediment mass transported at a given time can be assessed by simultaneous SSC and water flow velocity measurements. Fouling, including bio-fouling, has damaging impact on optical SSC measurements over the long term. In this study, an inexpensive, real-time, self-cleaning, optical sediment and flow velocity sensor was developed.

Laboratory experiments were conducted on a previously designed SSC sensor. A light modulation algorithm was designed to reduce the influence of ambient light, especially sunlight, on measurement accuracy. Statistical models to predict SSC based on measured light intensities were established and compared with neural network models. The statistical analysis showed that soil texture played an important role in SSC measurement accuracy while the designed sensor was capable of reducing the effect of water color on sensor performance. Neural-network models can further remove the influence of soil texture type on SSC measurement. The sensor design was simplified based on a stepwise selection analysis.

Long-term field experiments were conducted in Kansas and Georgia to evaluate the sensor performance, the effect of fouling, including bio-fouling, on sensor lenses, and the effect of temperature on the measurement. Methods of removing the fouling effect through data correction were developed. Results indicated that the designed optical SSC sensor was capable of providing rapid response to SSC fluctuations in water flow. Temperature of the water body has an insignificant impact on SSC measurement.

In order to reduce fouling, an air-blast cleaning mechanism was integrated into the optical sediment sensor. Laboratory experiments in a manually created fouling environment were conducted to observe the fouling process on sensor cases made of different materials, and to verify the effectiveness of air-blast cleaning in reducing fouling. Results indicated that air-blast cleaning mechanism was capable of reducing clay/silt fouling on sensor signals. The duration and frequency of air-blast cleaning can be determined and adjusted depending on actual field conditions. An air pressure drop test was conducted on the hose carrying pressurized air. Results showed negligible pressure drop.

A flow velocity measurement function based on the cross-correlation principle was integrated into the optical sediment sensor. An experiment was conducted in laboratory to examine the sensor performance on velocity measurement using a closed circulation system. A solution of blue colorant, Brilliant Blue FCF, was used as an artificial source to absorb light emitted by LEDs in the sensor and the signal variation patterns were measured. The results indicated that the cross-correlation-based velocity sensor was capable of measuring water flow velocity within in a certain velocity range using the dye injection method.

AN OPTICAL SENSOR FOR IN-STREAM MONITORING OF SUSPENDED SEDIMENT
CONCENTRATION

by

YALI ZHANG

B.S., Qingdao Agricultural University, China, 1997

M.S., South China Agricultural University, China, 2000

A DISSERTATION

submitted in partial fulfillment of the requirements for the degree

DOCTOR OF PHILOSOPHY

Department of Biological and Agricultural Engineering
College of Engineering

KANSAS STATE UNIVERSITY
Manhattan, Kansas

2009

Approved by:

Major Professor
Dr. Naiqian Zhang

Abstract

Suspended sediment concentration (SSC) in water is one of the most important parameters to evaluate water quality. Monitoring SSC provides important information on determining sediment transport for soil erosion research and soil/water conservation practices. Sediment mass transported at a given time can be assessed by simultaneous SSC and water flow velocity measurements. Fouling, including bio-fouling, has damaging impact on optical SSC measurements over the long term. In this study, an inexpensive, real-time, self-cleaning, optical sediment and flow velocity sensor was developed.

Laboratory experiments were conducted on a previously designed SSC sensor. A light modulation algorithm was designed to reduce the influence of ambient light, especially sunlight, on measurement accuracy. Statistical models to predict SSC based on measured light intensities were established and compared with neural network models. The statistical analysis showed that soil texture played an important role in SSC measurement accuracy while the designed sensor was capable of reducing the effect of water color on sensor performance. Neural-network models can further remove the influence of soil texture type on SSC measurement. The sensor design was simplified based on a stepwise selection analysis.

Long-term field experiments were conducted in Kansas and Georgia to evaluate the sensor performance, the effect of fouling, including bio-fouling, on sensor lenses, and the effect of temperature on the measurement. Methods of removing the fouling effect through data correction were developed. Results indicated that the designed optical SSC sensor was capable of providing rapid response to SSC fluctuations in water flow. Temperature of the water body has an insignificant impact on SSC measurement.

In order to reduce fouling, an air-blast cleaning mechanism was integrated into the optical sediment sensor. Laboratory experiments in a manually created fouling environment were conducted to observe the fouling process on sensor cases made of different materials, and to verify the effectiveness of air-blast cleaning in reducing fouling. Results indicated that air-blast cleaning mechanism was capable of reducing clay/silt fouling on sensor signals. The duration and frequency of air-blast cleaning can be determined and adjusted depending on actual field conditions. An air pressure drop test was conducted on the hose carrying pressurized air. Results showed negligible pressure drop.

A flow velocity measurement function based on the cross-correlation principle was integrated into the optical sediment sensor. An experiment was conducted in laboratory to examine the sensor performance on velocity measurement using a closed circulation system. A solution of blue colorant, Brilliant Blue FCF, was used as an artificial source to absorb light emitted by LEDs in the sensor and the signal variation patterns were measured. The results indicated that the cross-correlation-based velocity sensor was capable of measuring water flow velocity within in a certain velocity range using the dye injection method.

Table of Contents

List of Figures

List of Tables

Acknowledgements

CHAPTER 1 - INTRODUCTION

1.1 General Background

1.1.1 Suspended sediment and its impacts

Sediment is identified by the U.S. Environmental Protection Agency (EPA) as an important non-point source (NPS) pollutant (EPA, 2008) and the single most widespread pollutant affecting the beneficial uses of the Nation's rivers and streams (EPA, 1998). Sediment in natural watercourses commonly has two forms: suspended sediment and benthic sediment. In national water quality assessment glossary (USGS, 2009), suspended sediment refers to very fine soil particles that remain in suspension in water for a considerable period of time without contact with the bottom, in contrast to benthic sediment that moves downstream by rolling or sliding along the streambed.

Suspended sediment concentration (SSC) is defined as the ratio of the mass of dry sediment in a water-sediment mixture to the mass of the water-sediment mixture, which is expressed in milligrams of dry sediment per liter of water-sediment mixture (mg/L) (USGS, 2009).

When sediments stay in suspension, it has adverse impacts on aquatic ecosystems. Aquatic biota responds to both the concentration of suspended sediments and duration of exposure to excessive suspended sediment, much as they do for other environmental contaminants (Newcombe and MacDonald, 1991). Excessive sedimentation is considered the most important factor limiting fish habitat due to the fact that the increased light attenuation caused by sedimentation shortens the depth of the photic zone, and alters the vertical stratification of heat in the water column (Moore, 1978). Sedimentation has been linked to the increasing level of imperilment in the diverse fish fauna of the southeastern United States (Burkhead and Jelks, 2001), and one of the significant contributors to declines in populations of North American aquatic organisms (Henley et al., 2000).

Suspended sediment is also a potential source of contamination when it carries toxic chemicals during its transportation from industrial waste and sewage discharge, storm water runoff from city streets and farms, and natural sources. Contaminated sediment poses not only

ecological but also human health risks. EPA (1998) estimates that 10 percent of the nation's lakes, rivers, and bays have sediment contaminated with toxic chemicals that fish and bottom-dwelling organisms can accumulate and pass to the food chain. In addition, billions of dollars of economic activity are potentially affected by contaminated sediment, because of the loss of recreational and commercial use of contaminated water bodies and the increased cost of disposing of contaminated material (EPA, 1998).

1.1.2 Suspended sediment monitoring

Monitoring SSC is essential for assessing water quality and evaluating the extent of potential adverse impacts. Determining the amount of sediment being transported by rivers is also fundamental to determine the environmental impact on reservoirs and to estimate their life span (Cochrane et al., 2004). Water and waste treatment processes demand measurement of suspended sediments as one of the critical parameters for monitoring various treatment stages (Murren, 1993). Military activities may cause extensive soil erosion and reduced water quality especially when heavy military training vehicles pass unpaved roads and stream crossings. Many programs of Department of Defense's (DoD), including the Strategic Environmental Research and Development Program (SERDP), and the Environmental Security Technology Certification Program (ESTCP), have been working with various organizations to assess the impact of this pollution on surface water quality and to reduce soil erosion due to military activities by monitoring suspended sediment level in a long term (SERDP, 2009; ESTCP, 2009). In addition, accurate SSC monitoring helps to develop total maximum daily load (TMDL) for impaired waters, and to employ best management practices (BMPs) under section 303(d) of the Clean Water Act law (EPA, 2009).

Optical measurement is relatively simple and inexpensive. In-situ optical devices that measure transmitted or backscattered light caused by suspended sediment have been studied by many researchers and showed remarkable ability to record rapid temporal fluctuations in SSC (Maa, 1988; Daraigan et al., 2005; 2006; Bunt et al., 1999).

1.1.3 Fouling effect

Fouling is the accumulation of undesirable living or un-living material on a solid surface in an aquatic environment (EBSCO, 2009). Particularly, biofouling refers to the fouling that is

caused by the accumulation of bacteria, plants, algae, or animals on submerged surfaces (CTI, 2009). Fouling is often used interchangeably with biofouling.

Immersed surfaces without anti-fouling protection absorb inorganic material and macromolecules right after they are submerged in water (Delort et al., 2000). The colonization of bacterial and microbial then quickly occurs on these surfaces, resulting in a microfouling slime layer (a sticky coating). When the thickness of this layer is sufficient, it provides a food source to larger organisms, such as barnacles, mussels, polychaetes, and various species of bryozoans and hydroids, which results in a macrofouling - the development of the communities of larger and complex organisms (Delort et al., 2000; CTI, 2009).

Various factors have a significant impact on the degree of fouling, such as season, sunlight, temperature, flow rates, salinity and water depth. Winter months, less sunlight, colder temperature, higher and variable flow rate, a swing to extremely low or high salinity, and deeper waters generally lead to reduced fouling (CTI, 2009)..

Many researchers have reported the extremely damaging impact of fouling on submerged optical instruments (Lillycrop and Howell, 1996; Sherwood et al., 1989). It is one of the most prevalent hindrances in obtaining continuous, in situ, optical SSC measurements of long term, because the buildup of residue on the optical lens causes the degradation of measurement accuracy over time. In order to obtain long term, meaningful SSC measurement, a cleaning mechanism has to be considered in optical SSC sensor design.

1.1.4 Flow velocity measurement

Great interest has existed in the determination of sediment load to lakes, reservoirs, and rivers for resource mangers. Measurements of sediment transport can also provide information on soil loss rate due to erosion in a certain watershed (Walling, 1994). Flow velocity measurement is usually conducted with SSC measurement using separate sensors to assess sediment mass transport at a given time and depth so that the net sediment transport rate can be determined by calculating the time average of the product of the two measurements (Huntley and Hanes, 1987; Burkhead and Jelks, 2001). However, flow velocity and sediment concentration measurements that were conducted by different sensors could result in time mismatch between the measurements and high cost for equipment. An integrated sensor that can measure SSC and water flow velocity simultaneously is highly desirable.

1.2 Research Objectives

The overall mission of this research is to design a real-time, inexpensive, optical SSC sensor integrated with flow-velocity and self-cleaning mechanisms. The specific objectives of this proposed research are:

1) to further study and modify a real-time, optical SSC sensor based on a spectrum analysis conducted by a former student in the Instrumentation and Control Laboratory at Kansas State University;

2) to evaluate the sensor performance during long term SSC monitoring in field, including the sensor waterproof package, the signal stability, and effects of fouling on the sensor;

3) to design a lens cleaning mechanism for the optical sensor to reduce fouling effect;

4) to develop a stream flow-velocity mechanism and integrate it into the SSC sensor.

1.3 References

Bunt, J. A. C., P. Larcombe, C. F. Jago. 1999. Quantifying the response of optical backscatter devices and transmissometers to variations in suspended particulate matter. *Continental Shelf Research* 19: 1199-1220.

Burkhead, N. M., and H. L. Jelks. 2001. Effects of suspended sediment on the reproductive success of the tricolor shiner, a crevice-spawning minnow. *Transactions of the American Fisheries Society* 130(5): 959-968.

Cochrane, T. A., L. D. Norton, C. Castro-Filho, and J. H. Caviglione. 2004. Development of a river sediment transport monitoring system for large reservoirs. *Applied Engineering in Agriculture* 20(6):771-781.

CTI. 2009. Introduction to Fouling. Houston, TX: Champion Technologies, Inc. Available at www.champion-environ.com/marine-biofouling.asp. Accessed 10 June 2009.

Daraigan, S.G., M. Z. Matjafri, K. Abdullah, A. Abdul-Aziz, and A. A. Tajuddin. 2005. A simple instrument for measuring total suspended solids in polluted marine waters. In *Proceedings of 2005 Asian Conference on Sensors and the International Conference on New Techniques in Pharmaceutical and Biomedical Research*, 219-221. New York, NY: IEEE.

Daraigan, S. G., M. Z. Matjafri, K. Abdullah, L. H. San, and W. C. Jeng. 2006. Multi-spectral optical sensor based on light scattering for measuring total suspended solids. In

Proceedings of SPIE - The International Society for Optical Engineering 6201, 62010W-1-62010W-6. Bellingham, WA: SPIE.

Delort, E., N. Watanabe, H. Etoh, K. Sakata, and H.J. Ceccaldi. 2000. Analysis of initial fouling process in coastal environment: Effects of settlement, attachment, and metamorphosis promoters. *Marine Biotechnology* 2000(2): 224-230

Downing, J. 2006. Twenty-five years with OBS sensors: The good, the bad, and the ugly. *Continental Shelf Research* 26(17-18): 2299-2318.

EBSCO. 2009. Glossary of Terms: Flowmeter Specs. Birmingham, AL: Ebsco Industries Inc. Available at www.flowcontrolnetwork.com/news.asp?NewsID=932. Accessed 1 June 2009

EPA. 1998. Report of the Federal Advisory Committee on the Total maximum Daily Load (TMDL) Program: The National Advisory Council for Environmental Policy and Technology, EPA 100-R-98-006, 97 p., 7 appendixes.

EPA. 2008. Polluted Runoff (Nonpoint Source Pollution). Washington, DC: Environmental Protection Agency. Available at www.epa.gov/owow/NPS/qa.html. Accessed 1 March 2009.

EPA. 2009. Water quality standards and implementation plans. Washington, DC: Environmental Protection Agency. Available at frwebgate.access.gpo.gov/cgi-bin/getdoc.cgi?dbname=browse_usc&docid=Cite:+33USC1313. Accessed 3 March 2009.

ESTCP. 2009. The Environmental Security Technology Certification Program Homepage. Available at www.estcp.org. Accessed 4 March 2009.

Henley, W. F., M. A. Patterson, R. J. Neves, and A. Dennis Lemly. 2000. Effects of sedimentation and turbidity on lotic food webs: A concise review for natural resource managers. *Reviews in Fisheries Science* 8(2): 125-139.

Huntley, D. A., and D. M. Hanes. 1987. Direct measurement of suspended sediment transport. In *Proceedings of a Speciality Conference on Advances in Understanding of Coastal Sediment Processes,* 723-737. New York, NY: ASCE.

Lillycrop, L. S., G. L. Howell. 1996. In-situ Long-term Deployment of Water Quality Sensors Adversely Affected by Biological Fouling. In *OCEANS 96 MTS/IEEE Prospects for the 21st Century Conference Proceedings* 2: 693-697.

Maa, J. P.-Y. 1988. Laboratory measurements of instantaneous sediment concentration under waves. *IEEE Journal of Oceanic Engineering* 13(4):299-302.

Moore, P.G. 1978. Inorganic particulate suspensions in the sea and their effects on marine animals. *Oceanography and Marine Biology Annual Review* 15: 225-363.

Murren, C. 1993. Turbidity and particles in water and waste. *Control and Instrumentation* 25(6): 35-36.

Newcombe, C. P., and D. D. Macdonald. 1991. Effects of suspended sediments on aquatic ecosystems. *North American Journal of Fisheries Management* 11(1): 72-82.

SERDP. 2009. The Strategic Environmental Research and Development Program Homepage. Available at www.serdp.org. Accessed 4 March 2009.

Sherwood, C.R., D. Coats, and B. Walls. 1989. Current and suspended sediment measurements on the central california continental shelf. In *OCEANS '89. Proceedings*, 320-325. New York, NY: IEEE.

USGS. 2009. Water Science Glossary of Terms. Reston, VA: U.S. Geological Survey. Available at ga.water.usgs.gov/edu/dictionary.html#S. Accessed 8 June 2009.

Walling, D.E. 1994. Chapter 3: Measuring sediment yield from river basins. In *Soil Erosion Research Methods, 2nd ed*. 39-80. R. Lal, ed. Delray Beach, FL.: St. Lucie Press.

CHAPTER 2 - DESIGN OF A REAL-TIME, OPTICAL SEDIMENT CONCENTRATION SENSOR

Abstract. SSC in water is one of the most important parameters to evaluate the water quality. In this study, an optical sensor was developed to measure SSC in streams on a real-time basis. Three light emitting diodes (LED), emitting lights of different colors (blue-green, infrared, orange), were used as the light sources, and nine phototransistors were used to detect backscattered, scattered and transmitted lights at 45°, 90° and 180° angles for the LEDs. A light modulation algorithm was designed to remove the influence of ambient light, especially the sunlight, on measurement accuracy. Models to predict SSC based on measured light signals were established and compared in statistics and neural network. A statistical analysis showed that soil texture played an important role in SSC prediction while the designed sensor was capable of reducing the effect of water color on sensor performance. An R-square value of higher than 0.99 for the prediction model was achieved for individual soil type and the R-square value was reduced to 0.8845 when all soil types were combined. Neural-network models derived for the training and two validation data sets achieved R-square values of 0.9961, 0.9670, and 0.9476, respectively. The sensor design was simplified based on a statistical stepwise selection procedure.

Keywords. Suspended-sediment, concentration, prediction model, water quality.

2.1 Literature Review

2.1.1 Traditional method for SSC measurement

Various methods have been used to measure suspended sediments (Wren et al., 2000). The traditional method to determine SSC involves both field collection using bottles or automatic samplers, and laboratory procedures involving filtering, drying and weighting. Water samples should be taken back to the laboratory for filtration within 24 hours. Most other techniques are calibrated against the traditional sampling method. However, the traditional filtration method is time consuming and labor intensive. Although automatic samplers mitigate labor consumption to some extent, field personnel still need to replace sampling bottles inside samplers during rainy days due to the limited storage space within the samplers. Manual or

automatic sampling lacks the temporal resolution required to capture rapid and intermittent flushes of suspended sediment during storm events (Cochrane et al., 2004). The peak sediments concentrations which are responsible for carrying the vast majority of the total sediment load are usually missed with the traditional method (Burkhead and Jelks, 2001).

2.1.2 Acoustic measurement

Many researchers studied acoustic measurement for SSC (Hay and Sheng, 1992; Thorne and Hanes, 2002; Gartner, 2004). In acoustic techniques, high frequency sound (1-5 MHz) generated by a transducer is directed to the measurement volume (Wren and Kuhnle, 2002). The backscattered portion of the sound is directed back to the transducer. The strength of acoustic backscattered signals can be used to determine SSC with a pre-calibrated relationship between SSC in water and output signals provided by the acoustic instrument.

Acoustic measurement is non-intrusive to the water flow. It can conduct SSC measurement in a vertical range on the order of several meters (Wren et al., 2000). However, Acoustic measurement has its disadvantages. Acoustic signal tends to attenuate at high particle concentrations (Wren et al., 2000). Acoustic signal is also susceptible to absorption by biological materials. Acoustic devices usually have flow depth limitation so that they can't be used for SSC measurement in shallow rivers (Meral, 2008).

2.1.3 Remote sensing

Remote sensing techniques were used to measure SSC remotely through the infrared radiation reflected from a water body based on the relationship between the amount of radiation and SSC values (Li et al., 2003; Doxaran et al., 2003; Ruhl et al., 2001; Nilsson et al., 1996). Generally, the spectrometer that measures the reflected radiation is located on an air plane or satellite. Remote sensing method is able to measure broad areas. However, the resolution is low. With higher sediment concentrations in water body, the measuring depth is limited to the top meters of the water column (Wren et al., 2000).

2.1.4 Laser diffraction

The term laser diffraction is from light scattering physics. When angular scattering from a particle is examined in small forward angles, it appears identical to the diffraction pattern from an aperture with the same diameter. This property made it possible to consider particles as same-

sized apertures. For this reason, the method was called laser diffraction. A laser diffraction sensor uses a laser beam as the light source. The diffracted laser lights caused by particles with different size are detected by a series of ring-shaped detectors with a graduate increasing diameter (Wren et al., 2000). Thus, the diffraction angle of the laser beam, which is related to different particle sizes, is determined. The SSC is determined by summarizing the volume of the sediment at each particle size class if the particle density is known (Gray et al., 2009).

Current practice using laser diffraction technique to measure SSC is dominated by the Laser In-Situ Scattering and Transmissometry (LISST) series instruments made by Sequoia Scientific, Inc. of Bellevue, Washington. Agrawal and Pottsmith (2000; 2003) introduced two LISST series laser diffraction sensors that measure concentration and size distribution of suspended sediment. The LISST sensors measure the diffraction of a laser around the suspended particles, and infer the particle size distribution of the suspended sediment being measured based on the diffraction signal.

In situ laser sensors were tested in various watersheds as an alternative method for measuring the suspended sediment distribution and transport (Melis et al., 2002; Wei et al., 2007). A disadvantage of the LISST instrument is its large size, which causes a significant flow obstruction.

2.1.5 Digital image analysis

The rapid improvements in computer and imaging technology provide the possibility to use video and image analysis for SSC measurement. In this technique, a video camera records the water-sediment mixture on a real time basis. A computer-controlled analysis system is used to analyze SSC and the size distribution. The measurement accuracy is based on the resolution of the video system and the image processing method (Wren et al., 2000). The disadvantage of this SSC measurement is the large size of the housing of the equipment, which may cause flow disturbance when submerged in water. In addition, fouling on the glass wall of the housing, which the video device is faced, may reduce the measurement accuracy.

2.1.6 Capacitance sensors

Capacitance sensors have been used widely to measure water content in soils. Since sediment-water mixture also has solid and liquid phases, different partitions of sediment and water in the mixture can be determined by measuring the dielectric constant of the mixture. Li et

al. (2005) investigated a method to measuring SSC with two types of capacitance sensors, a parallel plate type and a cylindrical type. In their study, the relationships between the sediment concentration in flowing water and the output capacitance of capacitance sensor were established. Results showed that suspended sediment concentrations were linearly correlated with the outputs of capacitance sensors over a wide range. The capacitance sensor measurement is subject to temperature changes.

2.1.7 Optical measurement

Optical measurement has been proved to be a reliable method to measure SSC. Usually, it measures backscatter, scatter, or transmission of visible or infrared light through the water sediment samples.

Turbidity is often used as a surrogate measurement to estimate SSC in water after determining the correlation between turbidity and SSC (Gao et al., 2008; Sadar, 2002). However, this correlation can be inconsistent with large variability caused by constituents in water other than suspended sediment, such as finely divided inorganic and organic matters, soluble, colored organic compounds, and plankton and other microscopic organisms (EPA, 1999; APHA et al., 1998). Turbidity is an optical property, not a true measure of SSC (Riley, 1998; Davies-Colley and Smith, 2001). In addition, the establishment of suspended sediment/turbidity relationship is time-consuming (Sadar and Engelhardt, 1993), and this relationship is not explicitly transferable between different watersheds (Marquis, 2005).

Optical backscatterance (OBS) sediment sensors have been used by many researchers in sediment load and transport measurement (e.g. McKee et al., 2006; Kineke and Sternberg, 1992; Sherwood et al., 1989). OBS sensors measure light backscattered from soil particles in water and respond linearly to a wide range of SSC. Although OBS sensors tend to reach saturation at high sediment concentrations, the saturation problem can be overcome by careful adjustment of the instrument's gain (Kineke and Sternberg, 1992).

Transmitting light techniques are attractive in small sediment concentration ranges, although they cannot be used for relatively high suspended sediment concentrations due to the extreme light attenuation. SSC measurements have been successfully conducted using this method by many researchers (Gregory and Nelson, 1986; Maa, 1988; Daraigan et al., 2006).

Buttmann (2001) reported that scattered light is the most suitable parameter to measure sediment concentration since 90° scatterance is more constant over all particle sizes comparing with backscatterance and transmittance. Scatter light measurements were used by many researchers (Daraigan et al., 2005; 2006; Goldberg et al., 1987).

As a part of a research project supported by SERDP (Strategic Environmental Research and Development Program), "Assessing the impact of maneuver training on NPS pollution and water quality" (CP-1339), an optical sediment sensor was developed to measure pure sediment concentration in the Instrumentation and Control Laboratory at Kansas State University (Stoll, 2004). The sediment sensor was designed to be insensitive to non-soil, suspended and dissolved objects, such as algae, organic matter, various microorganisms, and soil properties, such as texture and color, so that the measurement reflects only soil sediment concentration. In order to reduce the influence of water type and soil texture on sediment measurement accuracy, the sensor used light sources of different wavelengths in the visible and infrared wavebands and light detectors arranged at different angles from the light sources (Stoll, 2004).

2.1.8 Objective

In order to examine the effects of water and soil on the measurement accuracy, the SSC sensor designed by Stoll (2004) was further studied and tested in this research. A simpler sensor design was achieved based on an statistics analysis. An algorithm was also developed to reduce the influence of ambient light on the measurement. An outdoor experiment was conducted to verify the effectiveness of the light modulation algorithm.

2.2 Methodology

2.2.1 Sensor design

The original design of the sensor was developed by Stoll (2004). Its "three-ring" design was based on two assumptions: 1) Sediment measurement errors caused by difference in water color may be reduced by using multiple light sources at different "feature wavelengths"; 2) Sediment measurement errors caused by difference in soil texture may be reduced by using light detectors placed at multiple angles from the light source.
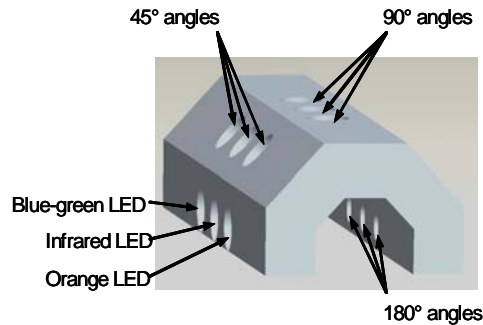
Figure 2.1 3-D view of the sediment sensor illustrating locations of light emitters and detectors (Stoll, 2004).

Based on an analysis of the spectral characteristics of three types of waters – distilled water, lake water, and stream water, Stoll (2004) selected three "feature wavelengths". LEDs with spectral responses peaking near these wavelengths were used in a prototype sensor as the light sources. For each LED, three phototransistors were strategically placed at various angles from the incident light to measure transmitted (180°), scattered (90°), and backscattered (45°) lights, respectively. Figure 2.1 shows the 3-D view of the sediment sensor illustrating locations of light emitters and detectors (Stoll, 2004). Figure 2.2 shows the prototype sensor with a waterproof package. A waterproof box with a rubber seal, purchased from Digi-Key Corporation (Thief River Falls, MN), was used as the sensor case. An aluminum tube with an internal diameter of 0.75 inch and thickness of 0.125 inch was cut to halves using a milling machine to be used as the "sensor tube". Holes were drilled on the sensor tube using the milling machine to ensure accurate sizes and orientations. Optical elements (LEDs and PTs) were glued in these holes using Epoxy. Connectors were soldered on these optical elements and a 12-pin panel receptacle screened in the sensor box with waterproof O-rings. A cable with a user-defined length linked the sensor through a 12-pin cable connector to its signal conditioning and processing circuitry.
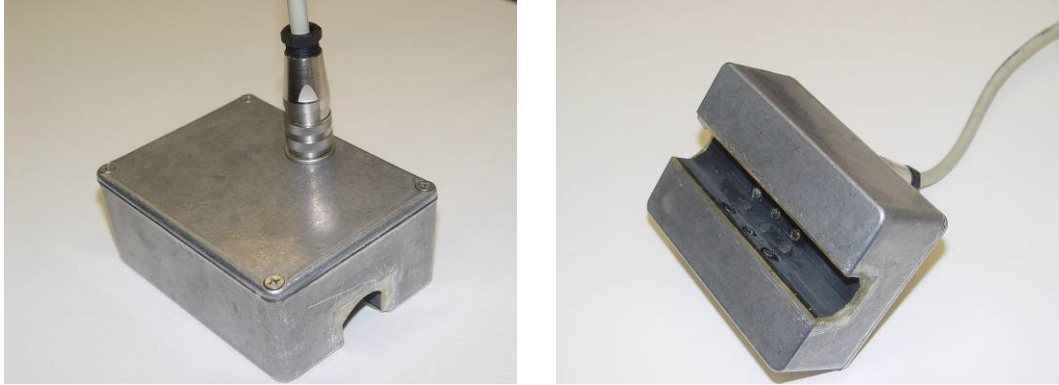
Figure 2.2 Prototype sensor in a waterproof package.

2.2.2 Light modulation algorithm to remove ambient light on SSC measurement

Optical sensors are sensitive to ambient light conditions. For field applications, sunlight usually has the strongest effect. In order to reduce the influence of ambient light on sediment measurement, a relative light index, "I_r" was used in the prediction model analysis:

$$I_r = I_{on} - I_{off} \qquad\qquad (2.1)$$

where:

I_{on} = signal recorded when LED is turned on (mV);

I_{off} = signal recorded when LED is turned off (mV);

When the LED is turned on, the signal detected by the phototransistors (I_{on}) reflects the combined effect of the LED and the ambient light. On the other hand, when the LED is turned off, the signal (I_{off}) reflects only the effect of the ambient light. If the signal is subtracted from the I_{on} signal, the effect of ambient light can be reduced. In this study, light modulation was accomplished using the datalogger. The frequency of modulation was programmed to be 50 Hz.

2.2.3 Laboratory experiments

2.2.3.1 Measurement system setup

Figure 2.3 illustrates the laboratory experiment setup for the prototype sensor. The setup consisted of the optical sediment sensor, a CR5000 datalogger (Campbell Scientific Inc., Logan,

Utah), a specially designed signal conditioning and processing board (Appendix A), a power supply, and a personal computer.
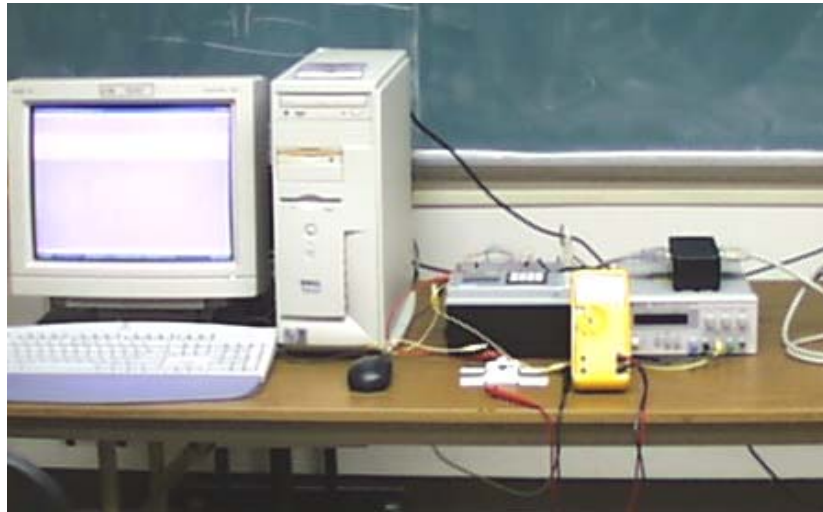
Figure 2.3 Prototype sensor laboratory experiment setup.

A pump-driven circulation system (Figure 2.4) was designed to maintain uniform sediment concentrations for the sensor test. A compact, submersible, centrifugal pump was used to drive the water/sediment mixture circulating in the system, which had a total volume of 2.5L. The CR5000 datalogger was programmed using the PC9000 software (Campbell Scientific Inc., Logan, Utah) to turn on and off each LED in a predefined sequence every second, while reading and processing the signals from the phototransistors (Appendix B). Data was downloaded from the datalogger for statistics and Neural Network analysis after the experiment was completed.
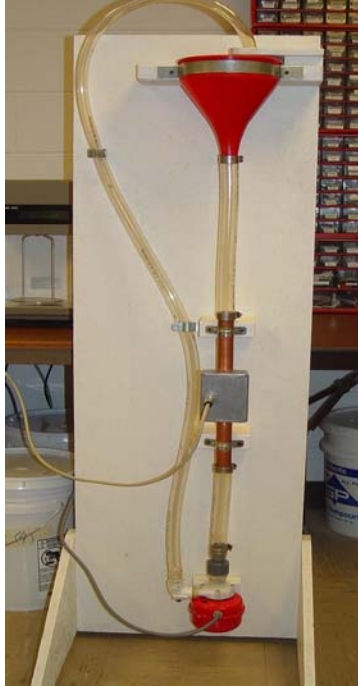
Figure 2.4 A Circulation system that provides uniform concentrations.

2.2.3.2 Experiment design

The prototype sensor was tested at combinations of four water types (Three-mile Creek at Fort Riley, Wildcat Creek in Manhattan, KS, Tuttle Creek Reservoir in Pottawatomie county, Kansas, and distilled water) and five soil types (sandy loam1, sandy loam2, clay, clay loam and silty clay loam). The texture compositions of the five soil types are given in Table 2.1. Water analyses for the water types are shown in Table 2.2.

Table 2.1 Texture compositions and sampling sites for five soil types.

Soil Type	Soil Sampling Site	Texture		
		% Sand	%Silt	%Clay
Sandy Loam 1	Stafford County, KS	74	20	6
Sandy Loam 2	Shawnee County, KS	50	44	6
Loam	Cherokee County, KS	32	50	18
Clay Loam	Wabaunsee County, KS	24	56	20
Silty Clay Loam	Marshall County, KS	14	54	32

Table 2.2 Water analysis results.

Water sample	Total Suspended Solids (mg/L)	pH	Ortho Phosphorus (ppb)	Ca Calcium (ppm)	K Potassium (ppm)	Mg Magnesium (ppm)	Na Sodium (ppm)	NH_4-N** (ppm)	NO_3-N (ppm)	Conductivity (dS/m)	Total Dissolved Solids*** (mg/L)	Total Nitrogen (ppm)	Total Phosphorus (ppm)
Three-Mile Creek Water	257	8.2	9	113	2.9	45	28	0.04	ND*	0.520	364	0.21	0.08
Tuttle Creek Water	2	8.2	205	86	13.9	23	35	0.05	1.23	0.440	308	1.56	0.23
Wildcat Creek Water	67	8.2	76	136	5.6	46	20	0.05	0.46	0.562	393	0.73	0.19
Distilled Water	ND	6.1	ND	ND	0.35	ND	0.63	0.09	0.02	8.81	6.2	ND	ND

*ND = None Detected;

**Detection limit of 0.01 ppm on NH4-N (Ammonium);

***A factor of 700 was used to convert electrical conductivity (dS/m) to total dissolved solids (mg/L).

2.2.3.2.1 Preliminary experiment on the circulation system

A preliminary experiment was designed to test the performance of the pump-driven circulation system in maintaining uniform concentrations. Seven concentrations were used in this experiment. At each concentration, one water sample was taken right after the datalogger took readings from the sensor. All 35 water samples were sent to the Soil Testing Laboratory at Kansas State University for SSC analysis.

2.2.3.2.2 Sensor experiment

A complete randomized factorial design experiment was conducted to study the effects of water color and soil composition on the signals, and to verify the effectiveness of the sensor design in reducing or removing the impacts of water color and soil composition on the accuracy of the prediction models in measuring SSC. The experiment was carefully designed to produce three statistically independent data sets as three replications by making three samples for each soil-water combination, one of which was used to train statistical and neural-network models for predicting SSC, whereas the remaining two sets were used to validate the models. Eleven soil concentrations were tested at each soil-water combination within the range 0~5000mg/L to cover possible sediment concentrations in natural streams. At each soil concentration, three repeated measures were taken. These eleven soil concentrations were selected on a base-100 logarithm scale (Figure 2.5) in order to create small intervals within the low concentration range and relative larger interval within the high concentration range.
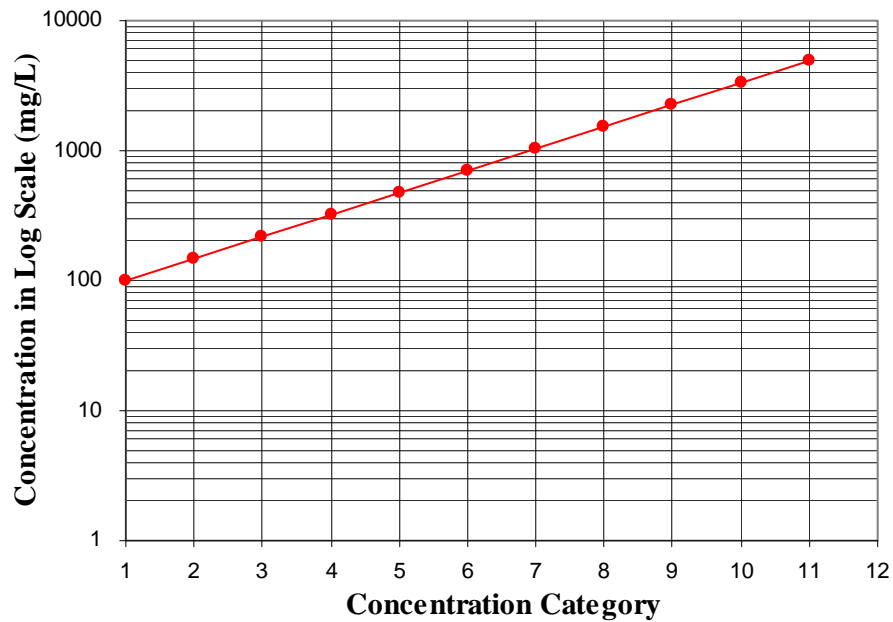
Figure 2.5 Concentration categories selections using a base-100 log curve.

2.2.4 Outdoor experiment

An outdoor experiment was conducted to test the effect of ambient light, especially the sunlight, on sensor signals, and the effectiveness of light modulation on SSC measurement accuracy. Only one soil type (sandy loam 2) was used in this experiment.

Figure 2.6 Circulation system used in outdoors experiment.

Because sun light conditions are not controllable, the experiment was conducted at different times in the day, from 9 am to 11 pm, over a period of two weeks, to obtain a wide range of ambient light intensity. Sensor signals recorded with all LEDs off in a completely dark environment were considered as the base line. An index, ambient light intensity (I), was created

by subtracting the base line value from sensor readings taken with all LEDs off under different light conditions to indicate various ambient light conditions.

$$I_A = I_{off} - I_b \tag{2.2}$$

where:

I_A = ambient light intensity (mV);

I_b = sensor signals recorded with all LEDs off in a completely dark environment (mV).

There were a total of 18 tests conducted in the outdoor experiment. For each test, twelve soil concentrations were created using another pump-driven circulation system (Figure 2.6). Gains of the signal conditioning circuits for each sensor were adjusted to avoid out-of-range data. Calibration models were once again established using the outdoor experiment data. To ensure the statistical correctness, the experiment data were divided into three statistically independent data sets for calibration, validation and test purposes, respectively.

2.3 Results

2.3.1 Preliminary experiment on the circulation system

Figure 2.7 shows the performance test results of the pump-driven circulation system. Large errors were observed for Sandy Loam 1 (contains 74% sand). This was due to the fact that it is relatively difficult for the circulation system to keep sandy soil particles floating all the time. Polynomial regression models between the actual concentration and target concentration for four soil types were developed (Table 2.3). They were used in data analysis to reduce prediction errors caused by the incapability of the circulation system in maintaining a uniform concentration distribution.
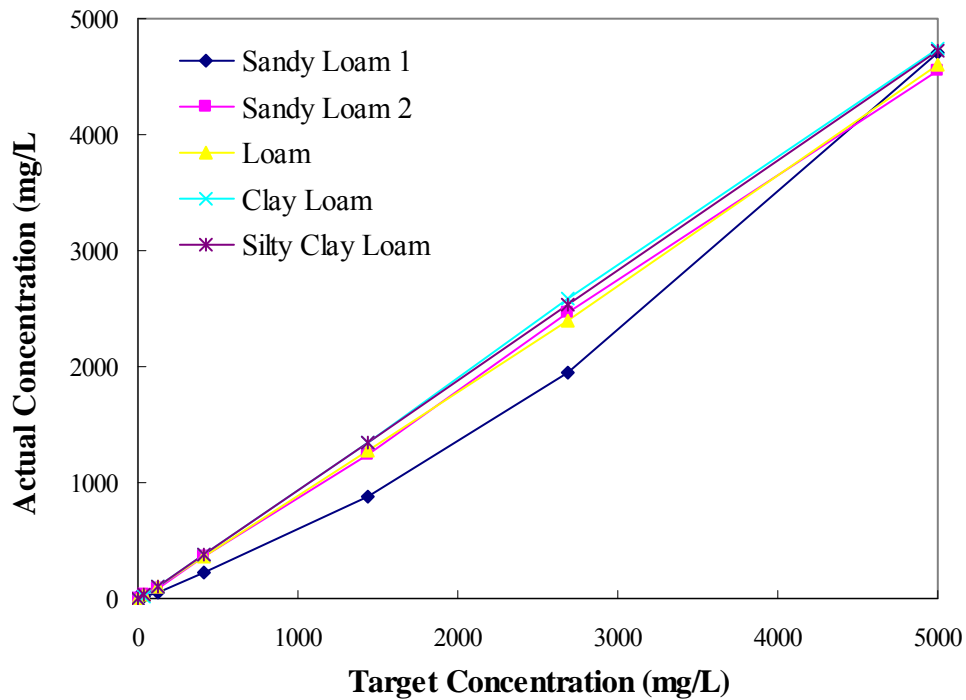
Figure 2.7 Results of the circulation system performance experiment for maintaining a uniform concentration distribution.

Table 2.3 Regression models between actual and target oncentrations.

Soil Type	Regression models	R-square value for the regression
Sandy Loam 1	Second order polynomial	1.0000
Sandy Loam 2	Linear model	0.9996
Loam	Linear model	0.9996
Clay Loam	Linear model	0.9999
Silty Clay Loam	Linear model	0.9999

2.3.2 Laboratory experiment results

Results of the laboratory experiment indicated that the sediment sensor had relatively better linear responses to SSC for sandy soil than clay soil. Two example calibration curves for Sandy Loam 1 soil and Silty Clay Loam soil with the same water (Three-mile Creek Water) were plotted in Figures 2.8 and 2.9, respectively. The signal for of backscattered light measured by phototransistors at 45° angle (BG45, IR45 and ORA45) increased with SSC. This was because that more soil particles at higher concentrations scattered more light. The transmitted light

measured by phototransistors at 180º angle (BG180, IR180 and ORA180) had a decreasing trend and tended to reach zero when SSC increased. This was due to the fact that more soil particles in water blocked more light. For the silty clay loam, the BG90 and ORA90 signals increased at lower sediment concentrations and then decreased at concentrations higher than 2000mg/L. The increasing trend of IR90 slows down at higher SSC for the silty clay loam. This was probably due to the fact that soil particles at higher concentrations partially blocked the light and partially scattered light. When the light emitted by LEDs was blocked more than that was scattered, the light detected at 90º angle showed a decreasing trend. On the contrary, when the light emitted by LEDs was scattered more than that was blocked with less soil particles at lower sediment concentrations, an increasing trend of the light detected at 90º angle was observed. For the sandy loam 1, the scattered light measured by phototransistors at 90º angle (BG90, IR90 and ORA90) did not have the same significant trend as that for the soil of silty clay loam. From these figures, it is clear that the impact of soil texture on sensor signals is not negligible.
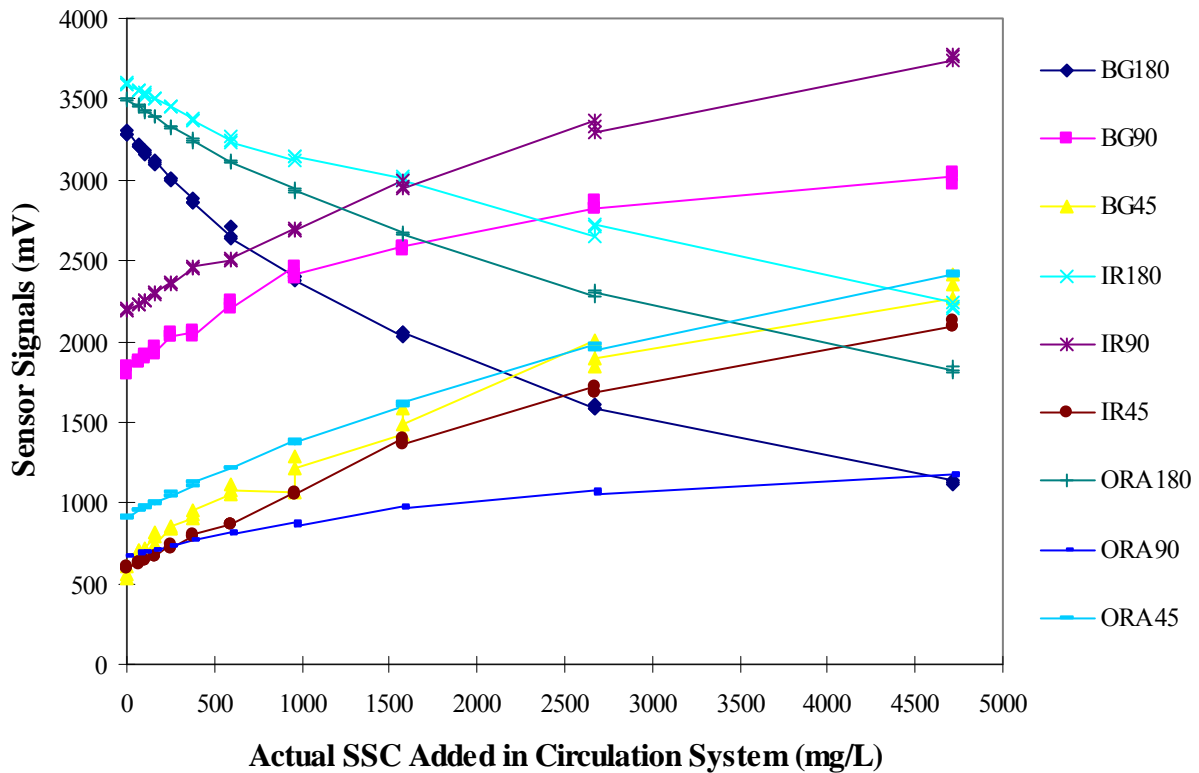
Figure 2.8 Sensor signals vs. actual SSC using sandy loam 1 and Three-Mile Creek water.
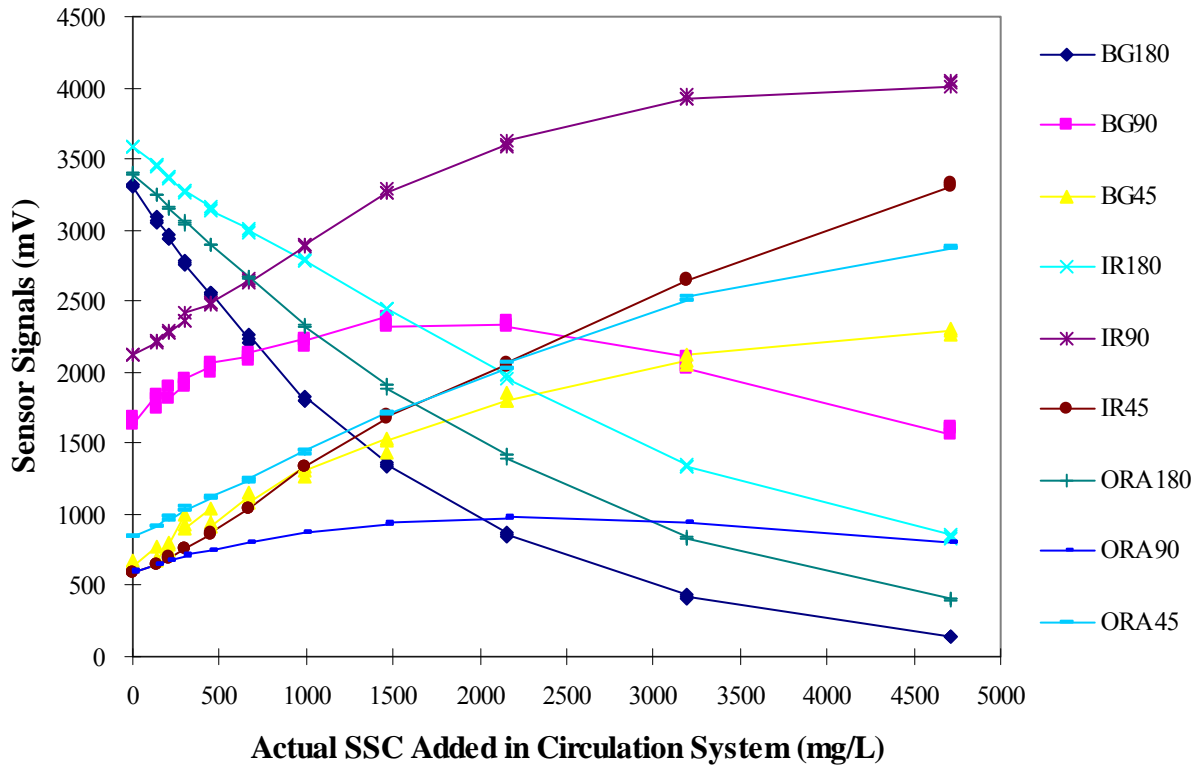
Figure 2.9 Sensor signals vs. actual SSC using silty clay loam and Three-Mile Creek water.

Comparison between Figure 2.8 and 2.9 also indicated that sensor output signal has a wider range for silty clay loam than that for sandy loam, which is especially obvious for backscattered signals at 45° angles and transmitted signals at 180° angles. This is most likely due to the fact that finer sediment has more surfaces for reflecting or blocking light per unit mass (Schoellhamer and Wright, 2003).

Since measurements of transmitted light are sensitive to SSC at lower concentrations and approaching zero at higher concentrations, whereas backscattered light measurements are more responsive at relatively high sediment concentrations. The combination of measurements of transmitted and backscattered lights made the optical sediment sensor useable within a wide SSC range.

2.3.3 Effect of soil texture on sensor signals

The "reg" procedure in SAS was used to develop a multiple regression model for each soil texture data and for combined 5 soil texture data in all waters using the calibration dataset.

These models were validated using the two validation datasets. The R-square values and RMS errors are summarized in Table 2.4. SSC prediction models established for individual soil types were capable of providing very accurate sediment concentration prediction with R-square values of higher than 0.95 for three datasets, indicating almost complete elimination of the influence of water color on measurement accuracy. However, the prediction accuracy was reduced when all 5 soil types were combined – R-square values were 0.8845, 0.8536 and 0.8717 for calibration and two validations, respectively.

Table 2.4 R-square values and RMS errors achieved for individual soil type using the calibration dataset and two validation datasets.

Soil type		Sandy loam 1	Sandy loam 2	Loam	Clay loam	Silty clay loam	Soil type combined
Calibration	R^2 value	0.9918	0.9995	0.9996	0.9991	0.9992	0.8845
	RMSE (mg/L)	131.49	32.84	30.06	46.01	42.00	481.91
Validation 1	R^2 value	0.9813	0.9989	0.9968	0.9950	0.9987	0.8536
	RMSE (mg/L)	216.66	118.67	133.80	117.21	71.97	544.92
Validation 2	R^2 value	0.9569	0.9854	0.9988	0.9923	0.9890	0.8717
	RMSE (mg/L)	304.00	187.09	61.41	151.70	174.57	511.53

Figure 2.10 shows the predicted SSC vs. actual SSC results using five separate prediction models developed for five individual soil texture types, whereas Figure 2.11 used the model developed across five soil texture types for calibration dataset. It is obvious that the prediction accuracy was greatly reduced when soil texture types were mixed. By observing Figure 2.11, it can also be found that the impact of sand content on the predicted concentration played an important role in SSC prediction. The SSC for soil type with a higher sand content tended to be underestimated and SSC for soil type with a lower sand content was relatively overestimated when using the combined model developed across all five soil types, indicating that the soil texture played an important role in SSC prediction accuracy. Figures 2.12 and 2.13 show predicted SSC vs. actual SSC results using the combined prediction model across all five soil types with combined water types for two validation datasets, respectively.
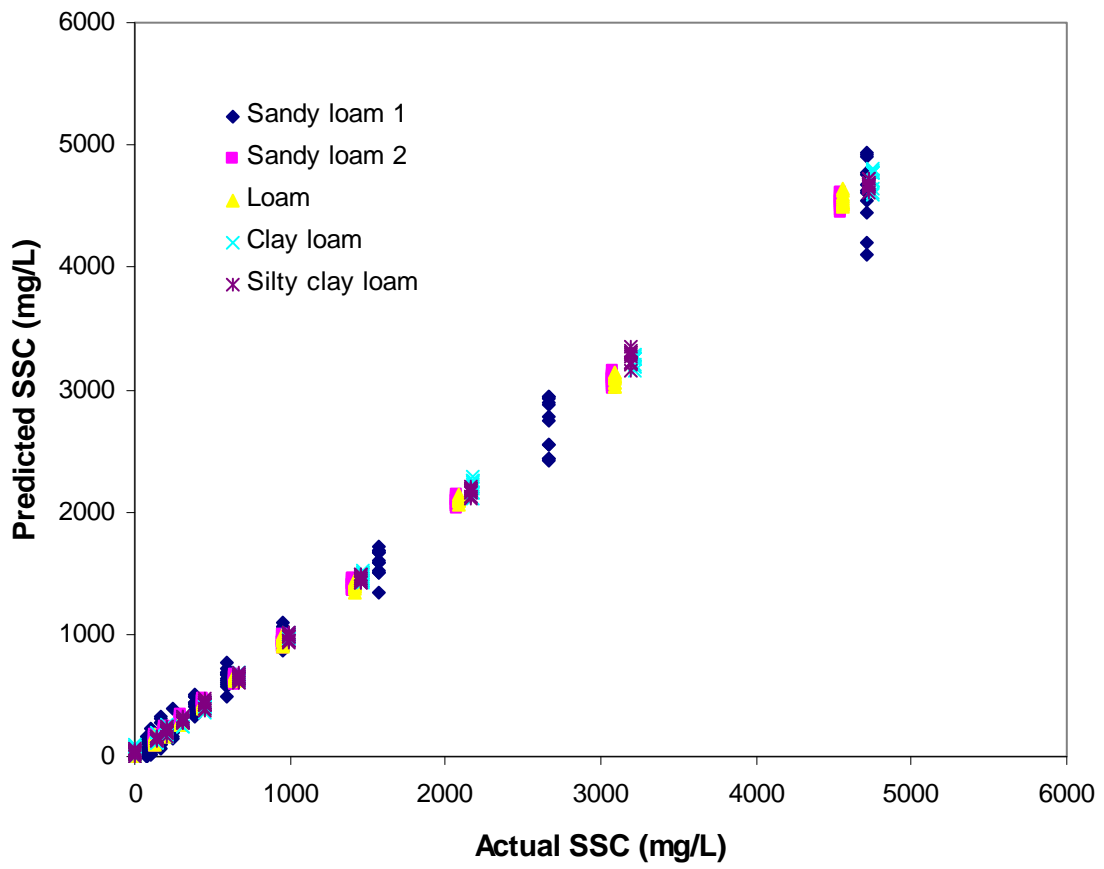
Figure 2.10 Predicted vs. actual SSC for calibration dataset using individual prediction model for each soil type with combined water types.
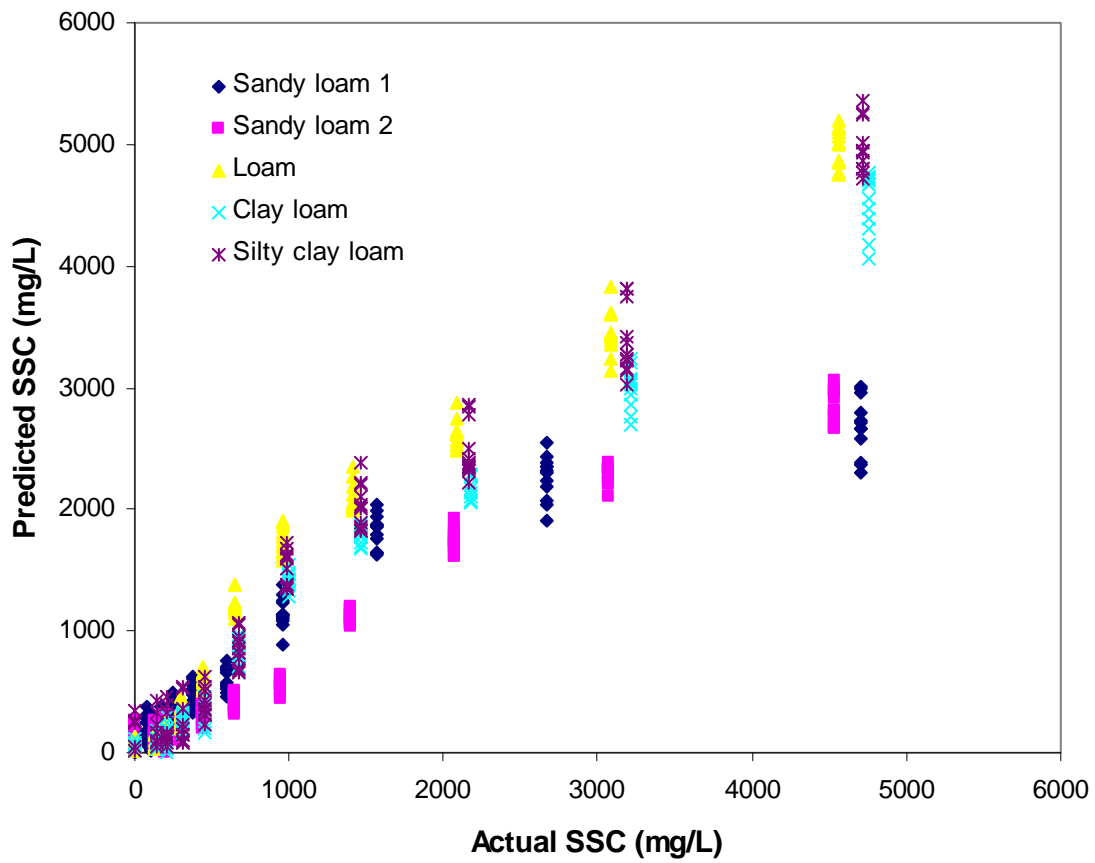
Figure 2.11 Predicted vs. actual SSC for calibration dataset using the combined prediction model across all five soil types with combined water types.
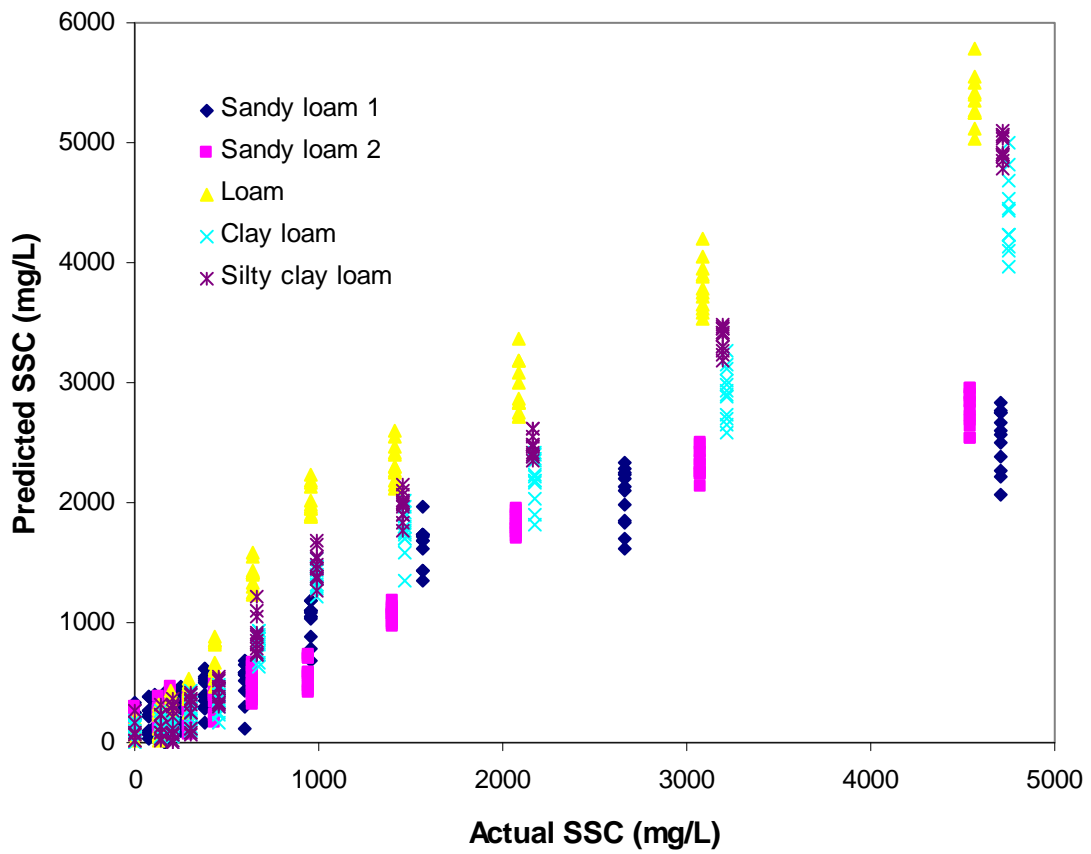
Figure 2.12 Predicted vs. actual SSC for validation dataset 1 using the combined prediction model across all five soil types with combined water types.
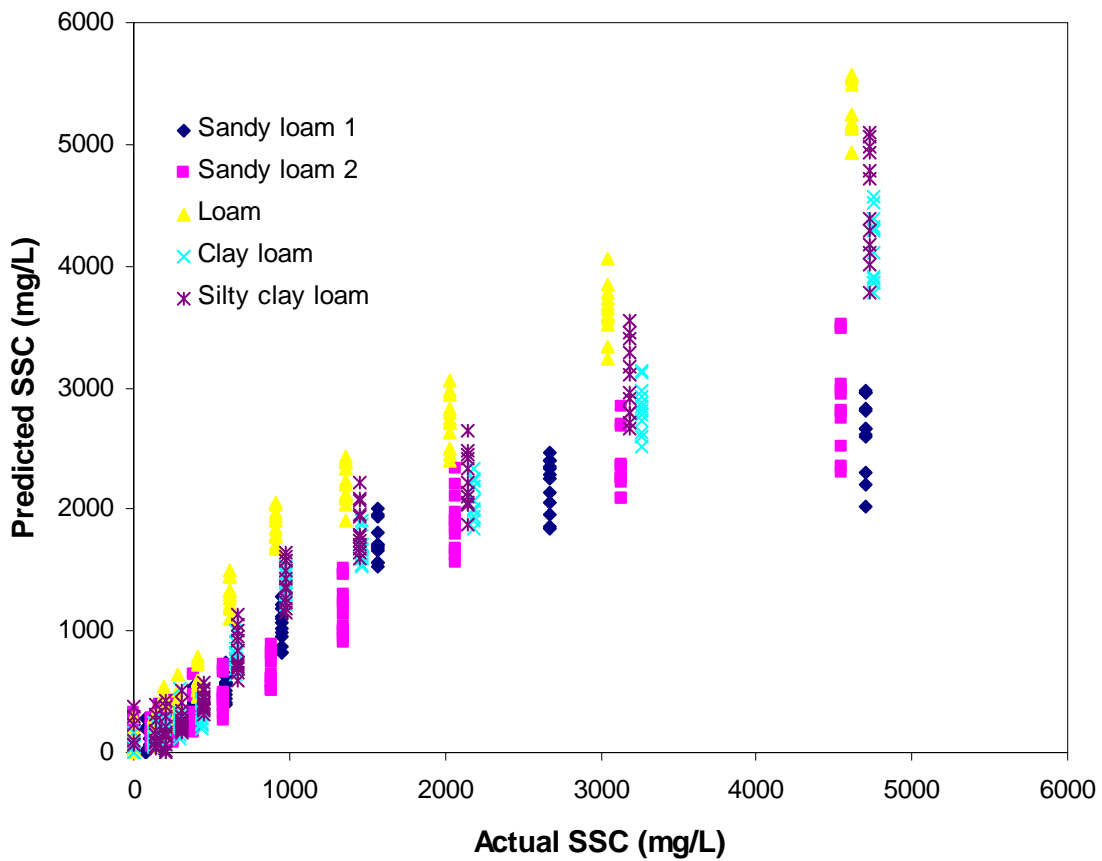
Figure 2.13 Predicted vs. actual SSC for validation dataset 2 using the combined prediction model across all five soil types with combined water types.

2.3.4 Effect of water type on sensor signals

When the "reg" procedure in SAS was used to develop a multiple regression model for each water type, R-square values of 0.9111, 0.9245, 0.9002 and 0.8959 were achieved for distilled Water, Wildcat Creek Water, Tuttle Creek Water and Three-Mile Creek Water, respectively (Table 2.5). When all 4 water types were combined across all soil texture types using the calibration dataset, the R-square value slightly reduced to 0.8845, which indicated that water color has relatively limited impact on SSC prediction accuracy.

Table 2.5 R-square values and RMS errors achieved across five soil types using the calibration dataset and two validation datasets.

Water type		Distilled water	Wildcat Creek water	Tuttle Creek water	Three-Mile Creek water	Water type combined
Calibration	R^2 value	0.9111	0.9245	0.9002	0.8959	0.8845
	RMSE	433.00	398.92	458.59	468.34	481.91
Validation 1	R^2 value	0.8043	0.7830	0.7887	0.8542	0.8536
	RMSE	651.37	780.62	678.85	584.11	544.92
Validation 2	R^2 value	0.7378	0.8701	0.7808	0.8681	0.8736
	RMSE	772.60	531.17	686.60	530.46	504.82

Figure 2.14 shows the predicted SSC vs. actual SSC using four prediction models developed for each individual water types, whereas Figure 2.15 used the model developed across four water types. It can be seen from these figures that prediction errors using individual models varied within a wide range. The SSC Measurement accuracy using the individual models (Figure 2.14) was not improved significantly compared to that using the four water types combined model (Figure 2.15), which further indicated the relatively small effect of water color on SSC measurement accuracy. These models were validated using two validation datasets as well. Figures 2.16 and 2.17 show predicted SSC vs. actual SSC results using the combined model for all four water with combined soil texture types for two validation datasets, respectively
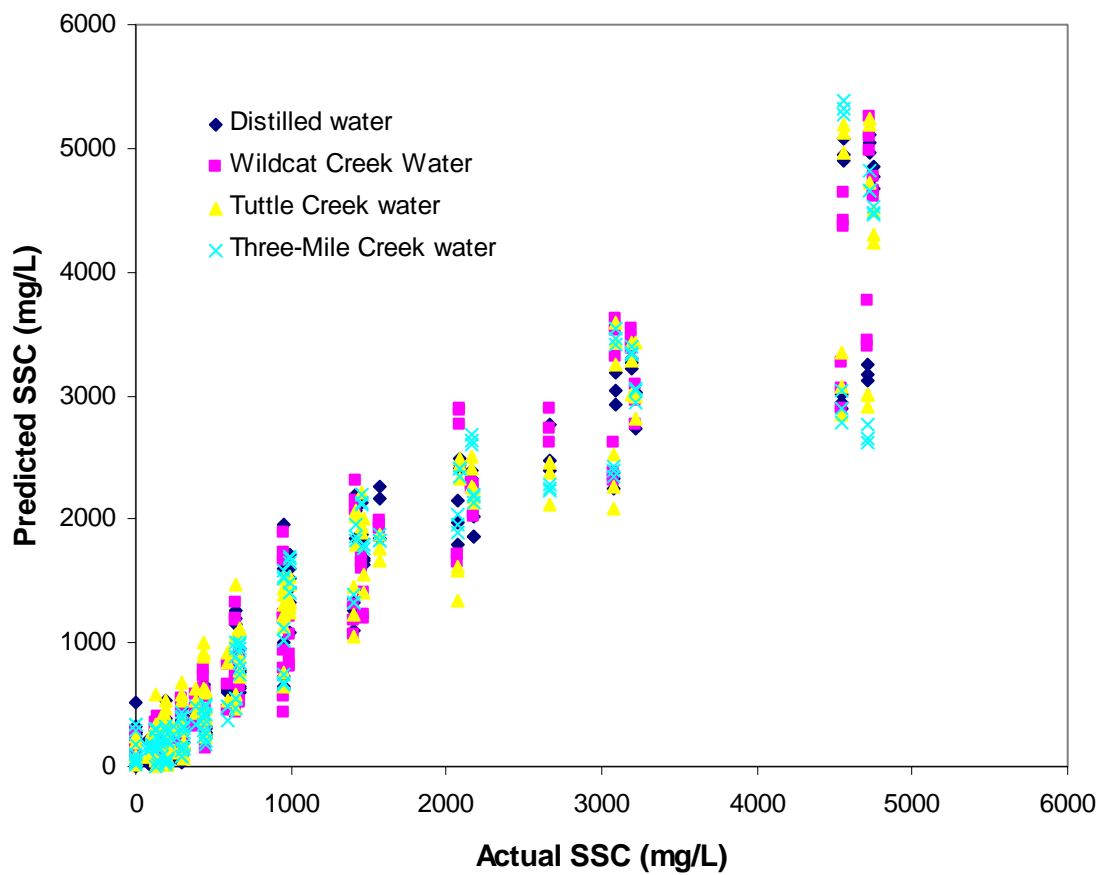
Figure 2.14 Predicted vs. actual SSC for calibration dataset using individual prediction models for each water with combined soil texture types.
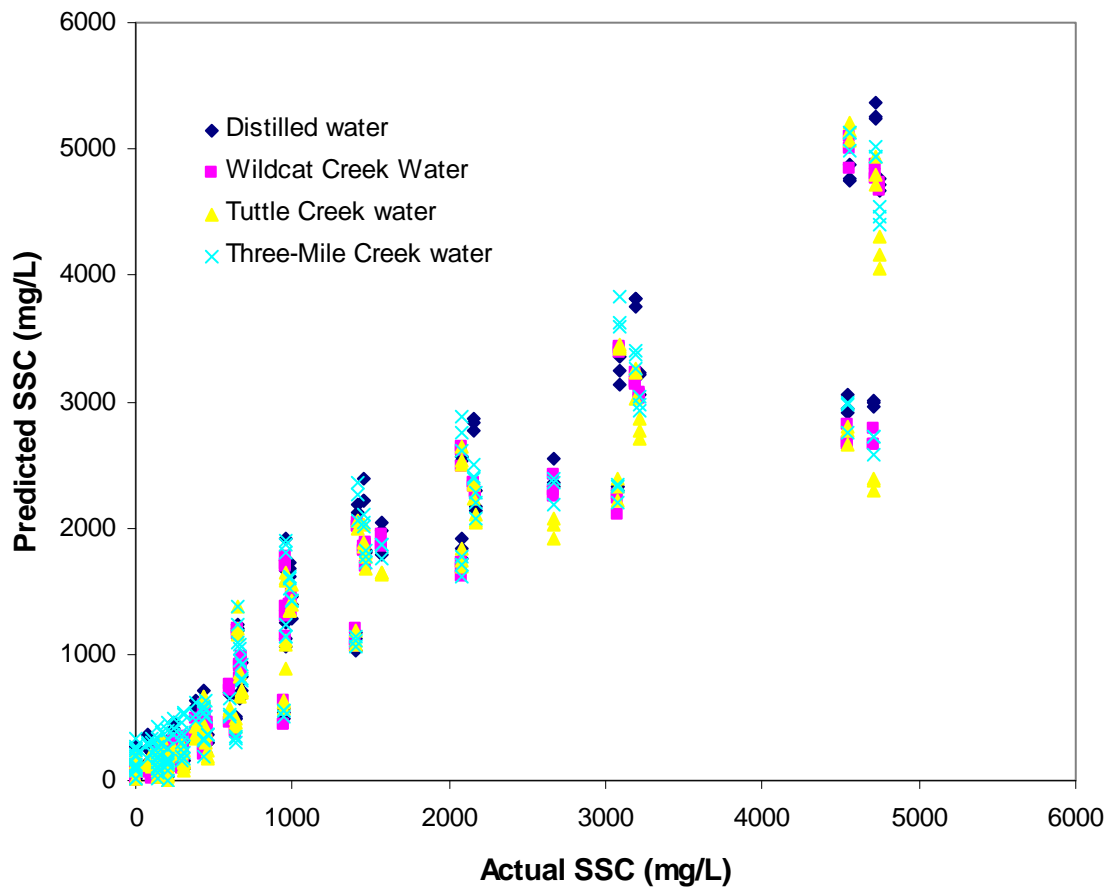
Figure 2.15 Predicted vs. actual SSC for calibration dataset using the combined model for all four water with combined soil texture types.
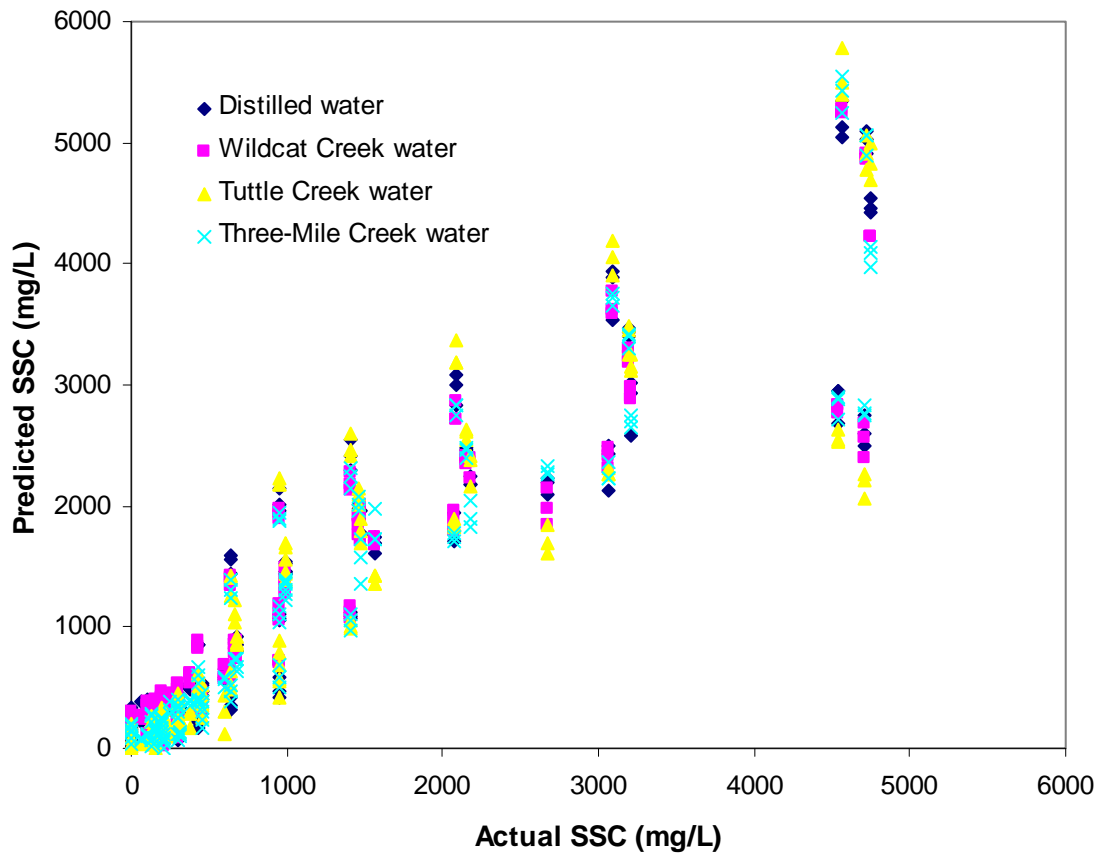
Figure 2.16 Predicted vs. actual SSC for validation dataset 1 using the combined model for all four water with combined soil texture types.
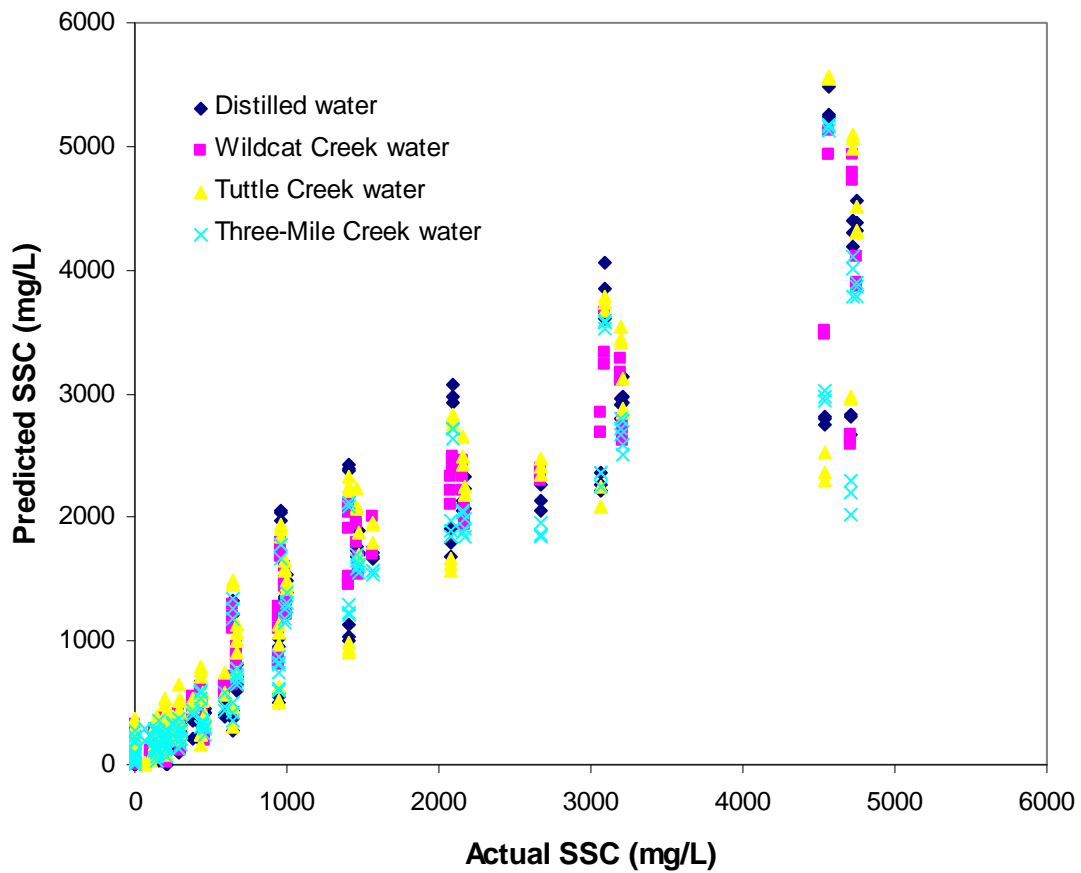
Figure 2.17 Predicted vs. actual SSC for validation dataset 2 using the combined model for all four water with combined soil texture types.

2.3.5 Neural-network models for SSC prediction in the indoor laboratory experiment

Neural-network models were developed based on experiment data obtained at combinations of four water types and five soil types (Appendix C). R-square values and RMS errors for neural-network models were derived for the training (calibration) and two validation data sets, respectively. Table 2.6 compares the results achieved from statistical and neural-network models. The R-square values for both calibration and validation datasets were greatly improved using the neural-network models. In the same time, RMS errors were decreased.

Table 2.6 R-square values and RMS errors achieved from statistical and neural-network models.

Model	Dataset	Training (calibration)	Validation 1	Validation 2
Neural-network models	R-square value	0.9961	0.9670	0.9476
	RMS error (mg/L)	88.66	259.41	326.17
Statistical models	R-square value	0.8845	0.8536	0.8736
	RMS error (mg/L)	481.91	544.92	504.82

Figures 2.18 and 2.19 show the predicted vs. actual SSC for calibration dataset using the neural-network model for all five soil types with combined water types. By comparing with Figures 2.11 and 2.15, it can be seen that prediction errors in Figures 2.18 and 2.19 had a relatively smaller range. These results indicated an improved result in reducing the influence of soil type on sediment concentration measurement using the neural-network models. Figures 2.20 and 2.22 show the predicted vs. actual SSC for all five soils with combined water types for validation datasets, respectively. Figures 2.21 and 2.23 show the predicted vs. actual SSC for all four water with combined soil texture types for validation datasets, respectively.
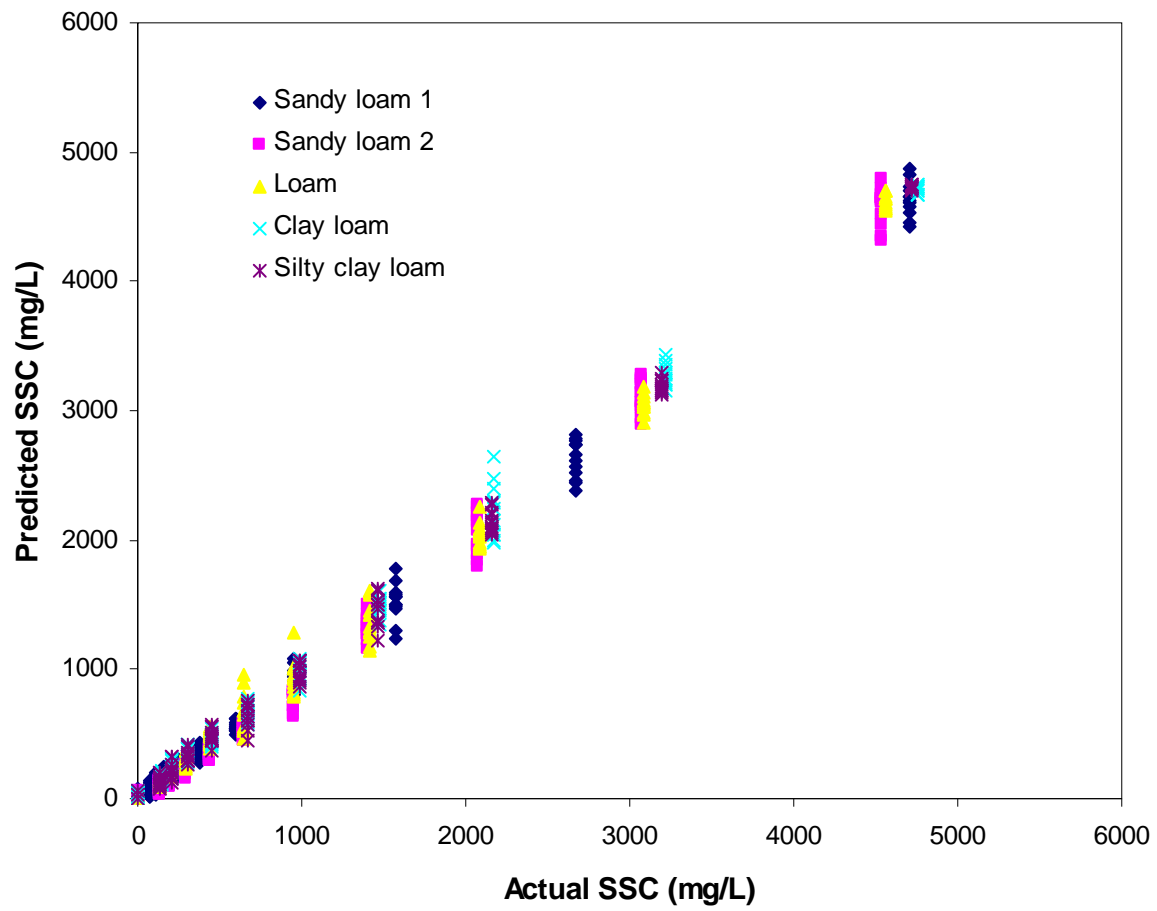
Figure 2.18 Predicted vs. actual SSC for calibration dataset using the model trained for all five soil types with combined water types.
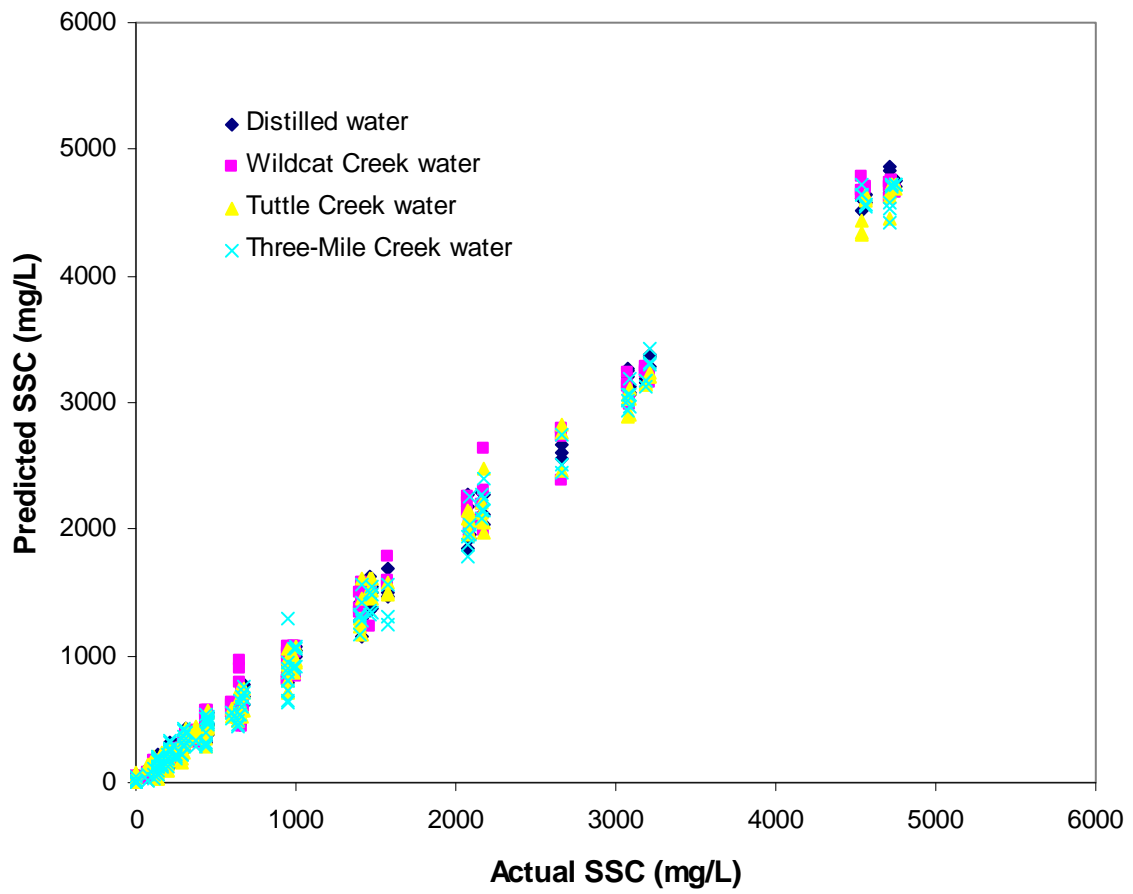
Figure 2.19 Predicted vs. actual SSC for calibration dataset using the model trained for all four water types with combined soil texture types.
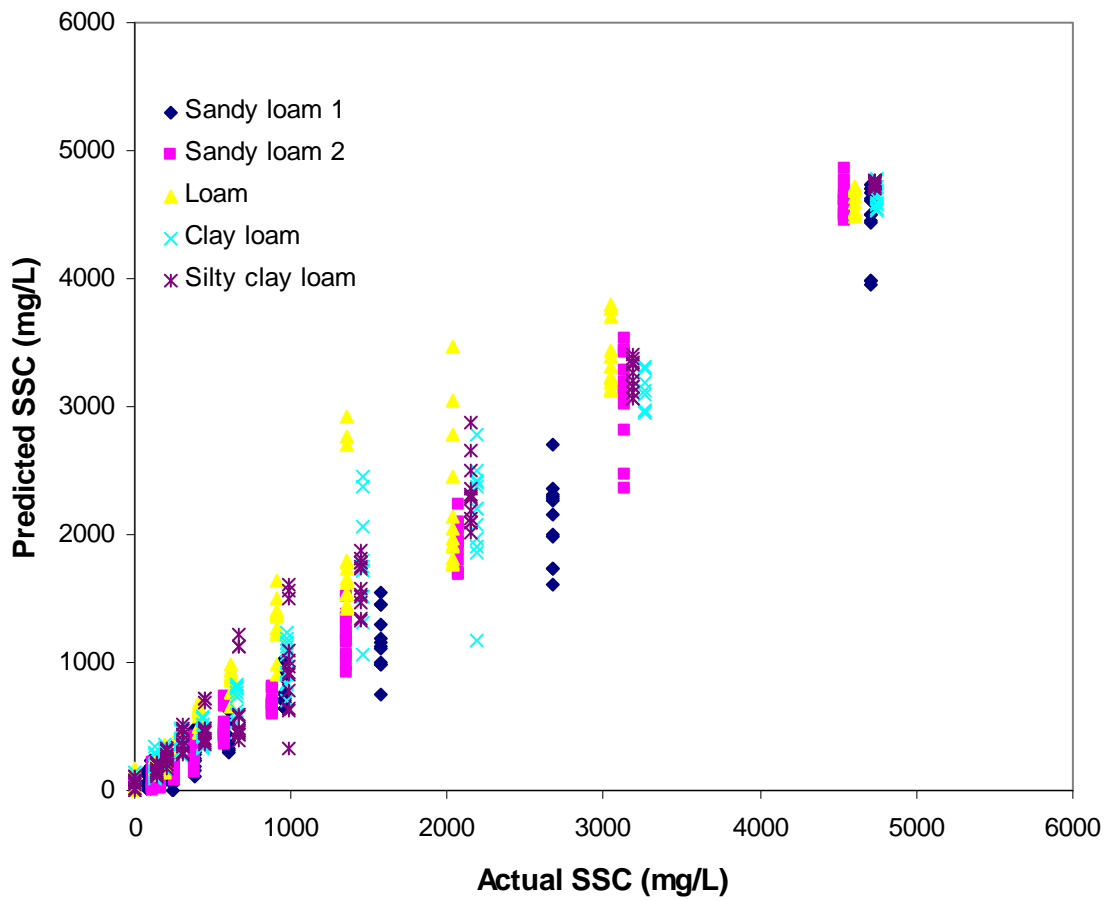
Figure 2.20 Predicted vs. actual SSC for validation dataset 1 using the model trained for all five soil types with combined water types.
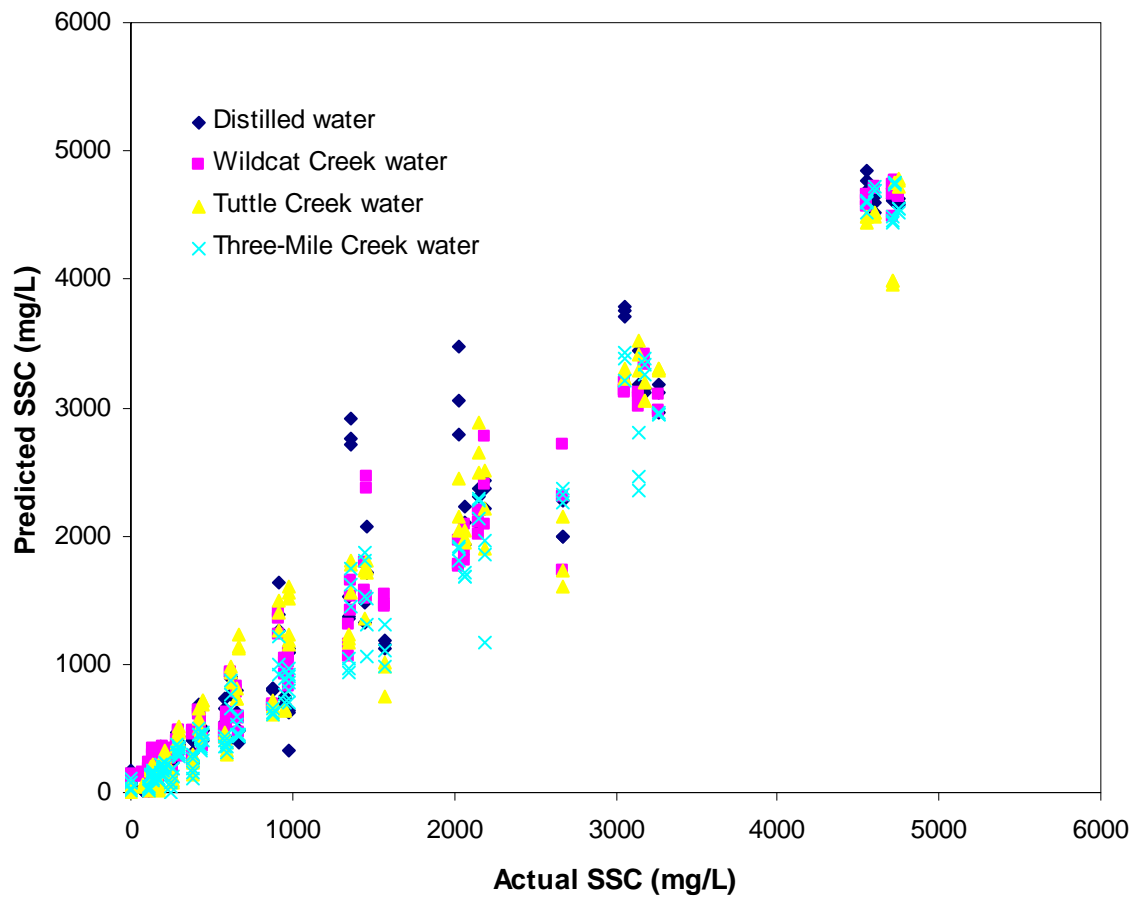
Figure 2.21 Predicted vs. actual SSC for validation dataset 1 using the model trained for all four water types with combined soil texture types.
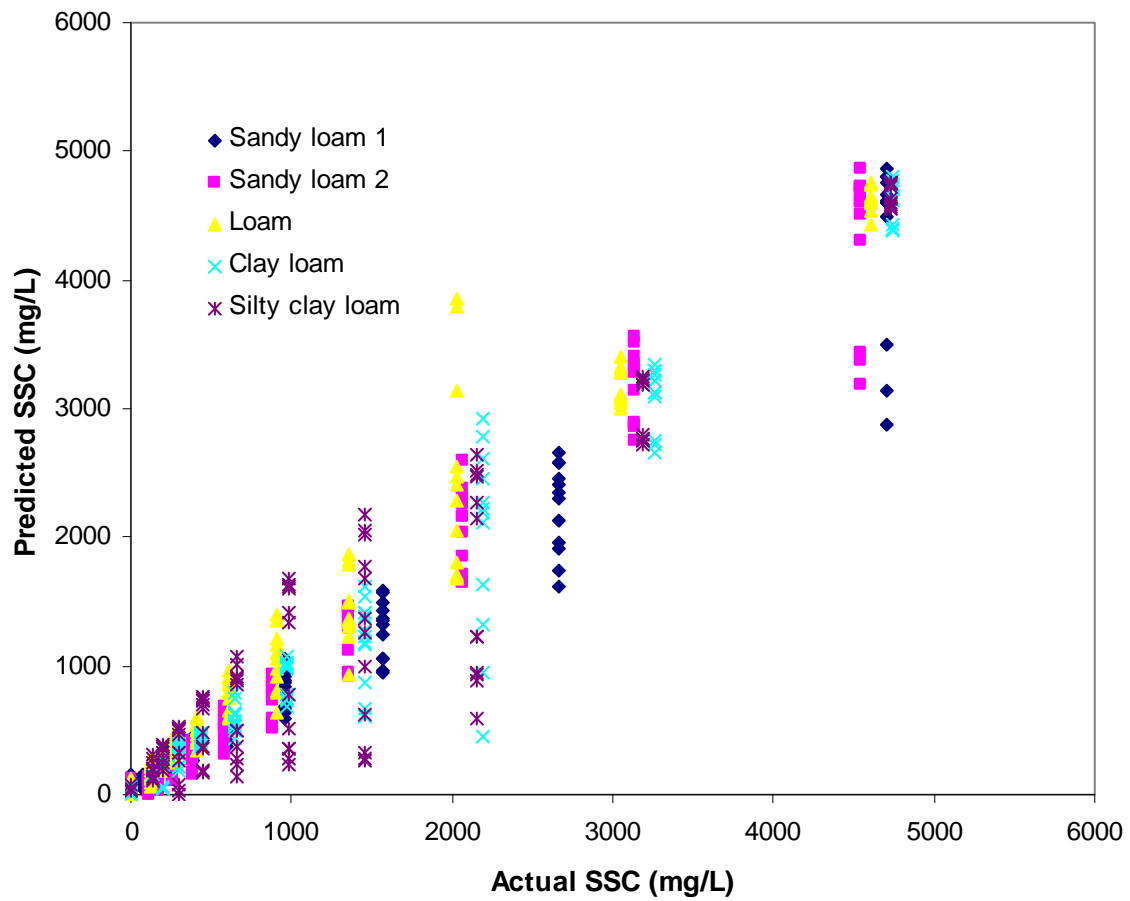
Figure 2.22 Predicted vs. actual SSC for validation dataset 2 using the model trained for all five soil types with combined water types.
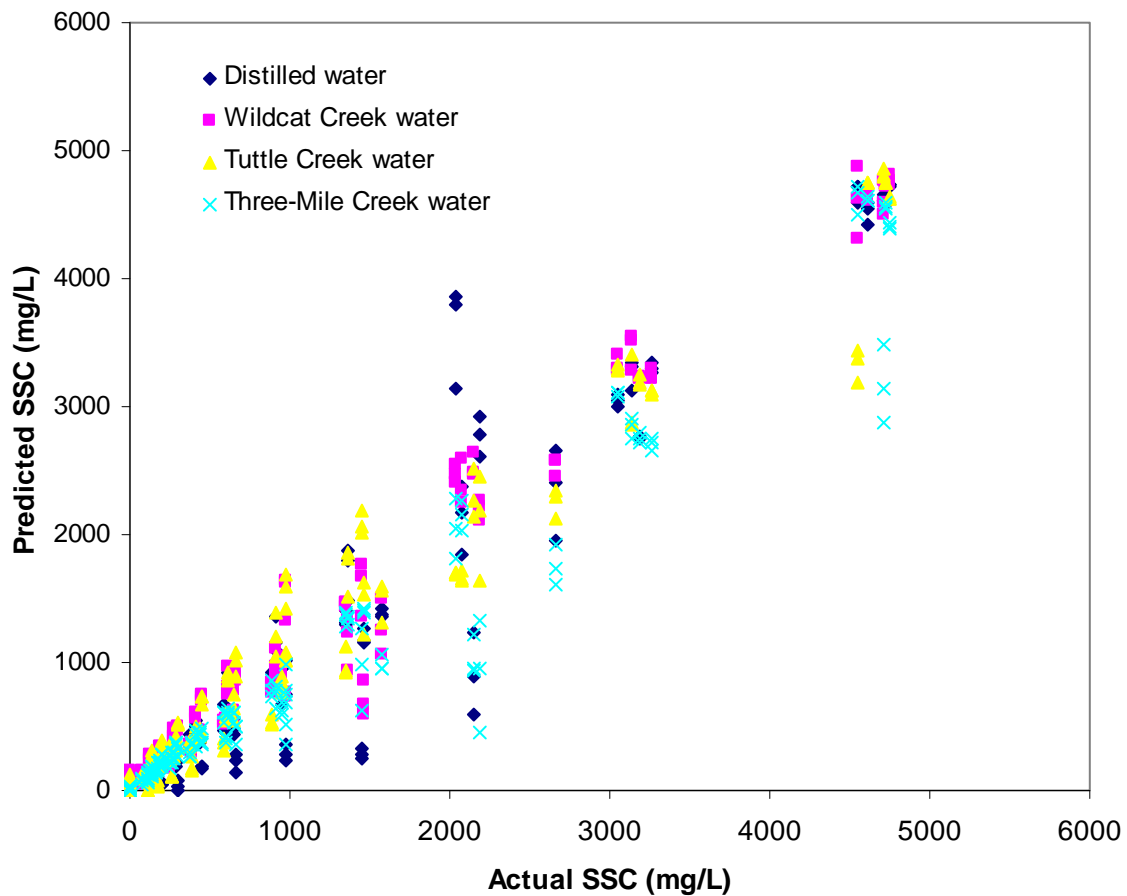
Figure 2.23 Predicted vs. actual SSC for validation dataset 2 using the model trained for all four water types with combined soil texture types.

2.3.6 Statistics analysis for the indoor laboratory experiment

The "mixed" procedure in SAS was used to analyze the data obtained from indoor laboratory experiment, in order to study the impact of water type, soil texture, and their interaction on SSC prediction accuracy (Appendix D). Water, soil, SSC, the interactions between water and soil, between SSC and water, and among concentration, water and soil, were considered as the fixed effects. Replications and the repeated measurements were considered as random effects. The results are summarized in Table 2.7.

Table 2.7 Results of statistics analysis for the indoor laboratory experiment.

Signal	Pr > F						
	Water	**Soil**	**Water*Soil**	**Conc.**	**Water*Conc.**	**Soil*Conc.**	**Water*Soil *Conc.**
BG45	0.1545	<0.0001	0.2533	<0.0001	0.0016	<0.0001	0.0004
BG90	<0.0001	<0.0001	<0.0001	<0.0001	0.1100	<0.0001	0.9108
BG180	0.1303	<0.0001	0.9959	<0.0001	0.9289	<0.0001	0.9996
IR45	0.0663	<0.0001	0.7487	<0.0001	0.0141	<0.0001	<0.0001
IR90	<0.0001	<0.0001	<0.0001	<0.0001	0.0459	<0.0001	0.0001
IR180	0.0691	<0.0001	0.5467	<0.0001	0.1034	<0.0001	0.1439
ORA45	0.8296	<0.0001	0.5817	<0.0001	<0.0001	<0.0001	<0.0001
ORA90	0.3560	<0.0001	0.0026	<0.0001	0.3077	<0.0001	0.1038
ORA180	0.0006	<0.0001	0.0004	<0.0001	0.8802	<0.0001	0.9288

Soil, SSC, and the interaction between soil and SSC were found to have a significant effect on sensor responses, P< 0.0001. Water type only has a significant effect on BG90, IR90, and ORA180 signals when the significance level $\alpha = 0.01$ was used, indicating water type has a relatively small effect on the sensor signals and the sensor was capable of partially removing the influence of water color on SSC prediction.

2.3.7 Sensor design simplification

In order to avoid over-fitting in prediction models and allow a simpler sensor design, the "stepwise" procedure in SAS was used to determine the most useful predictors among the 9 signals (Appendix E). The prediction results for the calibration dataset and the two validation datasets using the simplified model were compared in Table 2.8. As a result, BG90, IR45, ORA45 and ORA180 were selected in the final model. With these signals, an R-square value of 0.8750 with a RMS error of 537.4 was achieved across all water and soil types. The simplified model had slightly lower R-square values and slightly larger RMS errors compared to the model including all nine signals.

Table 2.8 Result comparison between the combined model (9 predictors) and the simplified model (4 predictors).

Dataset	Calibration		Validation 1		Validation 2	
	Combined model	Simplified model	Combined model	Simplified model	Combined model	Simplified model
R-square value	0.8845	0.8823	0.8536	0.8563	0.8736	0.8735
RMS error (mg/L)	481.91	484.62	544.92	534.05	504.82	484.62

Based on the statistical analysis, the optical sediment sensor was simplified from a "three-ring" design to a "two-ring" design (Figure 2.24).

(a)   (b)
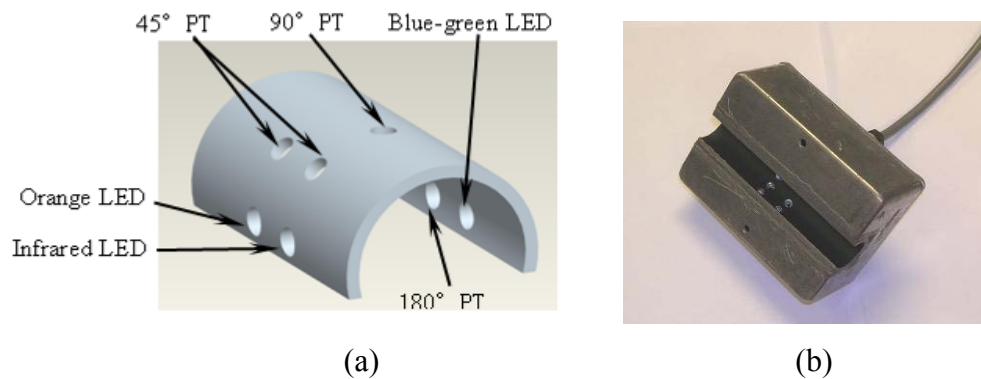
Figure 2.24 The simplified two-ring design. (a) 3-D view of the simplified design; (b) Waterproof package of the simplified design.

2.3.8 Outdoor experiments

A SAS program was used to evaluate the effectiveness of the light modulation in the outdoor experiment (Appendix F). Results are given in Figures 2.25-2.27. From Figures 2.25a, 2.26a, and 2.27a, it can be seen that signals for all four phototransistors increased with ambient light. However, when the relative light index "I_r" was used, the effect of ambient light intensity was basically eliminated (Figure 2.25b. 2.26b, and 2.27b). This result demonstrated the effectiveness of the light modulation in reducing the impact of ambient light on sensor measurement.
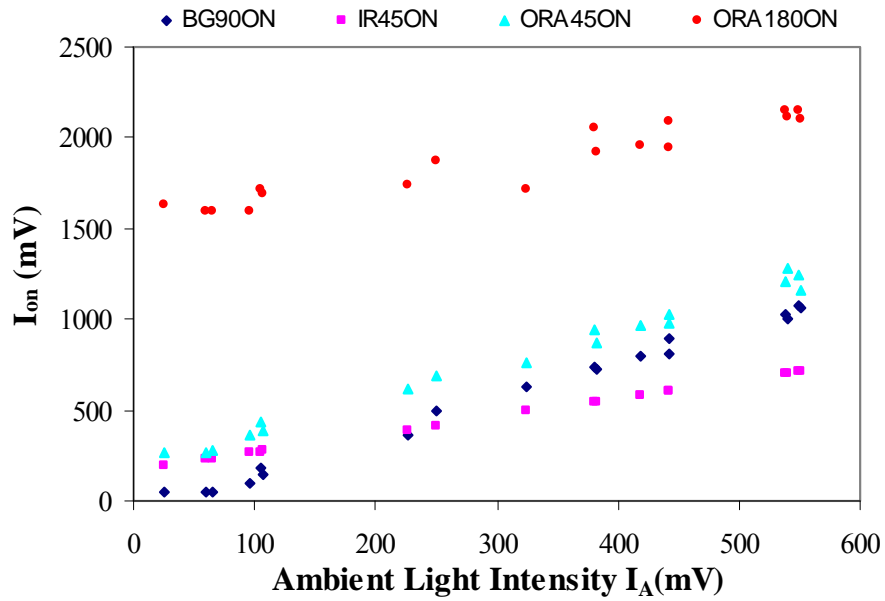
(a)
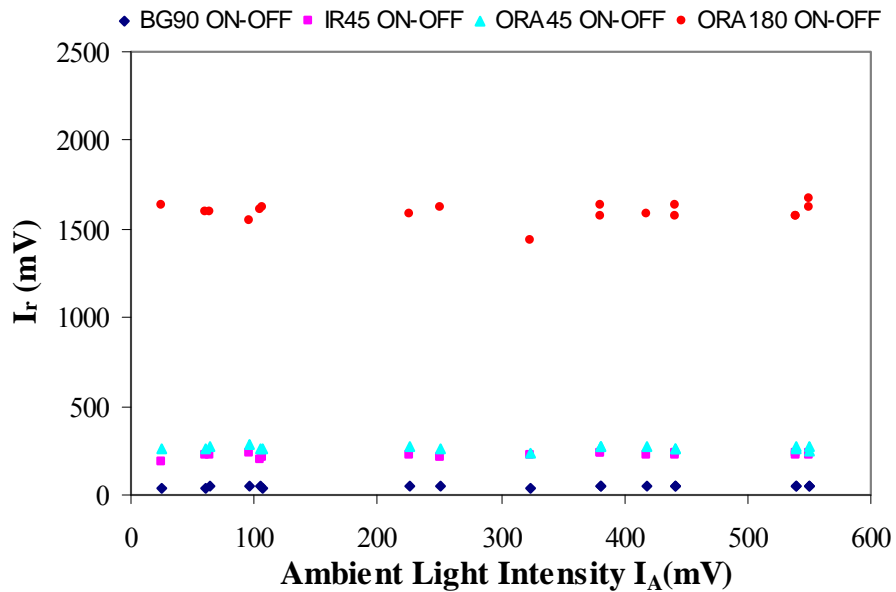
(b)

Figure 2.25 Comparison between non-modulated and modulated signals at concentration 200mg/L: (a) signals without light modulation; (b) signals with light modulation.
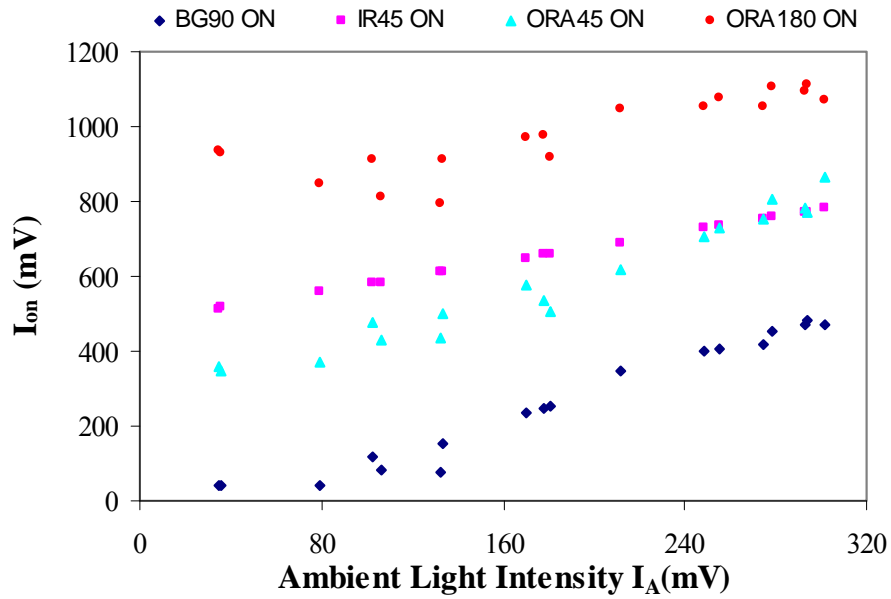
(a)
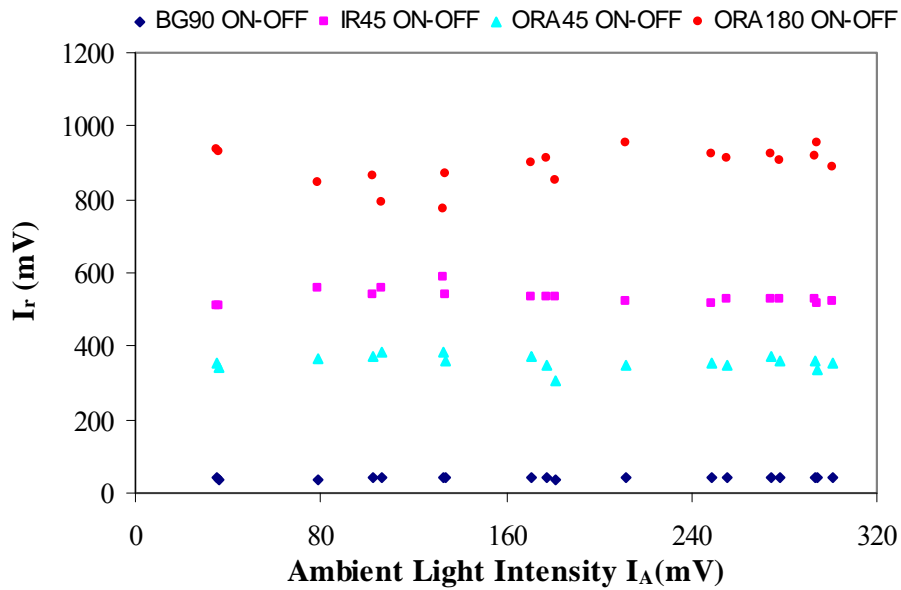
(b)

Figure 2.26 Comparison between non-modulated and modulated signals at concentration 1200mg/L: (a) signals without light modulation; (b) signals with light modulation.

.
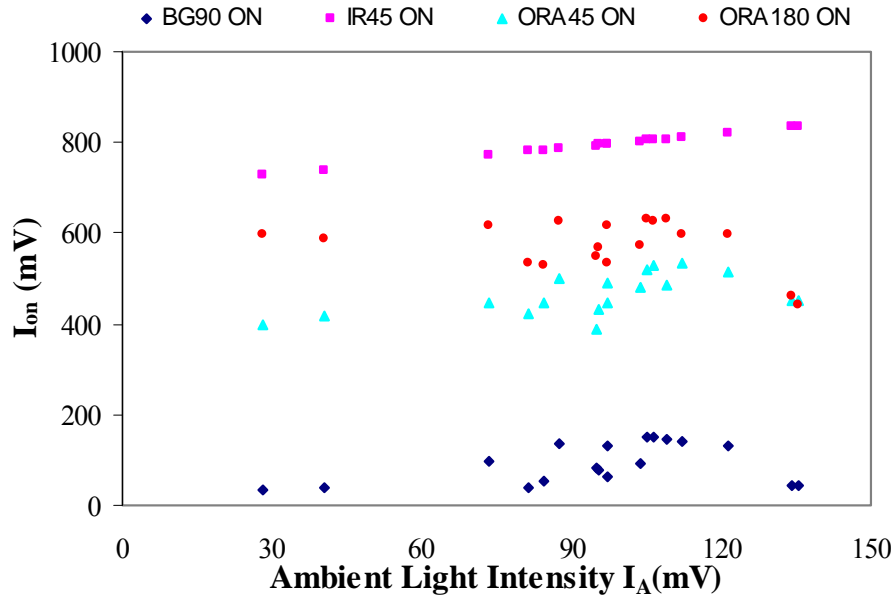
(a)
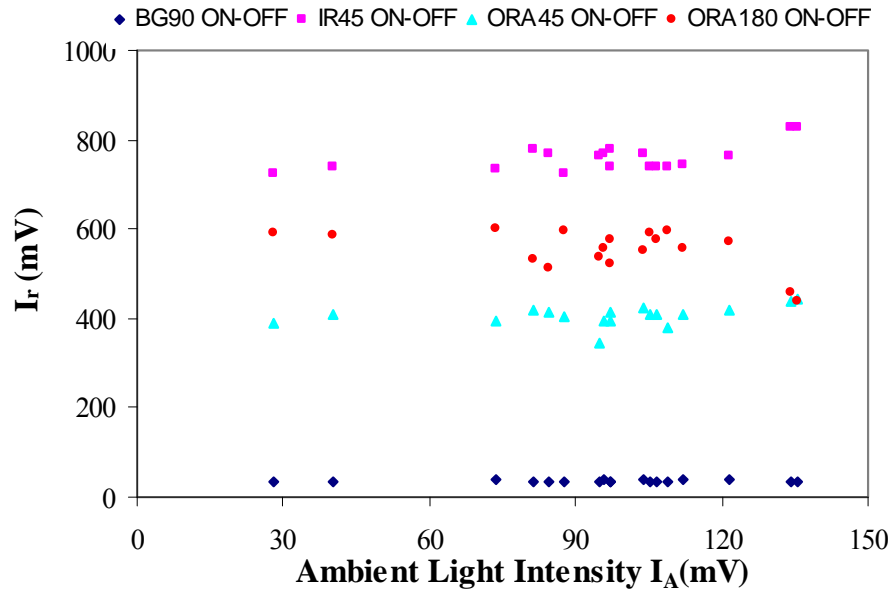
(b)

Figure 2.27 Comparison between non-modulated and modulated signals at concentration 200mg/L. (a) Signals without light modulation; (b) Signals with light modulation.

.

The light modulation algorithm resulted in accurate concentration measurement under variable, outdoor light conditions. Table 2.9 shows that, for the calibration and validation data sets, which were randomly selected from 18 tests conducted at different times in the day over a two-week periods, all the prediction models achieved R-square values of higher than 0.99. Figures 2.28 and 2.29 give comparisons between the predicted and actual concentrations for the calibration and validation datasets, respectively. Good predictions were achieved for the calibration and both validation datasets.

Table 2.9 R-square values and RM errors for the outdoor experiment.

Dataset	Calibration	Validation 1	Validation 2
R-square value	0.9954	0.9992	0.9924
RMS error (mg/L)	181.12	220.41	249.95
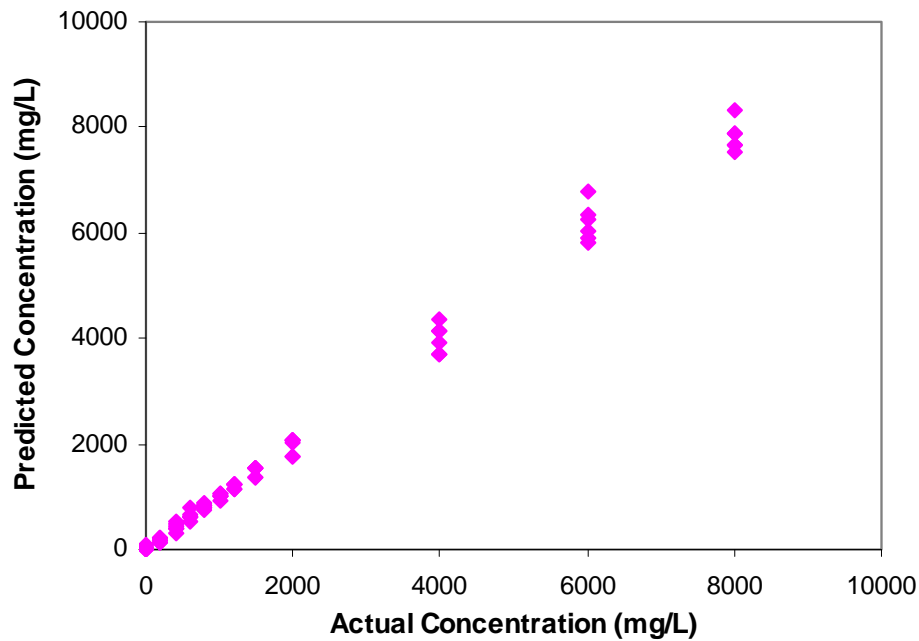
Figure 2.28 Predicted vs. actual SSC for the calibration data set in the outdoor experiment.
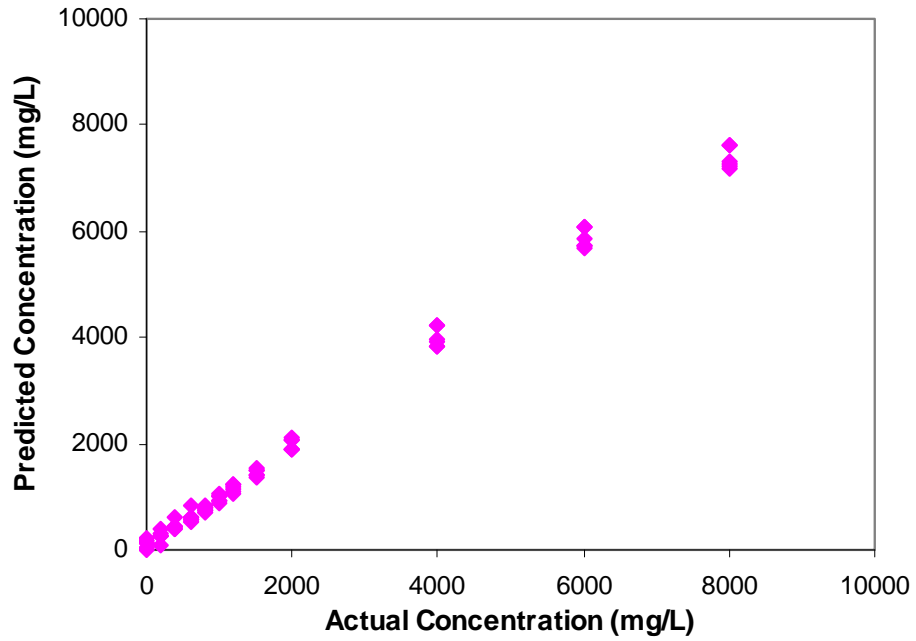
(a)
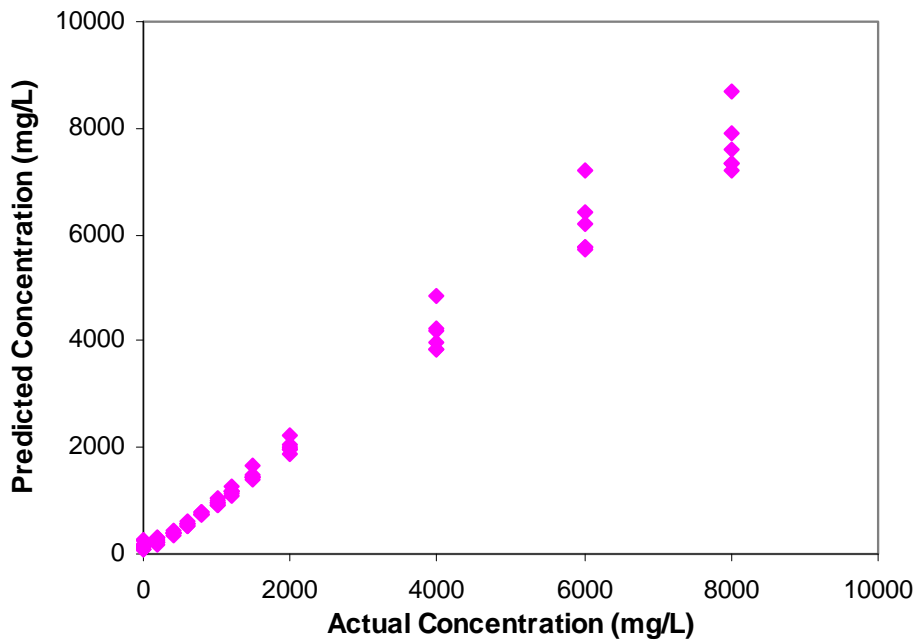
(b)

Figure 2.29 Predicted vs. actual SSC for the validation data sets in the outdoor experiment: (a) validation 1; (b) validation 2.

2.4 Conclusions

SSC sensor developed in this study was designed to measure soil sediment concentrations in water. Statistical analysis indicated a significant effect of soil texture on SSC measurement, $P<0.0001$, whereas water type has a relatively small effect on the sensor performance.

Multiple regression models were developed for individual soil types to predict SSC. R-square values of higher than 0.99 were achieved for sandy loam1, sandy loam2, loam, clay loam and silty clay loam, indicating that the influence of water color on measurement accuracy was almost completely eliminated for these soil texture types. When all five soil types were combined, the R-square value was reduced to 0.8845.

When multiple regression models for SSC measurement were established for individual water types, R-square values of 0.9111, 0.9245, 0.9002, and 0.8959 were achieved for distilled Water, Wildcat Creek Water, Tuttle Creek Water and Three-Mile Creek Water, respectively. When all four water types and five soil textures were combined, the R-square value was slightly reduced to 0.8845, indicating that water color had relatively limited impact on SSC measurement accuracy.

Neural-network models were developed to predict SSC using the sensor data. R-square values of 0.9961, 0.9670, and 0.9476, were achieved for the calibration and two validation datasets, respectively, indicating that the neural-network models can further remove the influence of soil texture type on SSC measurement and provide higher accuracy for SSC measurement.

In order to avoid over-fitting in prediction models and allow a simpler sensor design, a stepwise regression analysis was conducted to select from the nine optical signals the ones that were more effective in measuring SSC. The final model kept all three color LEDs and reduced the number of phototransistors from nine to four, which resulted in a simpler and more feasible design for the sensor. Based on this analysis, the optical sediment sensor was simplified from a "three-ring" design to a "two-ring" design.

An outdoor experiment demonstrated the effectiveness of light modulation and a relative light index of "I_r" in reducing the impact of ambient light, especially the sunlight, on SSC measurement. For a specific SSC, the relative light index maintained a relatively stable level when the ambient light varied significantly.

2.5 Acknowledgements

2.6 References

Agrawal, Y. C., and H. C. Pottsmith. 2000. Instruments for particle size and settling velocity observations in sediment transport. *Marine Geology* 168(1): 89-114.

Agrawal, Y. C., and H. C. Pottsmith. 2003. Laser diffraction sensors measure concentration and size distribution of suspended sediment. Available at: www.comm-tec.com/Library/Technical_Papers/Various/cool/p12Agrawal_Pottsmith.pdf. Accessed 1 March 2009.

APHA (American Public Health Association), AWWA (American Water Works Association), and WEF (Water Environment Federation). 1998. Standard Methods for the Examination of Water and Wastewater. 20th edition. Washington, DC: APHA.

Burkhead, N. M., and H. L. Jelks. 2001. Effects of suspended sediment on the reproductive success of the tricolor shiner, a crevice-spawning minnow. Transactions of the American *Fisheries Society* 130(5): 959-968.

Buttmann, M. 2001. Suspended solids measurement as reliable process control. In *ISA TECH EXPO Technology Update Conference Proceedings*, 413(1): 563-572. Houston, TX: Instrument Society of America.

Cochrane, T. A., L. D. Norton, C. Castro-Filho, J. H. Caviglione. 2004. Development of a river sediment transport monitoring system for large reservoirs. *Applied Engineering in Agriculture* 20(6):771-781.

Daraigan, S.G., M. Z. Matjafri, K. Abdullah, A. Abdul-Aziz, A. A. Tajuddin. 2005. A simple instrument for measuring total suspended solids in polluted marine waters. In *Proceedings of 2005 Asian Conference on Sensors and the International Conference on New Techniques in Pharmaceutical and Biomedical Research*, 219-221. New York, NY: IEEE.

Daraigan, S. G., M. Z. Matjafri, K. Abdullah, L. H. San, W. C. Jeng. 2006. Multi-spectral optical sensor based on light scattering for measuring total suspended solids. In *Proceedings of SPIE - The International Society for Optical Engineering* 6201, 62010W-1-62010W-6. Bellingham, WA: SPIE.

Davies-Colley, R. J., and D. G. Smith. 2001. Turbidity, suspended sediment, and water clarity: A review. *Journal of the American Water Resources Association* 37(5): 1085-1101.

Doxaran, D.; Froidefond, J.M.; Castaing, P. 2003. Remote-sensing reflectance of turbid sediment-dominated waters. Reduction of sediment type variations and changing illumination conditions effects by use of reflectance ratios. *Applied Optics* 42(15): 2623-2634.

EPA. 1999. Guidance manual for compliance with the interim enhanced surface water treatment rule: Turbidity provisions. Washington, D.C.: United States Environmental Protection Agency.

Gao, P., G.B. Pasternack, K.M. Bali, and W.W. Wallender. 2008. Estimating suspended sediment concentration using turbidity in an irrigation-dominated southeastern California watershed. *Journal of Irrigation and Drainage Engineering-ASCE* 134(2): 250-259.

Gartner, J.W. 2004. Estimating suspended solids concentrations from backscatter intensity measured by acoustic Doppler current profiler in San Francisco Bay, California. *Marine Geology* 211(304): 169-187.

Goldberg, M. C., K. M. Cunningham, and E. R. Weiner. 1987. Suspended sediment sensor. U.S. Patent No. 4696571.

Gray, J.R., T.S. Melis, E. Patino, M.C. Larsen, D.J. Topping, P.P. Rasmussen, and C. Figueroa-Alamo. 2009. U.S. Geological Survey Research on Surrogate Measurements for Suspended Sediment. Available at www.tucson.ars.ag.gov/icrw/Proceedings/Gray.pdf. Accessed 6 June 2009.

Gregory, J., and D. W. Nelson. 1986. Monitoring of aggregates in flowing suspensions. *Colloids and Surfaces A: Physicochemical and Engineering Aspects* 18(2): 175-188.

Hay, A.E., and J. Sheng. 1992. Vertical profiles of suspended sand concentration and size from multifrequency acoustic backscatter. *Journal of Geophysical Research* 97(c10): 15661-15677.

Kineke, G.C., R. W. Sternberg. 1992. Measurements of high concentration suspended sediments using the optical backscatterance sensor. *Marine Geology* 108(3-4): 253-258.

Li, R., Y.J. Kaufman, B. Gao, and C.O. Davis. 2003. Remote sensing of suspended sediment and shallow coastal waters. *IEEE Transactions on Geoscience and Remote Sensing* 41(3): 559-565.

Li, X, T. Lei, W. Wang, Q. Xu, and J. Zhao. 2005. Capacitance Sensors for Measuring Suspended Sediment Concentration. *Catena* 60: 227-237

Maa, J. P.-Y. 1988. Laboratory measurements of instantaneous sediment concentration under waves. *IEEE Journal of Oceanic Engineering* 13(4):299-302.

Marquis, P. 2005. Turbidity and suspended sediment as measures of water quality. *Watershed Management Bulletin* 9(1): 21-23.

McKee, L. J., N. K. Ganju, and D. H. Schoellhamer. 2006. Estimates of suspended sediment entering San Francisco Bay from the Sacramento and San Joaquin Delta, San Francisco Bay, California. *Journal of Hydrology* 323(1): 335-352.

Melis, T. S., D. J. Topping, and D. M. Rubin. 2002. Testing laser-based sensors for continuous in situ monitoring of suspended sediment in the Colorado River, Arizona. In *Proceedings of the Oslo Workshop (Erosion and Sediment Transport Measurement in Rivers: Technological and Methodological Advances)*, 21-27. Oslo, Norway: IAHS press.

Meral R. 2008. Laboratory evaluation of acoustic backscatter and LISST methods for measurements of suspended sediments. *Sensors* 8(2):979-993.

Nilsson, M. B., E. Dabakk, T. Korsman, and I. Renberg. 1996. Quantifying relationships between near-infrared reflectance spectra of lake sediments and water chemistry. *Environmental Science and Technology* 30(8): 2586-2590.

Riley, S. J. 1998. The sediment concentration-turbidity relation: its value in monitoring at Ranger Uranium Mine, Northern Territory, Australia. *Catena* 32(1): 1-14.

Ruhl, C.A., D.H. Schoellhamer, R.P. Stumpf, and C.L. Lindsay. 2001. Combined use of remote sensing and continuous monitoring to analyze the variability of suspended-sediment concentrations in San Francisco Bay, California. *Estuarine Coastal and Shelf Science* 53(6): 801-812.

Sadar, M. 2002. Turbidity Instrumentation – An Overview of Today's Available Technology. Reston, VA: USGS, Office of Surface Water. Available at: water.usgs.gov/osw/techniques/TSS/sadar.pdf. Accessed 20 March 2009.

Sadar, M. J., and T. L. Engelhardt. 1993. Turbidity and Suspended Solids: Determining Correlation of Nephelometric Turbidity Measurement to Suspended Solids in Industrial Samples. Available at www.hach.com/fmmimghach?/CODE%3ATURBIDITYANDSUSPENDE1574|1. Accessed 23 March 2009.

Schoellhamer, David H.; Wright, Scott A.. 2003. Continuous measurement of suspended-sediment discharge in rivers by use of optical backscatterance sensors. *IAHS-AISH Publication* (283): 28-36.

Sherwood, C.R., D. Coats, and B. Walls. 1989. Current and suspended sediment measurements on the central california continental shelf. In *OCEANS '89. Proceedings*, 320-325. New York, NY: IEEE.

Stoll, Q. M. 2004. Design of a real-time, optical sediment concentration sensor. MS thesis. Manhattan, Kansas: Kansas State University, Department of Biological and Agricultural Engineering.

Thorne, P. D., and D. M. Hanes. 2002. A review of acoustic measurement of small-scale sediment processes. *Continental Shelf Research* 22(4): 603-632.

Wei, J., X. Shi, X. Fang, and W. Zhang. 2007. Measurements of suspended particulate matter with laser in-situ scattering and transmissometry in the Jiaozhou Bay in China. *ACTA Ocenologica Sinica* 26(1): 55-65.

Wren, D. G., B. D. Barkdoll, R. A. Kuhnle and R. W. Derrow. 2000. Field techniques for suspended-sediment measurement. *Journal of Hydraulic Engineering* 126(2): 97-104.

Wren, D.G., and R.A. Kuhnle. 2002. Surrogate Techniques for Suspended-Sediment Measurement. Available at water.usgs.gov/osw/techniques/TSS/wren.pdf. Accessed 5 June 2009.

CHAPTER 3 - LONG-TERM FIELD EXPERIMENT OF A REAL TIME, OPTICAL SSC SENSOR

Abstract. Monitoring SSC in field settings is fundamental to determining sediment transportation for soil erosion research and soil/water conservation practices. Optical sensors have been proved to be powerful tools to measure SSC in a variety of environments in water flows. An optical sediment-concentration sensor was developed to allow long-term, real-time monitoring of sediment concentration. Field experiments were conducted at various sites to evaluate the sensor performance, the effect of fouling on sensor lenses, and the effect of temperature on the measurement. Results at two low-water crossings in Kansas and Georgia were analyzed and discussed. Methods of removing the fouling effect through data correction were also developed. Results indicated that the designed optical SSC sensor was capable of providing rapid response to SSC fluctuations in water flow. Temperature of water body has small impact on SSC measurement.

Keywords. Sediment, Optical sensor, Water quality, Low-water crossing, Fouling.

3.1 Literature Review

Optical sediment sensors have been studied by many researchers (McKee et al., 2006; Kineke and Sternberg, 1992; Sherwood et al., 1989). In situ optical sensors that measure backscattered or transmitted light caused by suspended sediment passing between the light source and detector have shown remarkable ability to measure SSC in a variety of environments in water (Downing ea al, 1981; Green and Boon, 1993). Optical measurement is relatively simple and inexpensive. However, several factors, such as fouling, were found to have impact on SSC measurement accuracy for long term monitoring in field settings (Sherwood et al., 1989).

An optical sensor that measures transmitted light is very sensitive to the existence of soil particles at low sediment concentration range and insensitive at high concentration range, whereas, an optical backscatter sensor has the opposite characteristics – it is relatively less sensitive at low concentration range but has a wide concentration measurement range. An optical SSC sensor was designed by Stoll (2004) for measuring pure suspended sediment in water integrated backscatter and transmittance measurements into one sensor frame. This design

overcame the above disadvantages and strengthened the sensor performance. The sensor used light emitting diodes (LED) as the light sources and silicon NPN phototransistors as the light detectors. The advantage of using LEDs is its relatively low power consumption and ability to be modulated electronically at rapid rates (Maffione and Dana, 1997). Laboratory experiments have proved that using light sources of different wavelengths in the visible and infrared wavebands can help reduce the effect of water color on sediment concentration measurement (Stoll, 2004).

3.2 Objectives

In order to evaluate the sensor performance on long-term SSC monitoring, field experiments were conducted at several experiment sites. Results of the experiments conducted at two low-water stream crossings (LWSC) in Kansas and Georgia were discussed in this dissertation. Effects of temperature and fouling on the SSC measurement were studied. Methods of correcting the fouling effect through data analysis were also discussed as well.

3.3 Methodology

3.3.1 Experiment sites

SSC sensors with simplified, two-ring design were used in the field study. Field experiments were conducted at four sites (Table 3.1).

Table 3.1 Experiment sites and time period.

Experiment site	Time period
Fort Riley, Kansas	August 16, 2005 ~ April 12, 2006
Fort Benning, Georgia	June 4, 2006 ~ February 1, 2007
Little Kitten Creek, Manhattan, Kansas	August 25, 2006 ~ April 29, 2009
Mission, Kansas	August 17, 2007 ~ August 19, 2008

At the Fort Riley site, there was no water in the creek during the test period. At the Mission site, insufficient data was available for analysis. Only data from Little Kitten Creek, Manhattan, Kansas and Fort Benning, Georgia were discussed in this chapter.

3.3.2 Sensor installation

The optical sensors have been deployed in various environments to measure sediment concentration. In order to avoid possible damages caused by log collision or high water flow during severe weather conditions, three types of mounting methods were tested at the experiment sites based on local conditions.

3.3.2.1 L-shaped metal plate

Two sensors were installed in Mission, Kansas to measure sediment concentrations in storm drainage water. A flat aluminum plate was bended to an "L" shape (90° angle). The short leg of the plate was anchored to the concrete base. The sensor was mounted to the long leg of the plate (Figure 3.1). This mounting method provided a simple solution for concrete surface. It also has the minimum disruption to surrounding environment without installing T-post in downtown area of the city of Mission.

Figure 3.1 Sensor mounted using an L-shaped aluminum plate at Mission, Kansas.

3.3.2.2 Galvanized steel pipe

Figure 3.2 gave a mounting solution to secure the sensor and protect the electric cables. A 1-1/4" galvanized steel pipe was driven into the ground. Three sensors were mounted to the pipe by U-bolts at three different heights to monitor the vertical profile of SSC. Sensor cables were enclosed in the galvanized steel pipe and PVC pipe to protect the cables from animal chewing.

Figure 3.2 Sensors were mounting using a galvanized steel pipe at Fort Riley, Kansas.

Figure 3.3 shows a mounting method using a stand fabricated from a galvanized steel pipe with a concrete bottom. The sensor was mounted using U-bolts to the pipe. The concrete bottom can stand at the stream bed due to its heavy weight. The top of the steel pipe was tied to a T-post for secure mounting.
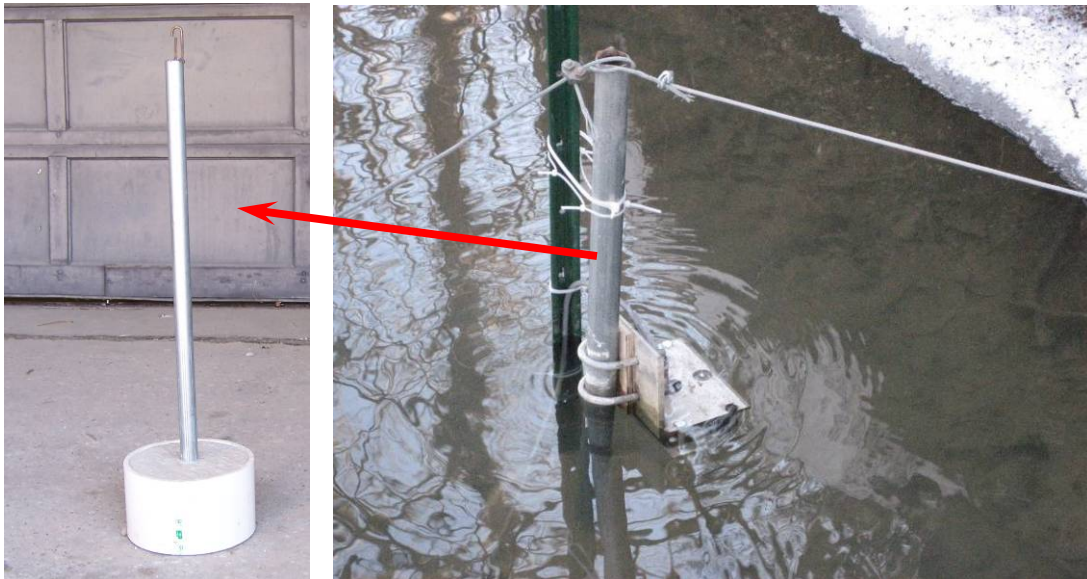
Figure 3.3 Sensor mounted using a galvanized steel pipe with a concrete bottom at Little Kitten Creek, Manhattan, Kansas.

3.3.2.3 T-post

The mounting method using a galvanized steel pipe with a concrete base (Figure 3.3) was replaced by heavy duty T-post mounting (Figure 3.4) at Little Kitten Creek, Manhattan, Kansas, due to the fact that the concrete base of the galvanized steel pipe was not driven into the stream bed and it was washed away by high speed water flow during heavy storms. Eliminating the galvanized pipe and directly using the T-post also simplify the mounting design. The sensor in Figure 3.4 was not covered by water because the photograph was taken during non-rain season.

Figure 3.4 Sensor was mounted using heavy duty metal stakes (green T-post) at Little Kitten Creek, Manhattan, Kansas.

Mounting method using PVC pipes and T-post shown in Figure 3.5 was proved to be feasible for installations in streams with water all the time. Two sensors were mounted to the PVC pipe at two different heights using U-bolts. Two U-bolts were also used to tie the sensor mounting unit to the T-post which was driven into the stream bed. The photograph shows the mounting method before the sensors were submerged into the water.

Figure 3.5 Sensors were mounted using PVC pipe and metal stakes (green T-post) at Fort Benning, Georgia.

3.3.3 Field setup of SSC monitoring system

3.3.3.1 Field setup at Little Kitten Creek, Manhattan, Kansas

The SSC measurement system at Little Kitten Creek in Manhattan, Kansas comprises an open-bottom optical sediment sensor, a signal conditioning circuit box, a CR10X datalogger manufactured by Campbell Scientific, Inc., and a 12 V deep cycle battery powered by a 15W solar panel manufactured by Brunton, Inc. The relative light index (I_r) was used to reduce the influence of ambient light on the measurement. A datalogger program developed using PC208W software (PC208W, 2000) was used to calibrate the sensor in the laboratory (Appendix G). Another datalogger program was developed using PC208W for the field experiment to control and take measurements every 10 seconds (Appendix H).

The sensor was installed in the mid-section of the creek, about 0.2 m above the creek bed to make sure it was submerged under water all the time. A 12 m-long cable that transmitted electrical current signals was enclosed in PVC pipes for protection. The PVC pipes were secured by steel bars that were driven into the creek bed and bank. A protection fence was built at the upstream side using metal stakes to protect the sensor from floating logs and other flotsam. The datalogger and the signal conditioning box were placed in a waterproof enclosure manufactured

by Campbell Scientific, Inc. (Figure 3.6b). The SSC measurement system was powered by a 12V deep cycle car battery, which was charged by a 15W solar panel.

<center>(a)</center> <center>(b)</center>

Figure 3.6 Little Kitten Creek site installation: a) Protection PVC pipe running from the creek to bank; b) waterproof enclosure that contains datalogger and the signal conditioning box.

Fluctuations in water body temperature potentially have adverse impacts on opto-electronic components and, therefore, cause errors in SSC measurement (Lawler and Brown, 1992; Orwin and Smart, 2005). In order to observe the temperature effect on optical sensor signals, a T-type thermocouple was enclosed in the PVC pipe along with the sensor cable. The measuring junction of the thermocouple wire was placed near the sensor to obtain an accurate temperature measurement. Datalogger was programmed to record temperature readings each time it took SSC measurement.

3.3.3.2 Field setup at Fort Benning, Georgia

A construction work at Fort Benning to "harden" a crossing site using articulated roadbed system (cable concrete) started on August 22, 2006, and was completed on October 22, 2006. Two SSC measurement systems and four optical sediment sensors continuously measured sediment concentrations at the site to study the effectiveness of the hardened structure on reducing soil erosion caused by military training. Each SSC measurement system comprises two SSC sensors, two signal conditioning circuit boxes, a CR10X datalogger manufactured by

<center>58</center>

Campbell Scientific, Inc., and a 12V deep cycle battery powered by a 15 W solar panel manufactured by Brunton, Inc (Figure 3.7). Dataloggers were programmed to control and take measurement every 1 minute. On each side of the creek, two sensors were installed about 30 m downstream of the crossing, with the "bottom" sensor about 0.1 m above the creek bed, and the top sensor about 0.25 m above the bottom sensor (Figure 3.5). Sensors were securely mounted with U-clamps and bolts on T-posts that were driven about 1 meter into the creek bed. Dataloggers were mounted in weatherproof enclosures. The 12V deep cycle batteries to power dataloggers were mounted on a wooden platform next to datalogger enclosures. The solar panel to charge the battery was mounted above the datalogger enclosure at a 45 degree angle to capture sunlight. Tree branches and foliage were removed from around the solar panels to ensure that sufficient sunlight would reach the solar panels. The measurement system on each bank was mounted sufficiently high to ensure that water levels would not submerge the data loggers, batteries, or solar panels when creek levels rose during storm events. Wiring from the sensors to the dataloggers was contained in PVC pipes running along the creek bottom. The PVC pipes were anchored to metal stakes driven securely into the creek bed with plastic wire ties to protect the cable from flotsam in the creek and from the current.

Figure 3.7 SSC measurement system installation at a LWSC in Fort Benning, Georgia.

3.3.4 Sensor calibration

Due to the variation of optical sensor signals caused by particle size and reflectivity, many researchers used different methods to calibrate their sediment sensors. Kineke and Sternberg (1992) used a pumping system to obtain water samples to calibrate their sensor in situ. Butt et al. (2002) investigated the possibility of calibrating sediment sensors in glycerol to avoid using complicated recirculation equipment for calibration since glycerol is a clear fluid with a higher viscosity than water. However, the conversion relationship between water and glycerol must be defined beforehand. More and more researchers calibrated their optical sediment sensors using the sediment taken from the bottom of the creek before the field installation, and by filtering water samples taken from the test site for laboratory calibration analysis after the field installation (Schoellhamer and Wright, 2003; Sherwood et al., 1989; Presto et al., 2006). Although it is quite difficult to obtain in situ water samples near the sensor, especially under severe weather conditions, taking water samples after the sensor was deployed provides an important check on the sensor performance (Downing, 1983).

The sensor calibration method used in this study included pre-calibration in the laboratory using the sediment from the bottom of the creek taken from the site before the field installation and post-calibration by collecting water samples close to the sensors after the field installation. The post-calibration was only conducted at Little Kitten Creek, Manhattan, Kansas during June 6, 2008 – January 11, 2009. This method involved filtering, drying and weighing process in laboratory to obtain real SSC values from water samples. Each grab sample was taken from the creek after manually cleaning the sensor lenses. The time when each water sample was taken was also recorded to find the corresponding sensor signals recorded at the same time. In the laboratory, water samples were filtered through 0.45 micron filters using a vacuum pump. SSC was calculated based on EPA method 160.2., adjusted by filtering the whole water-sediment mixture instead of only filtering a subset of the sample. All SSC data were used for sensor accuracy and signal stability analysis.

3.4 Results

Results from the field experiments at Little Kitten Creek, Manhattan, Kansas and Fort Benning, Georgia were discussed in the following sections.

3.4.1 Rapid response to SSC flux changes

The optical sediment sensor developed in this study was able to quickly respond to rapid, intermittent flushes of suspended sediment during storms. Figure 3.8 shows the sensor signals received during three storm events within a 31-hour period. Figure 3.9 shows the measured sediment concentrations. Rainfall data was provided by the NSF Long Term Ecological Research Program at Konza Prairie Biological Station. The station is 8 miles away from the experiment site.
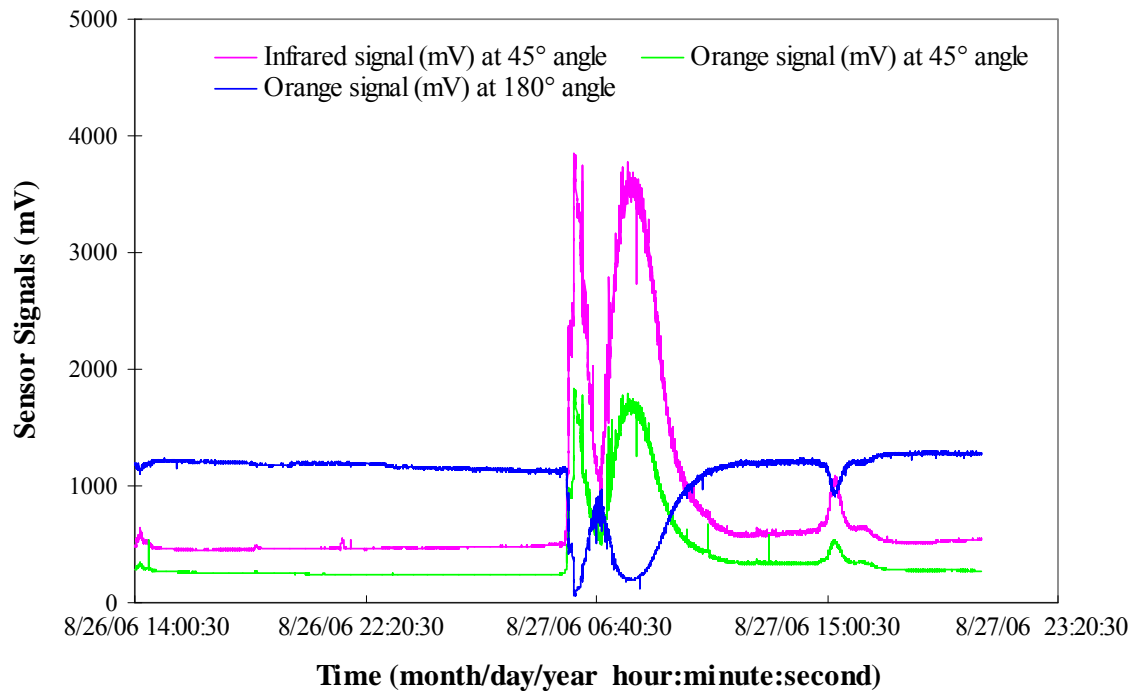
Figure 3.8 Sensor signals in three storm events recorded within a 31-hour period.
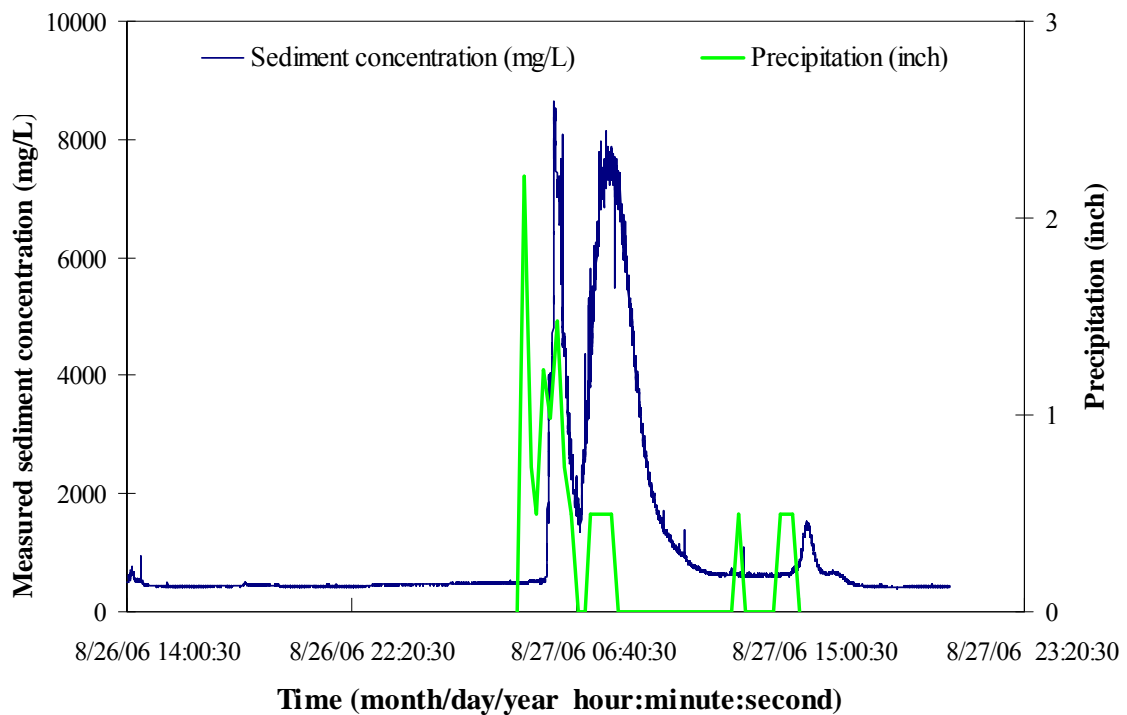
Figure 3.9 Measured SSC in three storm events recorded within a 31-hour period.

BG90 signal that represents scattered light detected by phototransistor at 90° degree from a blue-green LED was not shown in Figure 3.8. The gains of all signals (BG90, IR45, ORA45, and ORA180) were carefully adjusted in laboratory to meet two requirements: 1) signals should be within the measuring range of the datalogger under strong sunlight; 2) signals should be detectable under dark conditions. The adjustment of BG90 signal couldn't meet these requirements: when the gain was adjusted to avoid the signal from exceeding the range under strong sunlight, the signal would become too small to detect under dark conditions.

3.4.2 Fouling effect and correction

Fouling, including bio-fouling, on optical lenses has been a common problem for optical sensors exposed to various pollutants in water. Field experiments at Little Kitten Creek showed that fouling effect caused signal deterioration (Figure 3.10). This can be observed from the fact that, each time the sensor was manually cleaned, the signals went back to their original levels. Usually, fouling of the sensor lenses caused the transmitted signal to decrease and the

backscattered signal to increase. In order to maintain meaningful signals, the lenses need to be cleaned periodically.
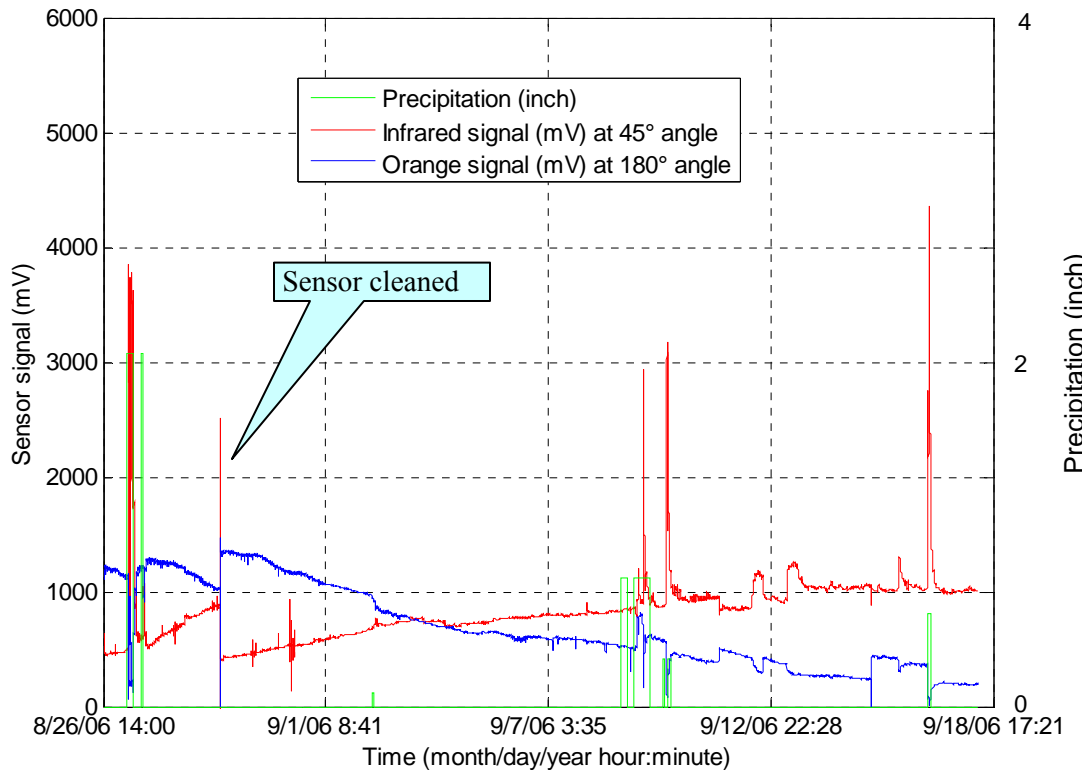
Figure 3.10 Signal deterioration due to fouling. Precipitation data source: www.weatherunderground.com.

During data post-processing, correction algorithms may be applied to restore the signals. In this study, a correction algorithm was developed by determining the fouling trend through a regression analysis on peak signal values taken during no-rain periods (Zhang et al., 2007). The fouling trend was then removed to restore the sensor signals. A MATLAB (MATLAB, 2006) program was developed to complete the signal correction (Appendix I). IR45 signal corrected using this algorithm and sediment concentration calculated using the corrected signal are shown in Figure 3.11 and 3.12, respectively.
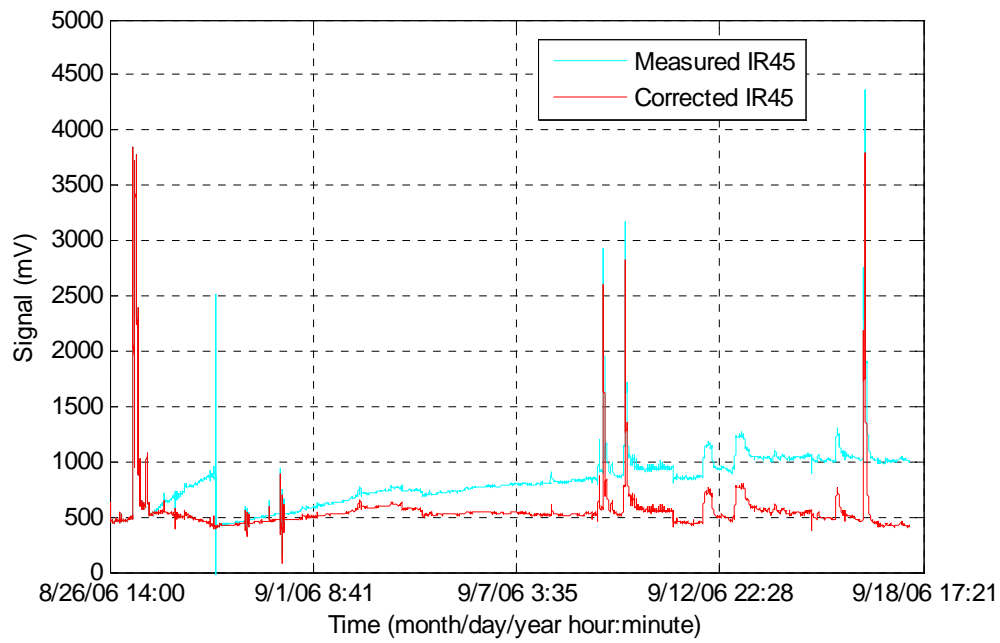
Figure 3.11 Backscattered signal (IR45) correction result.
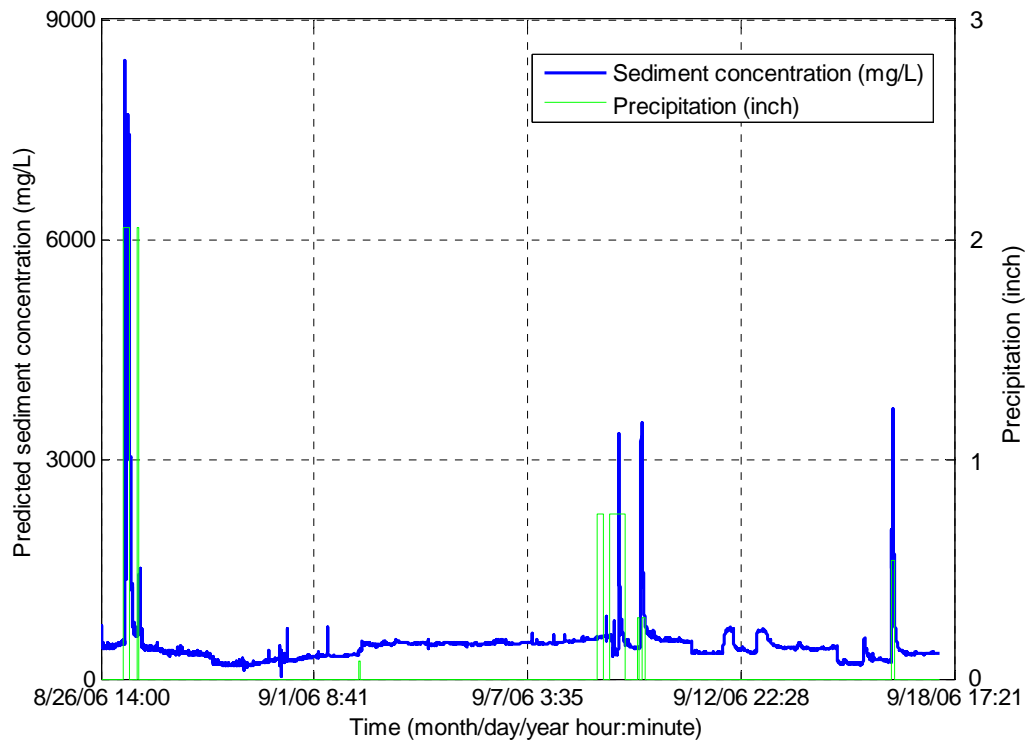
Figure 3.12 Sediment concentration data restored using the correction algorithm.

Precipitation data source: www.weatherunderground.com.

At Fort Benning site, the fouling effect is corrected by the same algorithm. Since fouling for individual sensors differed greatly, the regression models of fouling trend and the corresponding fouling correction were conducted based on data from individual sensors.

It can be observed that from Figure 3.13, the signals acquired at Fort Benning site during the winter time, especially in January, 2007, didn't show a significant fouling effect. This observation is related to the fact that, during winter, plant and animal growth and activities slow down significantly. Thus, it can probably be concluded that the fouling problem observed on the sensors signals is mainly a bio-fouling problem. The predicted sediment concentration based on the corrected sensor signals is shown in Figure 3.14.
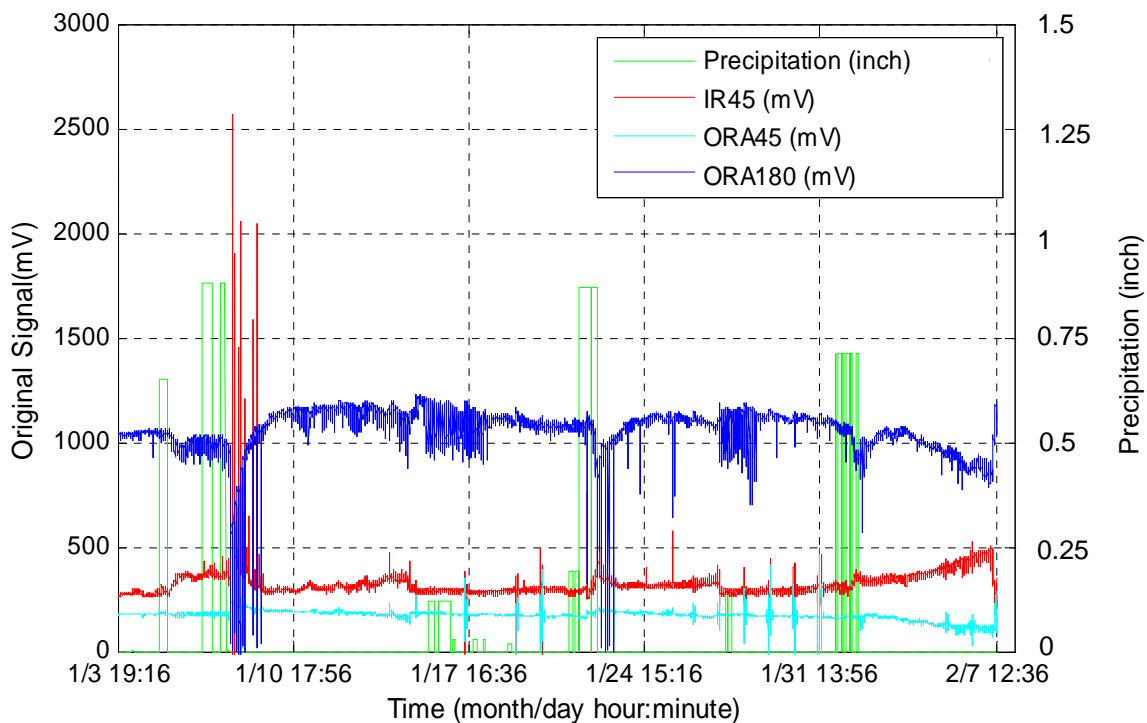
Figure 3.13 Unprocessed signals measured in January, 2007. Precipitation data source: www.weatherunderground.com.
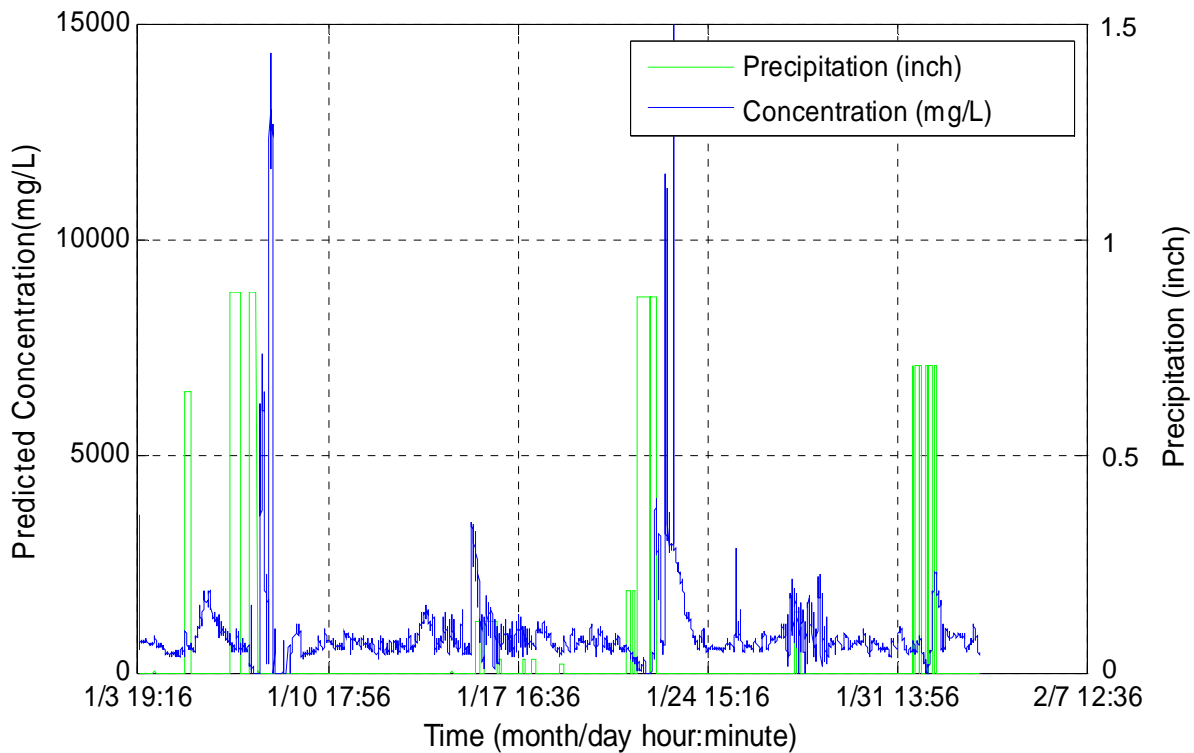
**Figure 3.14 Sediment concentration calculated by the corrected sensor signals.
Precipitation data source: www.weatherunderground.com.**

3.4.3 Clogging effect and correction

Two types of SSC sensor were used in the field experiment at Fort Benning: a closed-bottom design (Figure 3.15a) and an open-bottom design (Figure 3.15b).

a)   b)
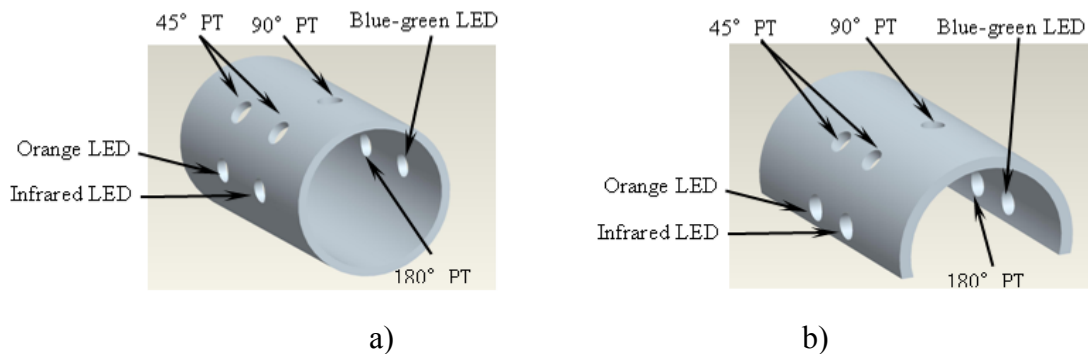
**Figure 3.15 Optical SSC sensor design used in field experiments. PT stands for
phototransistor. a) 3-D view of the closed-bottom design; b) 3-D view of the open-bottom
design.**

It was found that the closed-bottom design caused severe clogging problems. For the open-bottom design, the clogging problem improved significantly because there was no place for sediment to settle down at the bottom. A correction algorithm was applied to the data recorded by closed-bottom sensors in order to recover clogged signals. The MATLAB program (MATLAB, 2006) developed to correct the fouling effects also included corrections for clogging (Appendix I). The basic assumption for the clogging correction was that there should not be sudden rises or falls in the light signal unless materials covering the lenses are washed away within a short period of time. Based on this assumption, the clogging correction was done by removing sustained steep rises in the signals using a set of carefully selected thresholds, including 1) a threshold for the width of a moving-average window that smoothed the raw signals, 2) a signal rise/fall contrast threshold that detects the occurrence of sudden signal rises and falls, and 3) a threshold for the width of a moving-average window that smoothed the clogging-corrected signals as a preparation for a regression analysis that determines the fouling trends. The signal rise/fall contrast, C, was defined as follows.

$$C = \frac{S_{up}}{S_{down}}$$
(3.1)

where

S_{up} - slope for the trend when the signal is going up;

S_{down} - slope for the trend when the signal is going down.

Lower threshold values were used for the closed-bottom design because clogging occurred more frequently on the closed-bottom sensors. Using an orange signal measured at 180° angle (ORA180) as an example, Figure 3.16 compares the signals before and after clogging and fouling corrections.
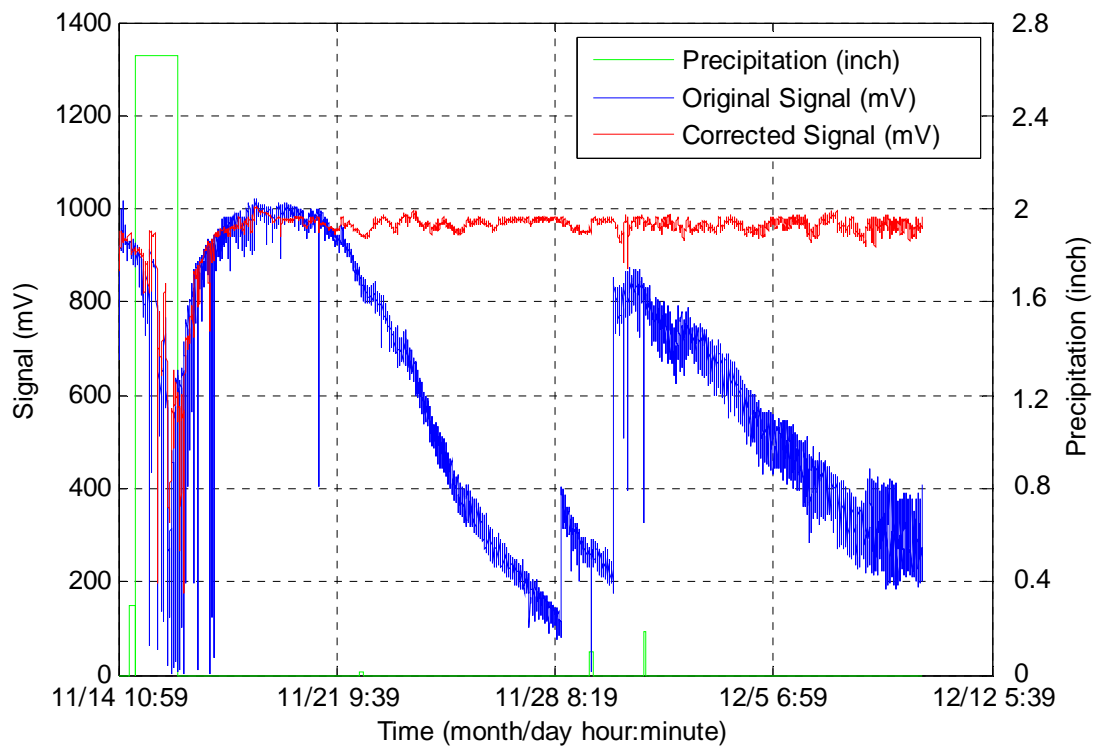
Figure 3.16 Original signal and signal corrected for clogging and fouling. Precipitation data source: www.weatherunderground.com.

From the data acquired at Fort Benning, it is clear that the open-bottom design provided higher-quality signals than the closed-bottom design, mainly because of reduced clogging problem.

Although during data post-processing, correction algorithms may be applied to restore the signals, an active lens cleaning method should be explored in the future to more effectively reduce the fouling problem.

3.4.4 Temperature effect on sensor performance

A total 270 grab water samples were manually taken from Little Kitten Creek, Manhattan, Kansas, during the period of June, 2008 to January, 2009. The lenses of the sensor were cleaned using a piece of soft cloth before each water sample was taken. 12 water samples were excluded as outliers (Table 3.2). The remaining 258 water samples were collected under various weather conditions within a temperature range of 1.6-22.4 $^{\circ}$C. The SSC of the water samples obtained

from laboratory weighting and drying process ranges from 0 – 4382 mg/L and the distribution was listed in Table 3.3.

Table 3.2 Outliers excluded from grab water samples.

Sampled Date and Time	Dried SSC (mg/L)	Reason for being outlier
00:19, Jun. 12, 2008	1719.04	Suspicious sampling time: no recorded sampling activities to match
00:19, Jun. 12, 2008	1764.48	
21:25, Jun. 24, 2008	989.18	Suspicious sampling time: no recorded rain event to match high SSC
21:25, Jun. 24, 2008	994.24	
21:44:30, Jun. 24, 2008	914.74	
21:44:30, Jun. 24, 2008	914.62	
10:00, Sep. 12, 2008	1257.96	Inaccurate sampling time and location
10:00, Sep. 12, 2008	1299.33	
11:29, Nov. 6, 2008	4.52	ORA45 signal was out of range due to strong sunlight
11:29, Nov. 6, 2008	6.55	
11:38, Nov. 6, 2008	2.11	
11:38, Nov. 6, 2008	2.79	

Table 3.3 The SSC distribution of all 258 grab water samples.

Dried SSC Range (mg/L)	Quantity
< 10	77 samples
10 ~ 100	61 samples
100 ~ 500	102 samples
500 ~ 1000	6 samples
>1000	12 samples

Figure 3.17 shows the temperature effect on the three output signals. Seventy-seven water samples with SSC concentration less than 10mg/L were used in order to exclude the effect of suspended sediment concentration on sensor signals. Regression models were established for all

69

three output signals to determine the temperature effect. Results showed that the temperature coefficients for ORA180, ORA45, and IR45 signals were 5.53mV/$^{\circ}$C, 3.74mV/$^{\circ}$C, and 3.36mV/$^{\circ}$C, respectively.
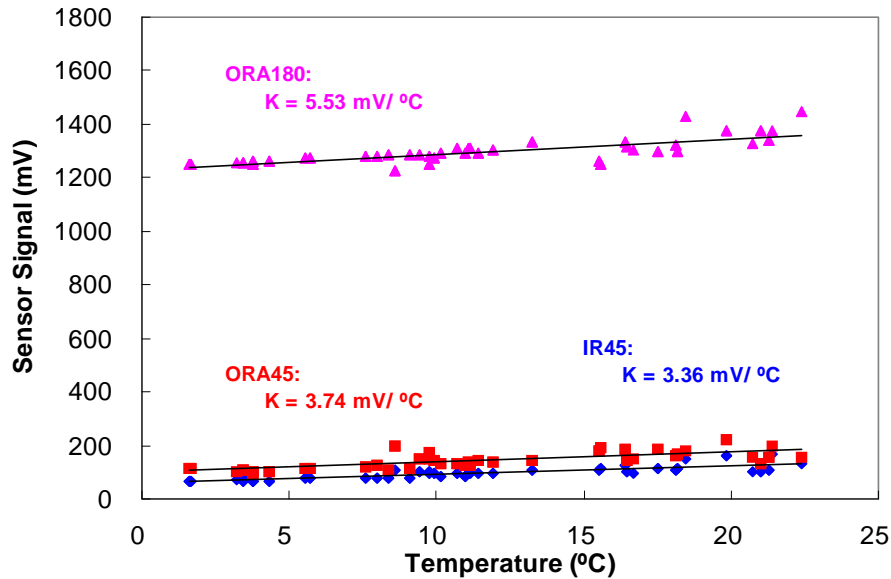
Figure 3.17 Temperature effect on sensor signals (K is temperature coefficient).

Temperature compensation based on these regression models was applied to SSC prediction analysis and the results before and after temperature compensation were shown in Figure 3.18 (SSC > 500 mg/L) and 3.19 (SSC < 500 mg/L). The R-square values for predicting SSC before and after temperature compensation were also compared for actual SSC higher and lower than 500mg/L, respectively. The results indicated that 1) R-square value is 0.9776 before temperature compensation and 0.9773 after compensation for SSC higher than 500mg/L; 2) R square value is 0.9015 before temperature compensation and 0.9057 after compensation for SSC lower than 500mg/L.
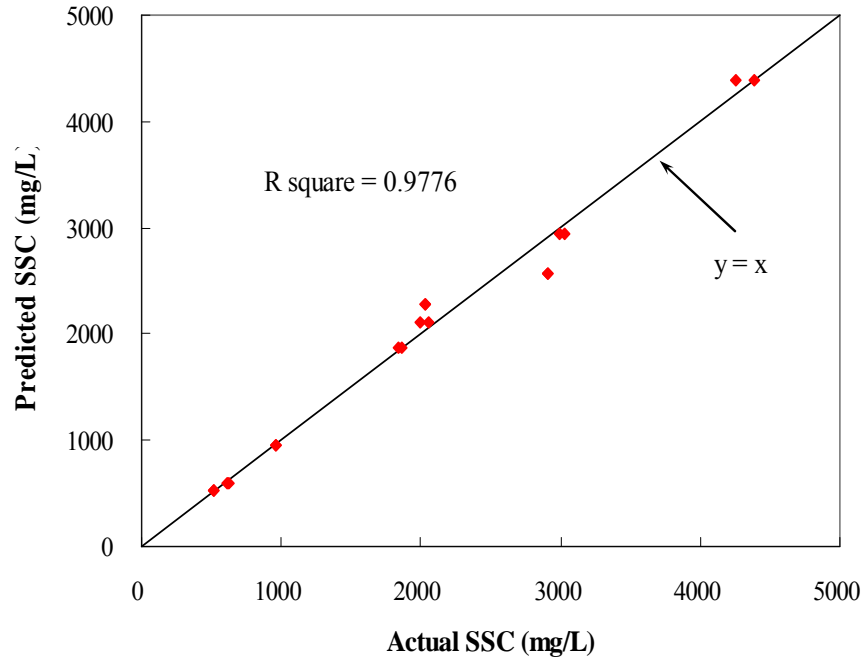
(a)
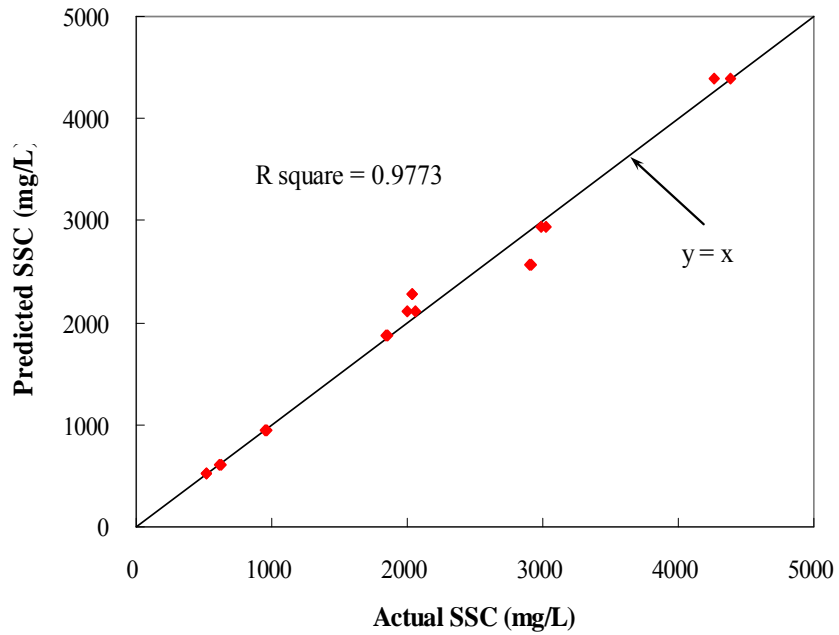
(b)

Figure 3.18 SSC prediction before and after temperature compensation (SSC> 500mg/L): a) before temperature compensation; b) after temperature compensation.
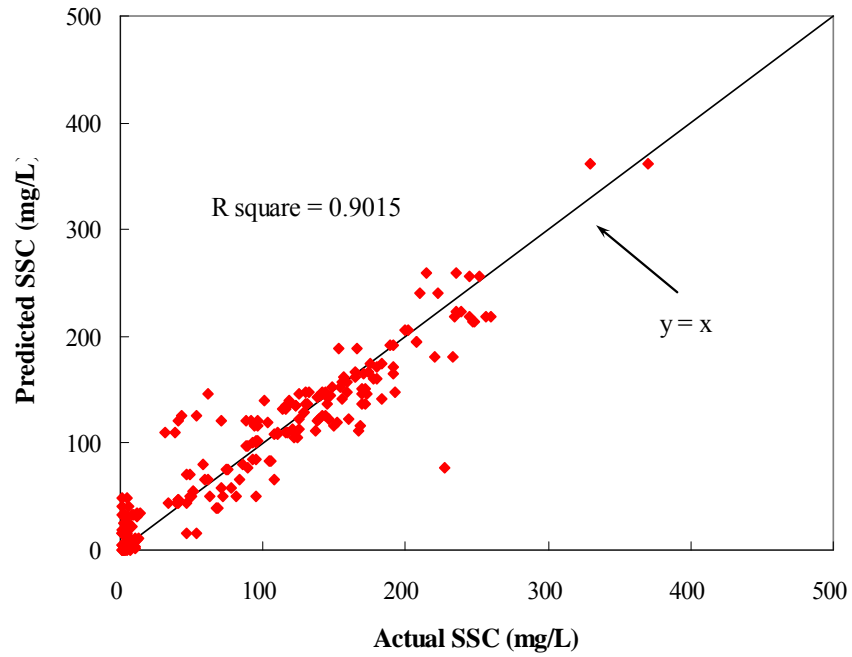
(a)
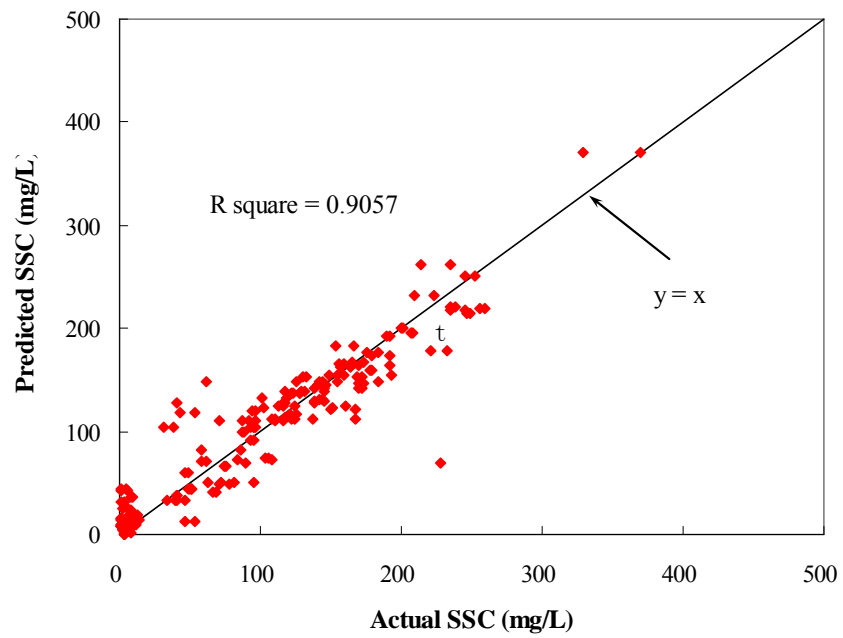
(b)

Figure 3.19 SSC prediction before and after temperature compensation (SSC< 500mg/L): a)
before temperature compensation; b) after temperature compensation.

An ANOVA analysis using the GLM procedure in SAS (SAS, 2003) was conducted to analyze the effects of actual SSC, temperature, and the interaction between actual SSC and temperature on predicted SSC (Appendix J). All 258 grab samples taken from Little Kitten Creek were used for the analysis. The results indicated that 1) there was a significant effect of interaction between actual SSC and temperature on predicted SSC when the significance level α = 0.01 was used (p=0.0021); 2) the temperature has no significant effect on predicted SSC (p=0.8336).

Based on above analysis, a conclusion can be drawn that temperature has limited effect on SSC measurement.

3.4.5 Individual signals at all measured SSC

Individual signals measured at the times the 258 grab samples were taken are plotted against the SSC in Figure 3.20. By observing the three signals, transmitted signals measured at 180° angle (ORA180) approached zero at higher SSC; two backscattered signals measured at 45° angle (IR45, ORA45) showed big variations at lower SSC. These observations indicated that the sensor was not capable of measuring SSC greater than 4500 mg/L or lower than 500 mg/L because large error would take place.
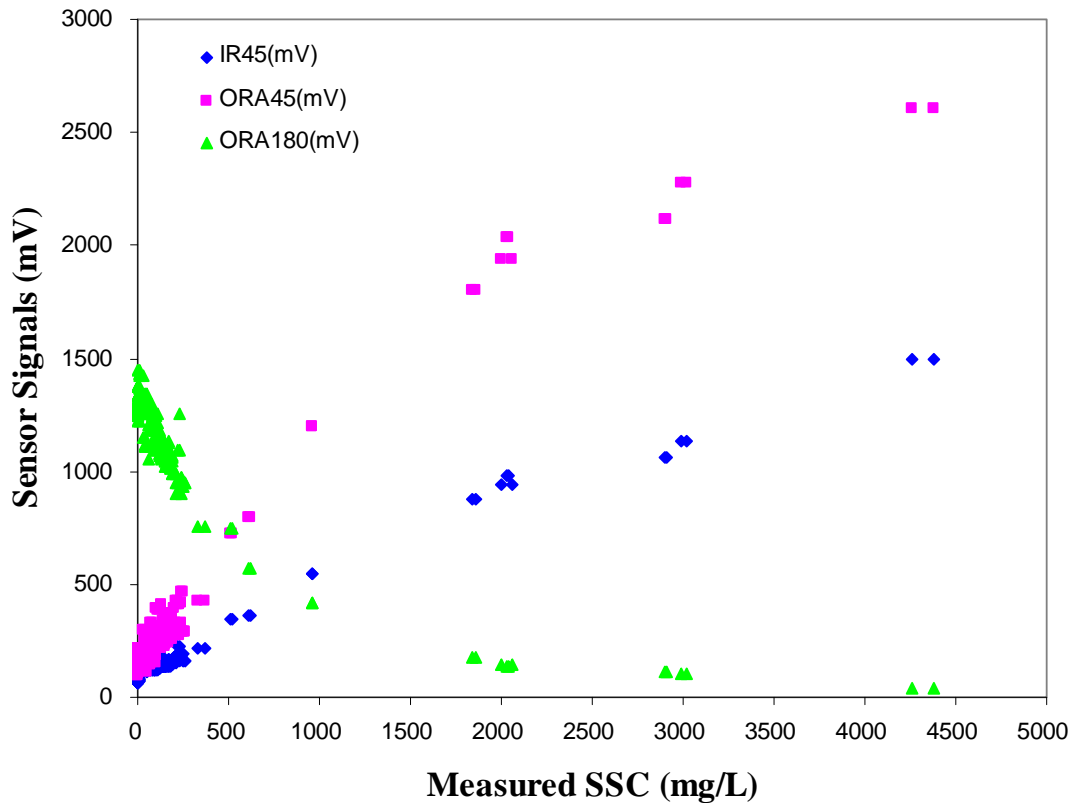
Figure 3.20 Individual signals at all measured SSC.

3.5 Conclusion

Long-term field experiments were conducted in Kansas and Georgia. Through these experiments, the performance of the optical sensors developed in this study was evaluated. Results showed that the optical sediment sensor was capable of long-term, real-time SSC monitoring.

Temperature effect on sensor measurement was analyzed. Results showed that the temperature coefficients for ORA180, ORA45, and IR45 signals were $5.53mV/^{o}C$, $3.74mV/^{o}C$, and $3.36mV/^{o}C$, respectively. For SSC greater than 500mg/L, R-square values of 0.9776 and 0.9773 were achieved before and after temperature compensation, respectively. For SSC lower than 500mg/L, the R square values of 0.9015 and 0.9057 were achieved before and after temperature compensation, respectively. An ANOVA analysis indicated that temperature had no significant effect on sensor signals (p=0.8336).

Signals of the optical sediment sensor deteriorated by lens fouling. Fouling of the sensor lenses caused the transmitted signal to decrease and the backscattered signal to increase. A fouling correction algorithm was developed by determining the fouling trend through a regression analysis on peak signal values taken during no-rain periods. The fouling trend was then removed to restore the sensor signals.

The field experiment at Fort Benning indicated that the open-bottom design provided higher-quality signals than the closed-bottom design, mainly because of reduced clogging and fouling problems. Furthermore, the fouling effect on signals was reduced significantly during winter seasons. Thus, it can be concluded that the fouling problem observed on the sensors was mainly a biofouling problem.

3.6 Acknowledgement

3.7 References

Butt, T., J. Miles, P. Ganderton, and P. Russell. 2002. A simple method for calibrating optical backscatter sensors in high concentrations of non-cohesive sediments. *Marine Geology* 192(4): 419-424.

Downing, J.P. 1983. An optical instrument for monitoring suspended particulates in ocean and laboratory. In *Proceedings OCEANS'83-Effective use of the sea: An update*, 1:199-202. New York, NY: IEEE.

Downing, John P.; Sternberg, R. W.; Lister, C. R. B. 1981. New instrumentation for the investigation of sediment suspension processes in the shallow marine environment. *Marine Geology* 42(1-4):19-34.

Green, M. O., and J. D. III Boon. 1993. Measurement of constituent concentrations in nonhomogeneous sediment suspensions using optical backscatter sensors. Marine Geology 110(1): 73-81.

Kineke, G.C.; Sternberg, R.W. 1992. Measurements of high concentration suspended sediments using the optical backscatterance sensor. *Marine Geology* 108(3-4): 253-258.

Lawler, D.M., Brown, R.M., 1992. A simple and inexpensive turbidity meter for the estimation of suspended sediment concentrations. *Hydrological Processes*. 6, 159–168.

Maffione, R. A., and D. V. Dana. 1997. Instruments and methods for measuring the backwardscattering coefficient of ocean waters. *Applied Optics* 36(24): 6057-6068.

MATLAB. 2006. Matrix Laboratory. Ver. 7.3.0.267 (R2006b). Natick, MA: The MathWorks, Inc.

McKee, Lester J., Neil K. Ganju, and David H. Schoellhamer. 2006. Estimates of suspended sediment entering San Francisco Bay from the Sacramento and San Joaquin Delta, San Francisco Bay, California. *Journal of Hydrology* 323(1): 335-352.

Orwin, J. F., and C.C. Smart. 2005. An inexpensive turbidimeter for monitoring suspended sediment. *Geomorphology* 68 (2005): 3 –15

PC208W. 2000. PC208W. Ver. 3.1a. Logan, UT: Campbell Scientific, Inc.

Presto, M. K., A. S. Ogston, C. D. Storlazzi, and M. E. Field. 2006. Temporal and spatial variability in the flow and dispersal of suspended-sediment on a fringing reef flat, Molokai, Hawaii. *Estuarine, Coastal and shelf Science* 67(1): 67-81.

SAS. 2003. *SAS Documentation*. Ver.9.1. Cary, N.C.: SAS Institute, Inc.

Schoellhamer, David H.; Wright, Scott A.. 2003. Continuous measurement of suspended-sediment discharge in rivers by use of optical backscatterance sensors. *IAHS-AISH Publication* (283): 28-36.

Sherwood, C.R., D. Coats, and B. Walls. 1989. Current and suspended sediment measurements on the central california continental shelf. In *OCEANS '89. Proceedings*, 320-325. New York, NY: IEEE.

Stoll, Q. M. 2004. Design of a real-time, optical sediment concentration sensor. MS thesis. Manhattan, Kansas: Kansas State University, Department of Biological and Agricultural Engineering.

Zhang, N., Y. Zhang, G. Grimm, and C. Johnson. 2007. Preliminary Report on Real-time Sediment-Concentration Monitoring Before, During, and After the Construction Work. Unpublished Material. Final report submitted to Aberdeen Test Center. July 1, 2007.

Zhang, Y., N. Zhang, Q. Stoll, D. Oard, J. Steichen, P. Woodford, P. Barnes, and S. Hutchinson. 2006. Monitoring sediment concentration at a low-water stream crossing using an optical sediment sensor. ASABE Paper No. 063091. St. Joseph, Mich.: ASABE.

CHAPTER 4 - AIR-BLAST CLEANING FOR OPTICAL SSC SENSORS

Abstract. Many researchers have reported the extremely damaging impact of fouling, including bio-fouling, on submerged optical instruments. It is one of the most prevalent hindrances in obtaining long-term, continuous, in situ optical SSC measurements. In order to solve this problem, an air-blast cleaning mechanism was integrated into a previously designed SSC sensor. Laboratory experiments in a manually created fouling environment were conducted to observe the fouling process on sensor cases made of different materials, and to verify the effectiveness of air-blast cleaning in reducing fouling. Results indicated that 1) sensors with an aluminum case experienced serious bio-fouling whereas sensors with polyethylene case didn't; 2) an air-blast cleaning mechanism was capable of reducing fouling effect on sensor signals. The duration and frequency of air-blast cleaning can be determined and adjusted depending on actual field conditions. Because long plastic tubing was required to provide pressurized air to the sensor in field installation, an air pressure drop test was also conducted on the hose between an air compressor and the sensor. Results showed negligible pressure drop.

Keywords. Air-blast cleaning, Sediment, Optical sensor, Fouling.

4.1 Literature Review

Fouling of moored optical instruments is the most prevalent deterrent in obtaining long-term, continuous, optical SSC measurements. Various lens-cleaning techniques have been studied by many researchers and optical sensor manufacturers.

A wide variety of antifoulant coatings have been attempted (Manov et al., 2004). However, many antifoulants are tributyltin (TBT)-based, which has a direct negative environmental impact and has been found to cause surface roughness (McLean et al., 1997).

Flemming et al. (1998) used a pulsing jet of fresh water from two small tubes to flush directly onto the glass window every half hour for 20 seconds to prevent fouling on sensor lenses. Suspended solids sensors manufactured by RWT (2009) are equipped with a jet-cleaning system to blast air or water on a timed basis. D15/76 system is a turbidity monitor unit manufactured by

Analytical Technology, Inc. that uses a burst of compressed air to automatically clean the sensor and maintain reliable measurements (ATI, 2009).

Lillycrop and Howell (1996) developed an optical lens protection method that fills the sampling cell with a biologically resistant reference fluid when a measurement is not taking place. The reference fluid is replaced with the water to be measured before the measurement and is brought back to the cell immediately after the measurement.

Ridd and Larcombe (1994) described a simple wiper mechanism, in which a soft rubber pad is mounted upon a small wiper blade that rotates like a windshield wiper on a vehicle. Another DTS-12 turbidity sensor manufactured by FTS (2009) also uses a self-cleaning wiper system. Fondriest Environmental, Inc. uses a wiper mechanism on their YSI 6136 turbidity sensor to clean residue buildup on the surface of the sensor for fouling prevention (FEI, 2009).

WTW (2009) integrates an ultrasonic module that can generate a permanent oscillation on the optical windows in the micrometer range to avoid biofouling on their VisoTurb® 700 IQ and ViSolid® 700 IQ sensors. The ultrasound source has maximum vibration amplitudes at the center of the measurement window to minimize its impact on SSC measurements, because the light paths were placed away from the center. An oceanographic sensor with in-situ cleaning and bio-fouling prevention system developed by Edgerton (1977) entails the use of sonic energy which varies in frequency and energy intensity level. In the industrial cleaning processes, ultrasonic cleaning is used for a wide range of applications to remove swarf or other polishing residue from parts that are immersed in oil, grease, or paint. This technique usually involves the proper temperature and chemistry selection, and relatively longer cleaning time (Maxsonic Inc., 2006).

Besides active lens cleaning techniques discussed above, proper algorithms were also used by researchers to remove fouling on sensor signals obtained from specially designed optical structures. Buttmann (2001) and Postolache et al. (2007) suggested that fouling of the optics could be compensated using a four-beam technology. The four-beam sensing method includes two light sources and two light detectors. Each light source has one detector at 90° and the other one at 180° angle. Two light sources were switched on alternatively while two light detectors took readings. From the four readings, a rationmetric algorithm was used to calculate turbidity values (HEI, 2009).

During data post-processing, correction algorithms could be applied to restore the signals. For example, Zhang et al. (2007) developed a correction algorithm to determine and remove the fouling trend found through a regression analysis on peak signal values taken during no-rain periods.

4.2 Objective

Taking into account the cost and simplicity, a method of air-blast cleaning to reduce fouling on optical lenses of the previously designed optical sensor was investigated. Different cleaning durations and intervals were used in the laboratory cleaning experiments. Fouling on SSC sensors with aluminum and polyethylene cases were studied and compared.

4.3 Methodology

4.3.1 Sensors with embedded air passages used in laboratory cleaning experiments

Optical SSC sensors designed in 2006 with an aluminum case (Figure 4.1a) and in 2008 with a polyethylene case (Figure 4.1b) were used in laboratory cleaning experiments. Air passages were embedded in the sediment sensors. For the sensor with an aluminum case, positions of three air outlets were selected based on the available space in the sensor tube. For the sensor with a polyethylene case, two air outlets were placed on the two LED/PT rings, about 135° from the orange LEDs. The other two air outlets were designed to give an extra air-blast for better cleaning. The stretch-out views of the sensor tube with air outlets for the aluminum and polyethylene case sensors are showed in Figure 4.2 and Figure 4.3, respectively.

(a)   **(b)**

Figure 4.1 Two types of sensors used for cleaning experiments: (a) SSC sensor design with an aluminum case (2005); (b) SSC sensor design with a polyethylene case (2008)
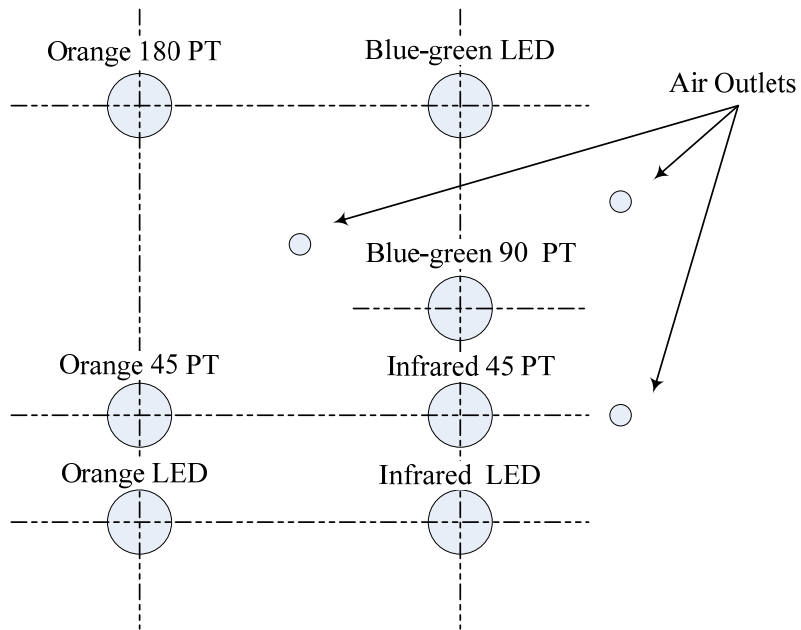
Figure 4.2 The stretch-out view of air outlets in the sensor tube with an aluminum case.
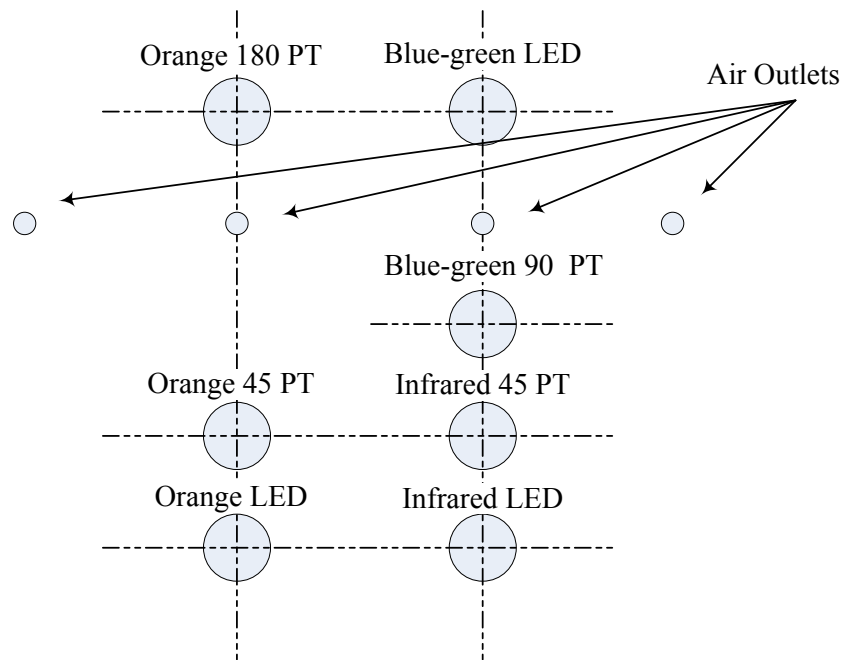
Figure 4.3 The stretch-out view of air outlets in the sensor tube with a polyethylene case.

4.3.2 Laboratory cleaning experiment

Four laboratory cleaning experiments were conducted.

4.3.2.1 Aluminum sensors with 12-hour cleaning intervals

An indoor experiment was conducted from July 15 to August 23, 2008 to study fouling on sensors with aluminum cases and to test the effectiveness of air-blast cleaning. Figure 4.4 shows the laboratory setup for the experiment, which consisted of two sensors with aluminum case, a 10-Gallon fish tank, a 12V normally closed solenoid valve (Aerocon Systems Co., San Jose, CA), a submergible air pump, a 12V air compressor equipped with a 3.5 liter air tank (Omega Research and development, Inc., Douglasville, GA), two signal conditioning and processing units, a relay circuit to drive the air compressor, a Campbell Scientific CR10X datalogger (Campbell Scientific Inc., Logan, UT), and a car battery as the power supply.

Figure 4.4 Laboratory setup of air-blast cleaning experiment.

The fish tank was divided into two chambers with a rigid plastic sheet. Two sensors with aluminum cases were placed side by side in one chamber of the tank and an air pump was placed in the other chamber to keep the water circulating and to maintain sediments suspended all the time during the experiment. One sensor was designed to have embedded air passages so that it could be cleaned when pressurized air blasts water into the sensor. The other sensor had no embedded air passages and it was used for comparison. The air compressor worked as a high pressure air source with the maximum output air pressure of 115 psi. The pressure was regulated

to 60 psi in this experiment and introduced to the sensor through embedded air passages. The CR10X datalogger was programmed to turn on a solenoid valve for two seconds every 12 hours to clean the sensor (Appendix K). Water in the fish tank was taken from Little Kitten Creek, Manhattan, Kansas, with high suspended sediment concentration.

4.3.2.2 Aluminum sensors with 2-minute cleaning intervals

A cleaning experiment using Little Kitten Creek water with a higher cleaning frequency was conducted from October 31 to November 19, 2008. Air-blast cleaning mechanism was activated for 2 seconds every 2 minutes, before taking each measurement. Air pressure of 70 psi was used. Two aluminum sensors were tested.

4.3.2.3 Polyethylene sensors with 2-minute cleaning intervals

A cleaning experiment using two polyethylene sensors was conducted during November 26 ~ December 12, 2008. Water for the experiment was taken from Tuttle Creek Lake, Manhattan, Kansas, to intentionally create an aqueous environment rich in biological organism in order to investigate the bio-fouling effect on polyethylene sensors. Air-blast cleaning mechanism was activated for 2 seconds every 2 minutes before each measurement was taken. Air pressure of 70 psi was used.

4.3.2.4 Comparison between aluminum sensor and polyethylene sensor

In order to compare the differences in fouling between sensors with aluminum and polyethylene cases, and the effects of air-blast cleaning on these sensors, an experiment was conducted during December 19, 2008 to January 6, 2009 using two aluminum sensors and two polyethylene sensors in a small swimming pool with a capacity of 70 gallons. Water with high sediment concentration was taken from Little Kitten Creek. A submersed pump was used to circulate the water to create fouling. Four sensors were placed away from the pump to avoid erosion of the fouling buildup caused by the high-speed water flow at the pump outlet. Lagoon water from the research unit of Animal Science Department of Kansas State University was also added to the swimming pool to enrich a bio-fouling environment. Air-blast cleaning mechanism was activated every 12 hours with a cleaning duration of 2 seconds.

4.3.3 Pressure drop test

A pressure drop test with 50 feet air tubing was also conducted to investigate air pressure loss in long paths. Five pressure settings (41, 63, 81, 91 and 105 psi) were used in this experiment. The air system consisted of an air compressor with a 3.5 liter tank, a pressure reducing valve, a solenoid valve, three pressure gauges, a 12V car battery, and necessary air fittings (Figure 4.5). Pressure gauge 1 measures the air pressure at the outlet of the pressure reducing valve; gauge 2 measures the pressure at the outlet of the solenoid valve; gauge 3 measures the outlet pressure at the sensor end. The pressure difference between gauge 1 and 3 was considered pressure loss after 50 feet plastic tubing.
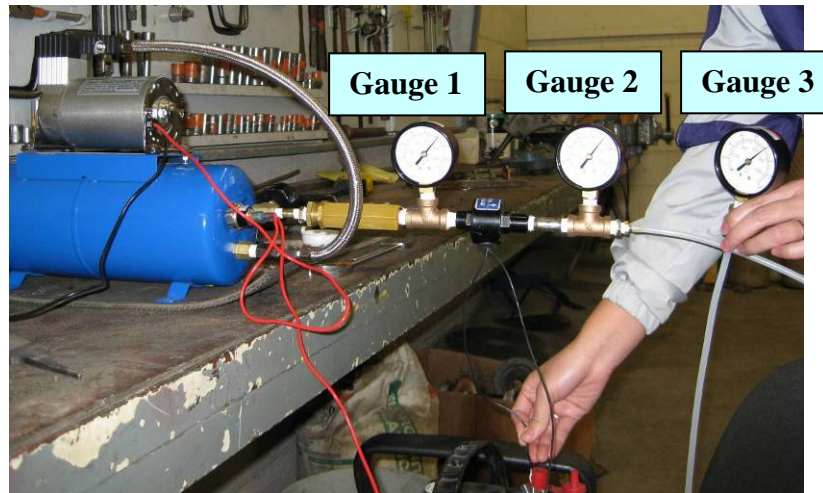
Figure 4.5 Pressure drop test setup.

4.4 Results and Discussion

Two types of fouling were observed and discussed in this dissertation, including bio-fouling (refers to the organic growth on the sensor's surfaces while submerged in water) and clay/silt fouling (refers to the accumulation of finer soil particles on sensor's surfaces and lenses).

4.4.1 Aluminum sensors with 12-hour cleaning intervals

Sensor signals in Figure 4.6 indicated signal deterioration caused by fouling and signal recovery due to air-blast cleaning. The transmitted signal and backscattered signals went back to their normal levels after each cleaning. Figure 4.7 shows signals measured from the sensor

without cleaning mechanism. Fouling of the sensor lenses caused the transmitted signal (ORA180) to decrease and the backscattered signal (IR45 and ORA45) to increase except the sudden changes (Figure 4.7). These sudden changes were probably due to washout of the fouling materials accumulated on the lens by the water flow. Obviously, these signal variations made the sensor useless in SSC measurement. Comparison between Figure 4.6 and 4.7 indicated that the air-blast cleaning mechanism was capable of reducing fouling effect on sediment sensors.
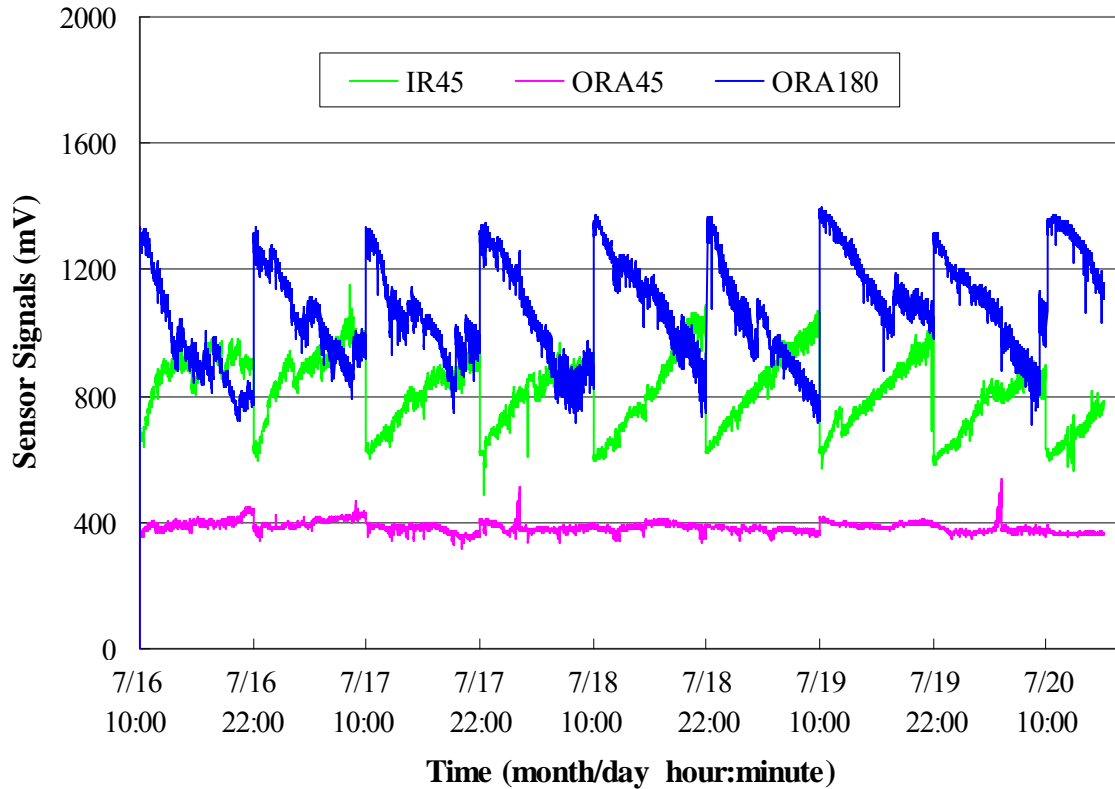
Figure 4.6 Signal deterioration due to fouling and recovery due to air-blast cleaning. Air-blast cleaning mechanism was activated for 2 minutes every 12 hours.
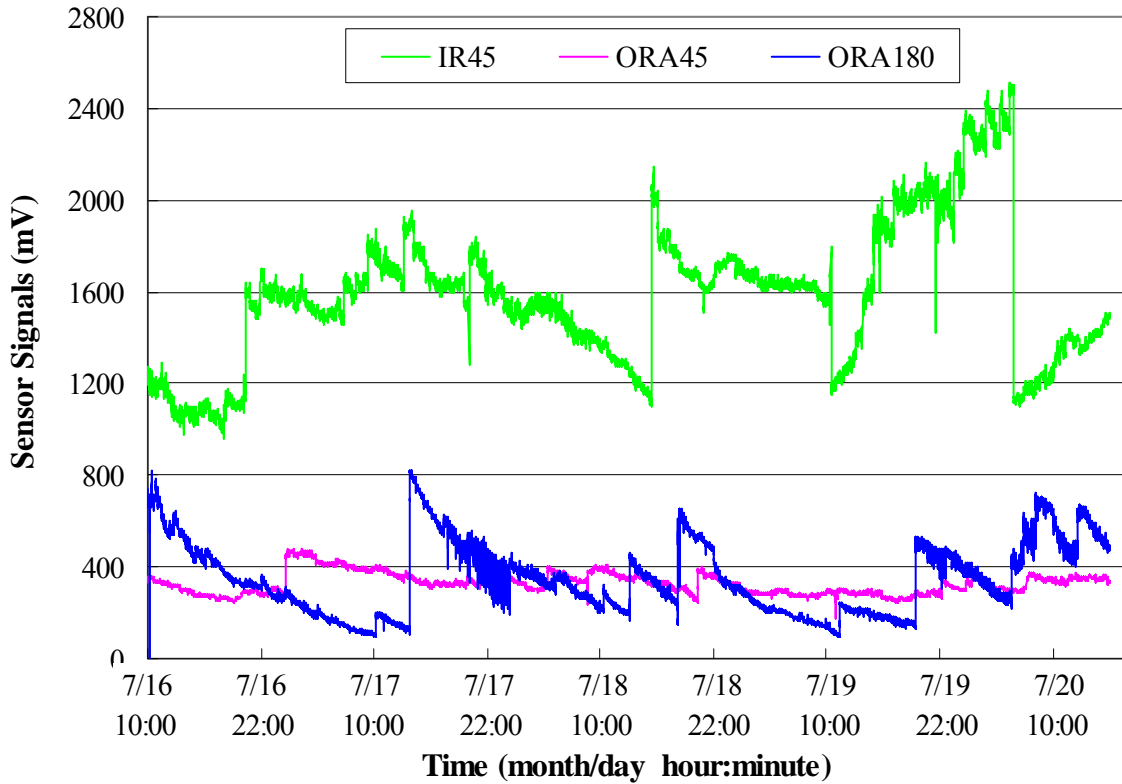
Figure 4.7 Signal deterioration due to fouling measured from the sensor without air-blast cleaning. Air-blast cleaning mechanism was activated for 2 minutes every 12 hours.

Clay/silt coating or the growth of biological organisms on optical lenses is the most possible cause for deterioration of the light signals. When fouling occurred on the lenses of the LEDs, lights detected at remote transistors at all angles would reduce. When fouling occurred on the lens of a phototransistsor placed 180º from the light source, less transmitted light would be detected. On the other hand, when fouling occurred on the lens of a photo detector placed 45º from the light source, less backscattered light would be detected. However, the fact that two backscattered signals were increasing due to fouling was probably because the buildups of clay/silt or bacteria on lenses caused more scattered light, which was detected by phototransistor at 45º angle.

Cleaning results obtained from the aluminum sensor during July 15 to August 23, 2008 were shown in Figure 4.8. Sharp spikes due to air-blast cleaning were clearly observed on IR45 and ORA180 signals during the first 28 days of the experiment (before August 6). Less fouling effect was observed on ORA45 signal. Signals deterioration was accelerated after August 11,

2008. The results indicated that the cleaning mechanism could only maintain the lenses clean for a limited period of time (28 days in this experiment), beyond which the mechanism only had a limited effect on reducing fouling.
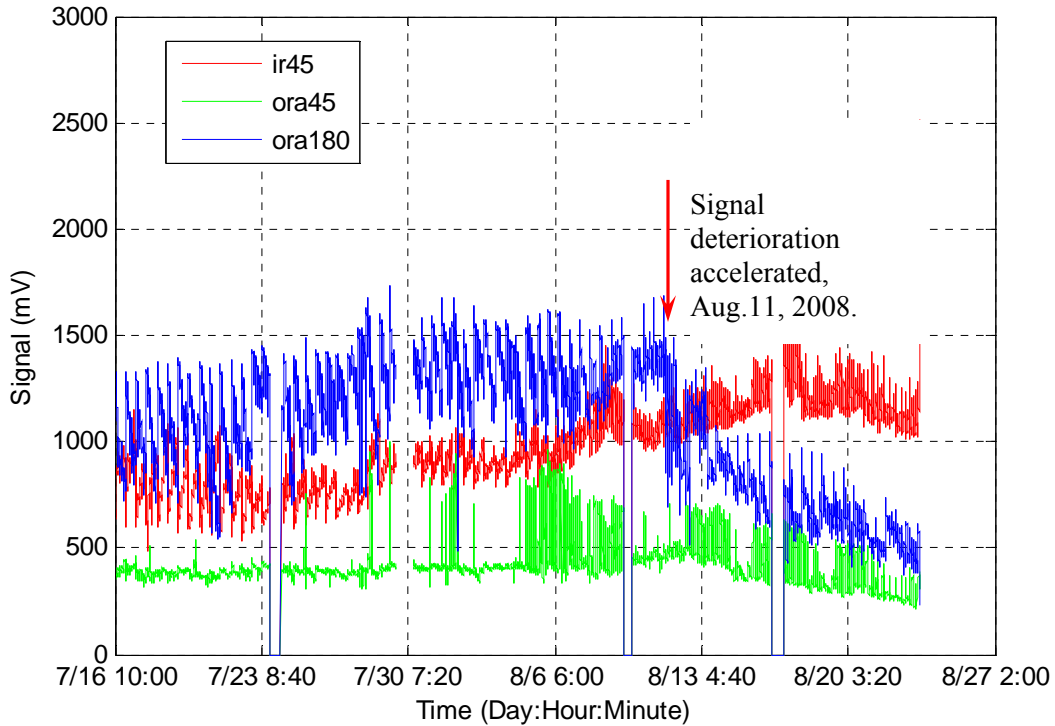
Figure 4.8 Signal measured from the sensor with air-blast cleaing within a 40-day period. Signals deterioration was accelerated after 28 days.

Sensor cases were painted black using ultra flat paint before the experiment. However, paint around the optical component and sharp edges of drilled holes were washed off easily and the metal surfaces were then exposed to the fouling environment. Photographs indicating fouling effects on sensor aluminum case and sensor tube are shown in Figure 4.9.

Sensor with air-blast cleaning   Sensor without cleaning

(a)

Sensor with air-blast cleaning   Sensor without cleaning
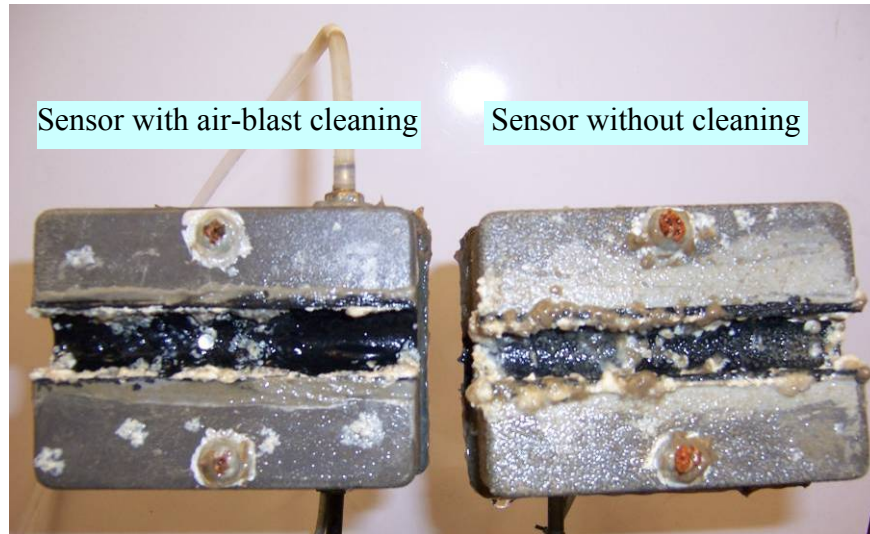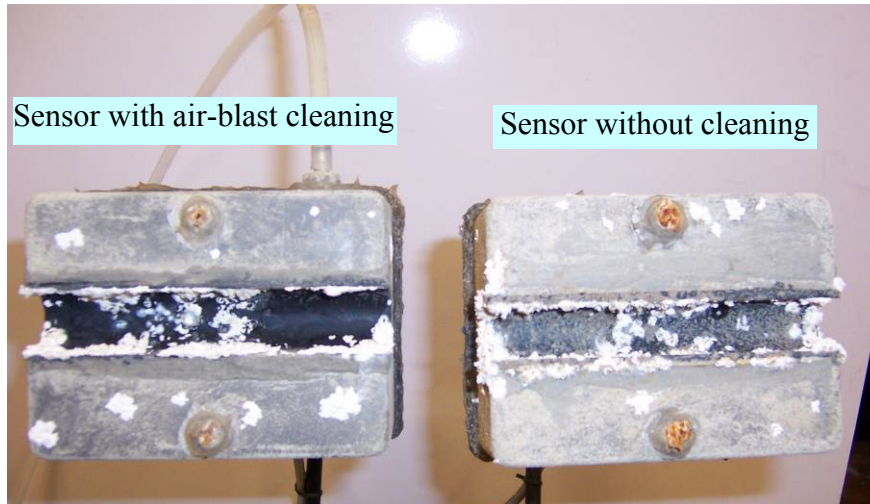
(b)

Figure 4.9 Photographs showing clay/silt fouling and bacterial fouling on sensors after a 40-day cleaning experiment (July 15 ~ August 23, 2008): (a) photographs taken right after the sensor were taken out from water when sensors were still wet, (b) photographs taken two days after the sensors were taken out from water.

Sticky materials were observed to adhere to sensor cases and bare metal surfaces around optical components for both cleaned and uncleaned sensors due to improper painting. They were hard to remove. This was probably due to bio-fouling caused by bacterial growth on the metal surfaces. A thin clay/silt layer was only observed on sensor case and lenses of optical components on the sensor without cleaning. Air-blast cleaning was more effective in remove

clay/silt fouling. Results also indicated that cleaning twice per day might not be sufficient under extremely dirty environment. For field deployment, the cleaning frequency and duration will need to be adjusted based on actual field conditions.

The sticky fouling materials were scraped off the aluminum sensors and cultured in two sheep blood agar plates (SBAP) under 37ºC and 25ºC, respectively. The growth medium was prepared with 50ml/L (5%) defibrinated sheep blood, 20g tryptone, 15g agar agar, and 1000ml H_2O. After culturing for 6 days, a number of bacterial colonies, such as Staphylococcus, Streptococcus, Enterococcus, Heterotroph, Pseudomonas, Bacillus, were observed in both plates. The growth patterns under two temperatures were identical. The culture results proved that the fouling observed on metal surfaces was bio-fouling caused by bacteria.

4.4.2 Aluminum sensors with 2-minute cleaning intervals

Sensor signals with 2-minute cleaning intervals (Figure 4.10) indicated that air-blast cleaning with higher frequency helped reduce fouling, especially for the ORA180 signal. Sensor signals without cleaning (Figure 4.11) showed serious signal deterioration on both IR45 and ORA180 signals. After a 12-day cleaning experiment (November 12, 2008), signal deterioration on both sensors accelerated due to serious fouling. By comparing Figure 4.10a and 4.10b, less fouling was observed on ORA45 signal, even without air-blast cleaning.
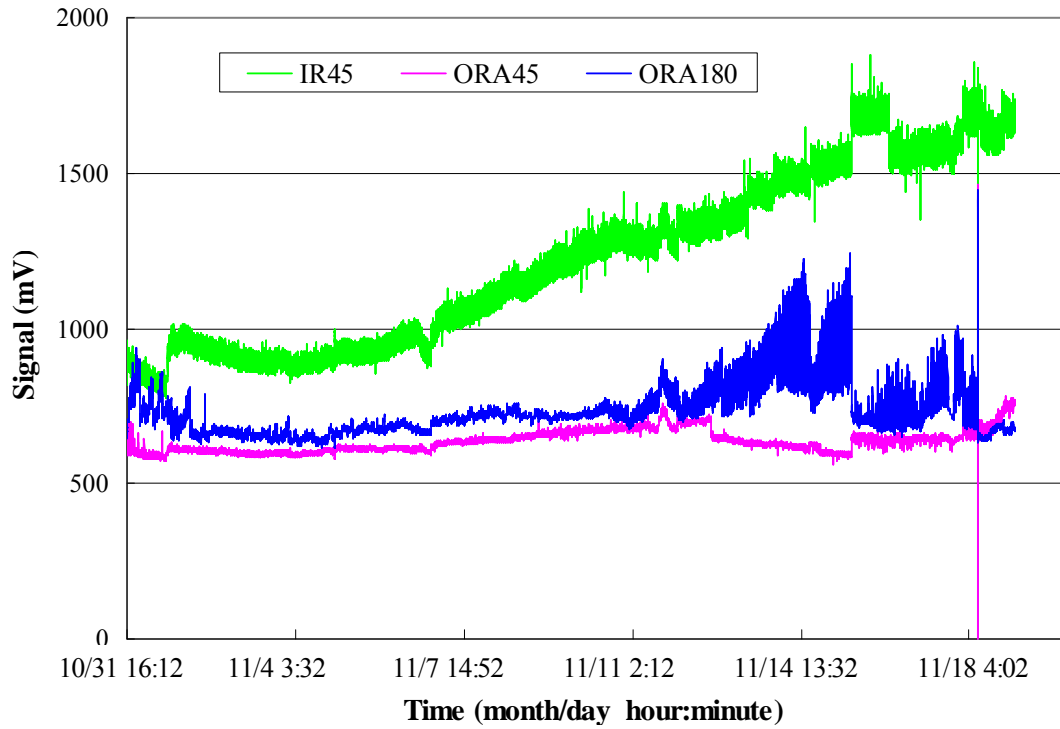
(a)
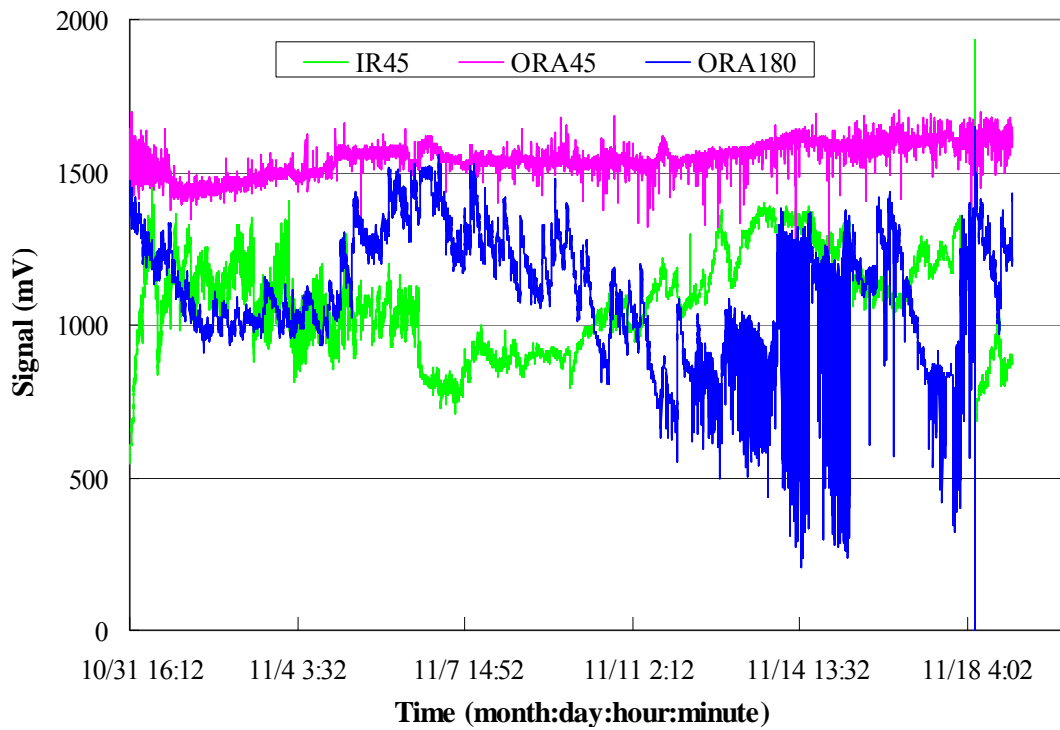
(b)

Figure 4.10 Signals measured from aluminum sensors with 2-minute cleaning intervals:

(a) sensor with air-blast cleaning; (b) sensor without Cleaning.

90

By observing photographs of the sensors taken 20 days after the experiment started (Figure 4.11), bio-fouling spots were found on aluminum case of both sensors (Figure 4.11a). However, clay/silt fouling was only found on the sensor without the cleaning mechanism (Figure 4.11b). Results shown in Figure 4.10 and photographs shown in Figure 4.11 both verified that 1) air-blast cleaning at 2-minute intervals was more effective in removing clay/silt fouling than that at 12-hour intervals; 2) Bio-fouling persisted even when the cleaning was activated at 2-minute intervals; 3) To avoid bio-fouling, aluminum material should not be used. Manov et al. (2004) suggested that copper-based materials could be employed for optical sensors for long-term submersed deployments due to the fact that copper can significantly reduce marine fouling.
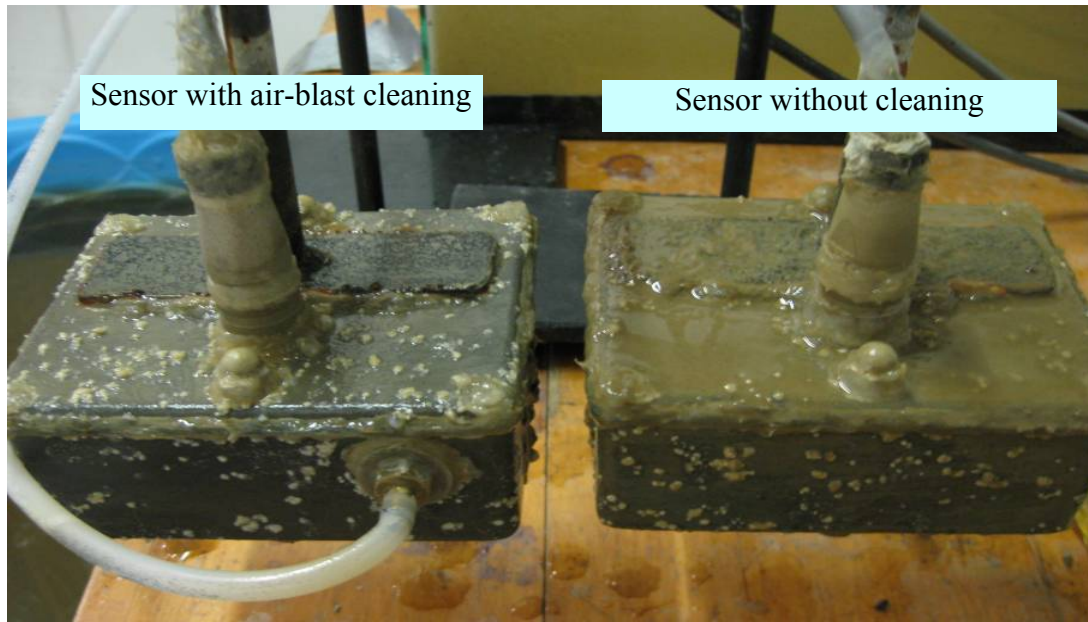
(a)
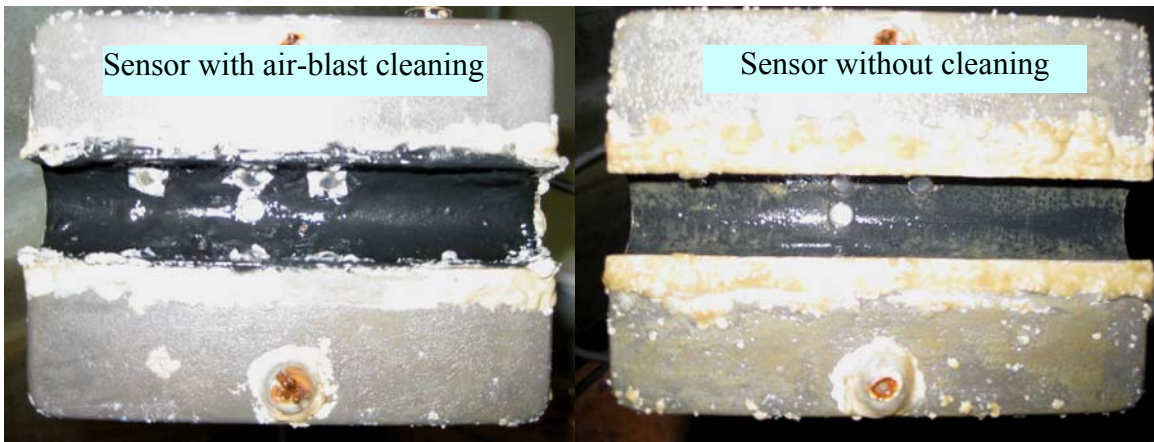
(b)

Figure 4.11 Photographs showing clay/silt fouling and bacterial fouling on sensors after a 20-day cleaning experiment (October 31 – November 19, 2008): (a) bacterial fouling spots on both sensor cases; (b) clay/silt fouling only on the tube surface of the sensor without cleaning.

4.4.3 Polyethylene sensors with 2-minute cleaning intervals

Figure 4.12 shows the signals recorded for the sensors with and without cleaning during the 17-day experiment. For the sensor with cleaning at 2-minute intervals (Figure 4.12a), signals

were relatively clean when compared with signals shown in Figure 4.10a. Figure 4.13 shows photographs taken after the experiment was completed. There were no bio-fouling spots found on either sensor. Bio-fouling around optical components and on sensor cases was observed on aluminum sensors during the previous experiment. It was not found on the polyethylene sensors during this experiment.

Figure 4.12a shows an increasing trend on the transmitted signals (ORA180) and a decreasing trend on the backscattered signals (IR45 and ORA45), which was probably due to the continuous settling of the suspended sediment in the fishing tank. Lower concentration of suspended sediments resulted in stronger transmitted signal and weaker backscattered signal. Without frequent lens cleaning, fouling on sensor lenses caused transmitted signals to decrease and backscattered signal to increase, as can be seen in Figure 4.12b, where an obvious decreasing trend and an increasing trend are observed on the ORA180 and IR45 signal, respectively. It is noticed from Figure 4.12b that the ORA45 signal displayed a relatively smaller fouling comparing to other two signals. The reason is unknown.
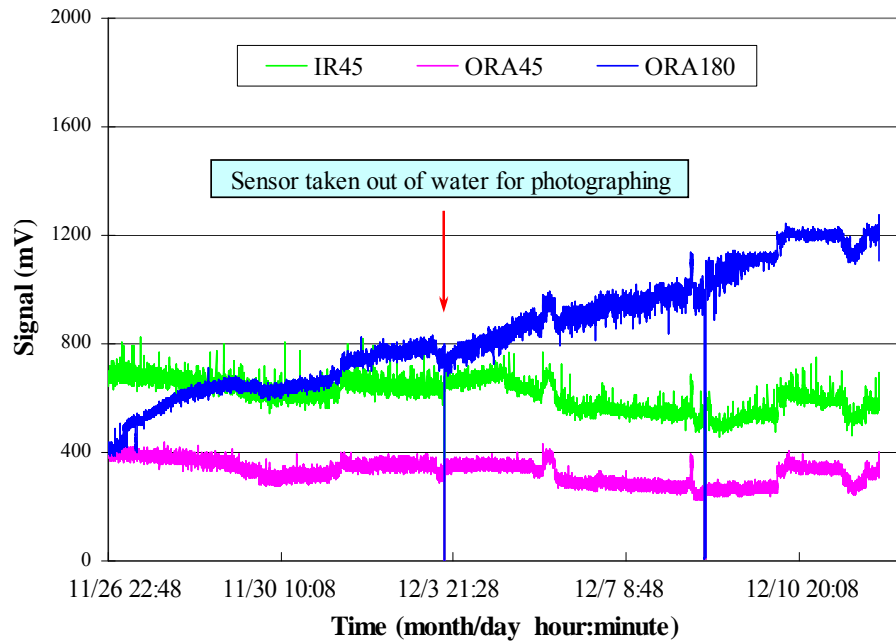
(a)
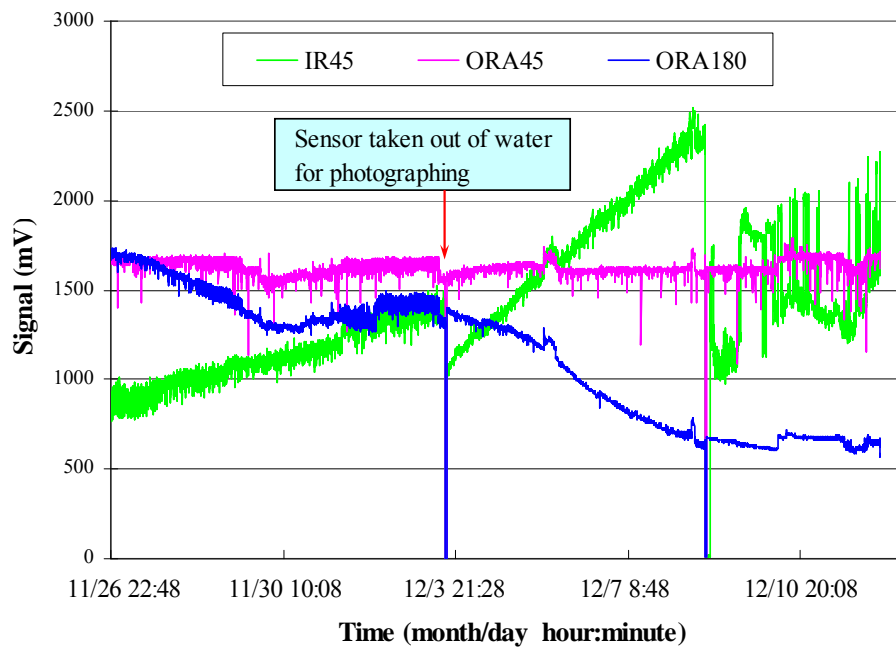
(b)

Figure 4.12 Indoor cleaning experiment using two polyethylene sensors: (a) signals of the sensor with cleaning; (b) signals of the sensor without cleaning.

Sensor with air-blast cleaning   Sensor without air-blast cleaning

(a)
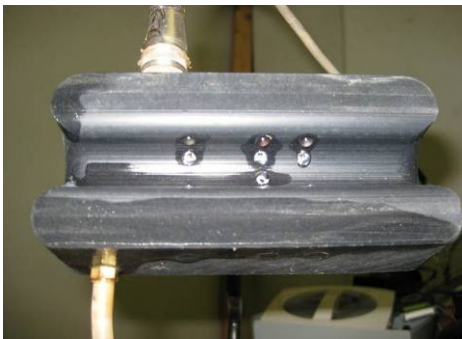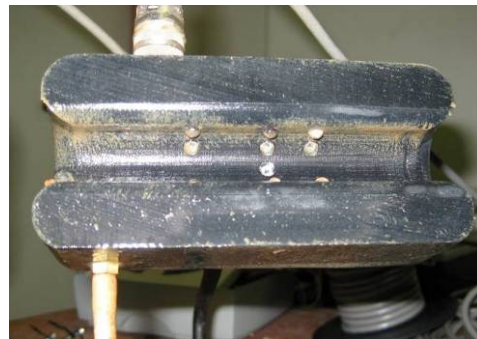
Sensor with air-blast cleaning   Sensor without air-blast cleaning

(b)

Figure 4.13 Photographs comparing sensors with and without air-blast cleaning after a 16-day cleaning experiment (November 26 ~ December 12, 2008) was completed: (a) side view; (b) bottom view.

Careful observation of clay/silt fouling on the sensor without air-blast cleaning (Figure 4.13) indicates that, clay/silt was accumulated at places where LEDs and PTs of 0 and 180 degrees were located. Future design of the sediment sensor may consider placing optics further away from sensor edges to avoid fouling on lenses due to clay/silt accumulation on these places.

4.4.4 Comparison between aluminum sensor and polyethylene sensor

Sensor signals from the aluminum and polyethylene sensors with 12-hour cleaning intervals are shown in Figure 4.14a and 4.15a, respectively, indicating signal deterioration by fouling and signal recovery due to air-blast cleaning. Signals measured from the aluminum sensor without cleaning (Figure 4.14b) clearly indicated that fouling of the sensor lenses caused the transmitted signal (ORA180) to decrease and the backscattered signals (IR45 and ORA45) to increase. Signals measured from the polyethylene sensor without cleaning (Figure 4.15b) showed a similar decreasing trend for ORA180 signal and increasing trend for IR45 signal caused by fouling. Fouling had a relatively small effect on ORA45 signal.
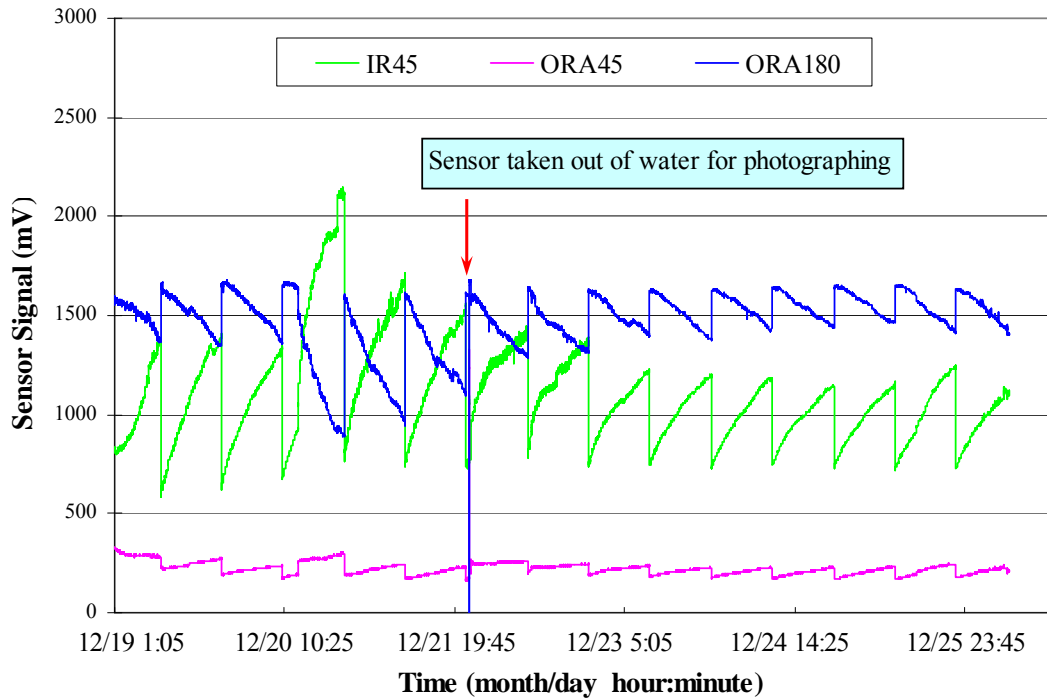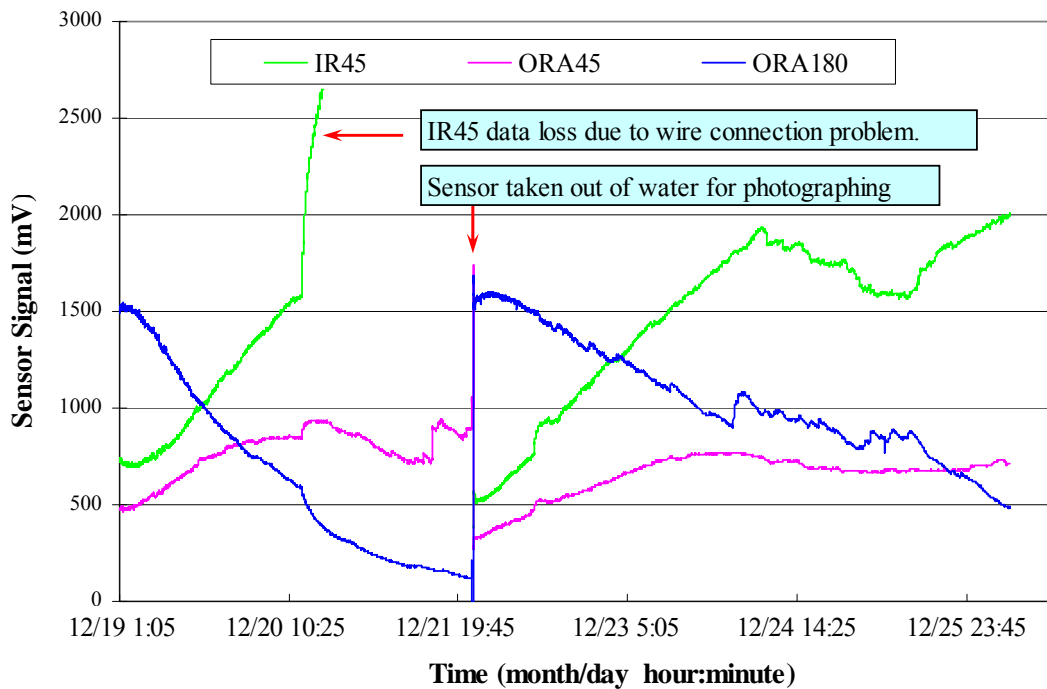
Figure 4.14 Signals recorded during the four sensor comparison experiment: (a) polyethylene sensor with air-blast cleaning; (b) polyethylene sensor without cleaning.
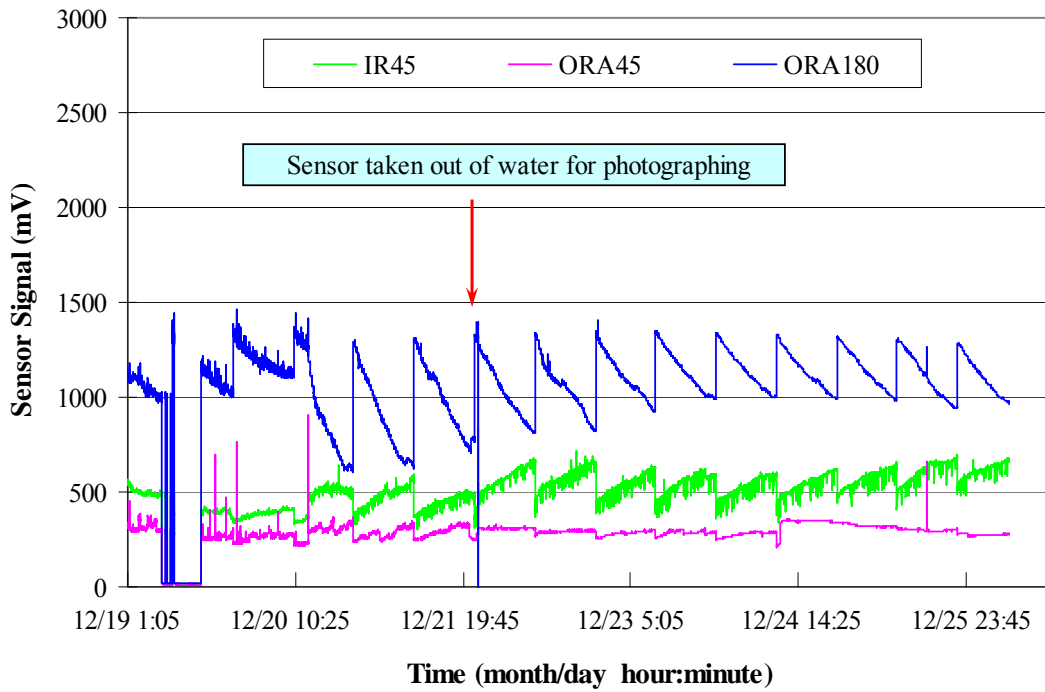
(a)
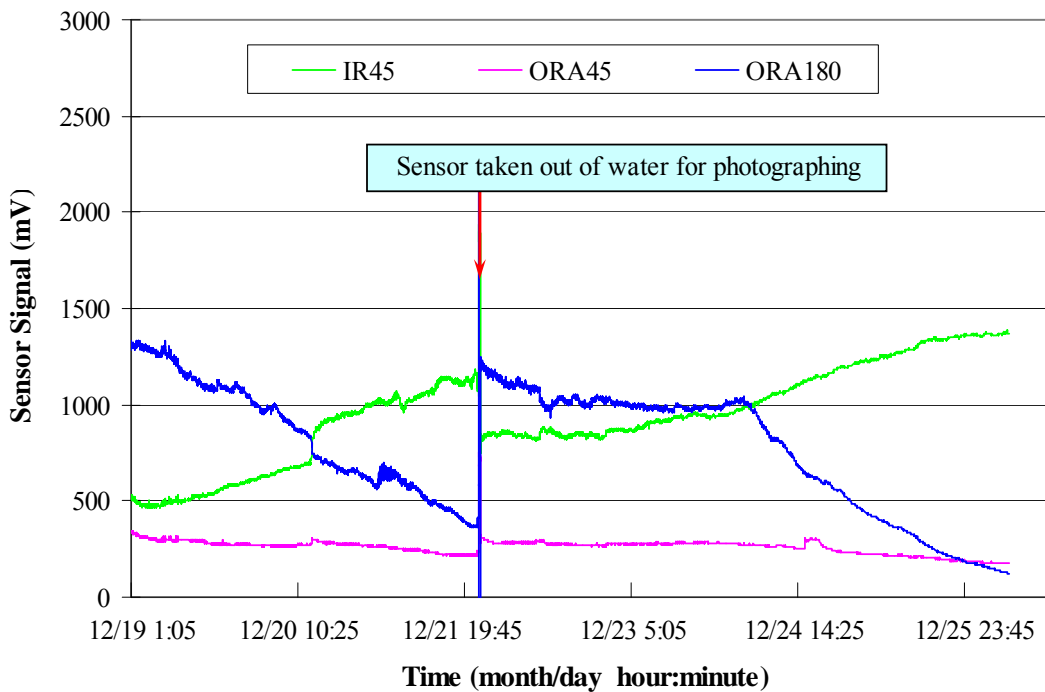
(b)

Figure 4.15 Signals recorded during the four-sensor comparison experiment: (a) aluminum sensor with air-blast cleaning; (b) aluminum sensor without cleaning.

Observation of the sensors after they were operating under water for four days showed that air-blast cleaning was effective in removing clay/silt fouling (Figure 4.16 and 4.18). Observations made 18 days after the start of the experiment showed that both clay/silt fouling and bio-fouling persisted on both aluminum sensors, even with air-blast cleaning (Figure 4.17). On both polyethylene sensors, however, only clay/silt fouling was observed (Figure 4.19). Activating the air-blast cleaning mechanism every 12 hours was not sufficient to completely eliminate clay/silt fouling, when clay/silt continuously accumulated for a long term. By observing the sensors without air-blast cleaning (Figure 4.17 and 4.19), the majority amount of clay/silt was again found at sensor edges where LEDs and PTs were located at 0 and 180 degrees. For the sensors with air-blast cleaning (Figure 4.17 and 4.19), sensor edges were clean. However, there was still small amount of clay/silt found at places where PTs were located at 45 and 90 degrees. In order to have a better cleaning result, more frequent cleaning and modification of the embedded air paths should be considered.
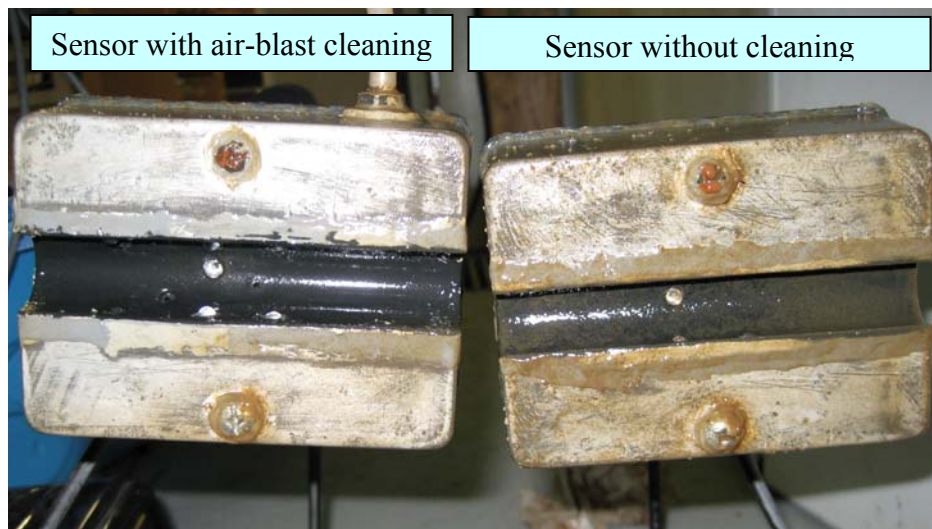
Figure 4.16 Aluminum sensors after working in water for four days (December 19 ~ 23, 2008).
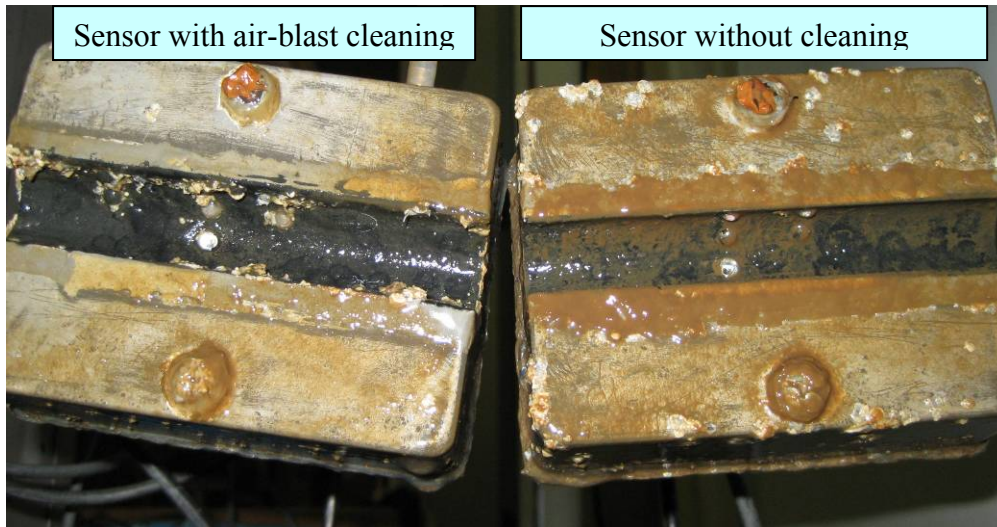
Figure 4.17 Aluminum sensors after working in water for 18 days (December 19, 2008 ~ January 6, 2009).
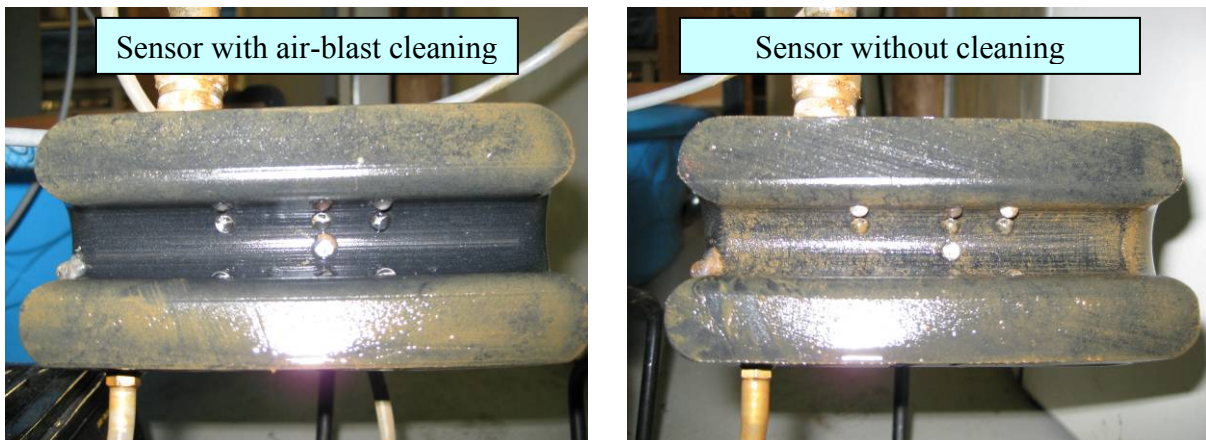
Figure 4.18 Polyethylene sensor after working in water for four days (December 19 ~ 23, 2008).
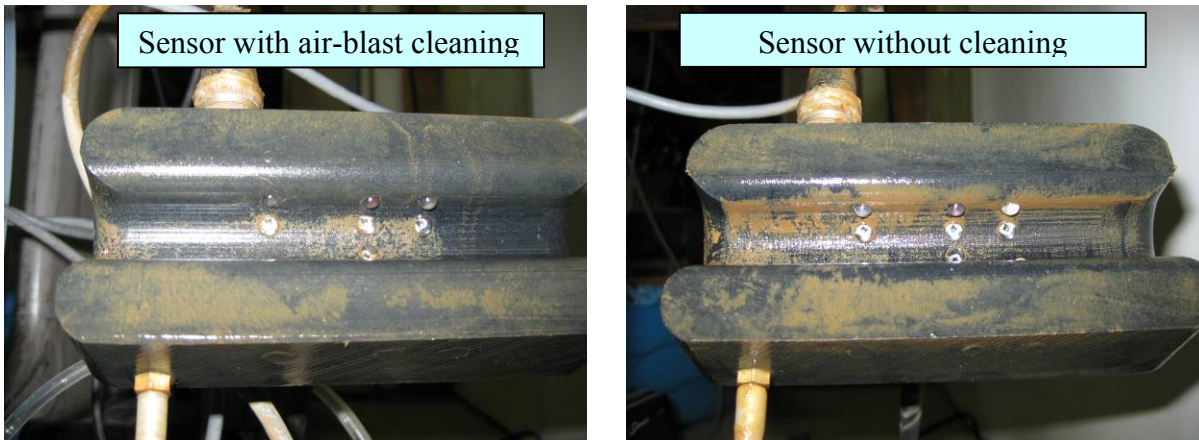
Figure 4.19 Polyethylene sensor after working in water for 18 days (December 19, 2008 ~ January 6, 2009).

4.4.4 Pressure drop test

The pressure drop test result is shown in Table 4.1. The air-blast cleaning system had a pressure loss of less than 0.2 psi with 50 feet tubing. Because the maximum distance between the sensor and air compressor in actual field installations will be less than 50 feet, air pressure drop will not cause problems for the system.

Table 4.1 Air pressure drop test.

Gauge 1 (psi)	Gauge 2 (psi)	Gauge 3 (psi)	Total pressure drop (psi)
105	104.9	104.8	0.2
91	90.5	90.5	0.5
81	80	79.9	0.2
63	63	63	0
41	41	41	0

4.4.5 Cost estimation

Table 4.2 shows estimated costs of the components required to build a complete air-blast cleaning system.

Table 4.2 Cost estimation for one complete set of air-blast cleaning system.

Component	Estimated cost ($)
Air Compressor	170
Solenoid Valve	100
Pressure Reducing Valve	100
Air Fittings and Plastic Tubings	20
Electronics Components (Wires, Circuit Board)	10
Total Estimated Cost	400

4.5 Conclusion

Two types of fouling - clay/silt fouling due to clay/silt accumulation on sensor lenses and bio-fouling due to bacterial contamination - were observed on the SSC sensors. Both fouling effects caused transmitted signals to decrease and backscattered signals to increase.

Clay/silt fouling and bio-fouling were both observed on sensors with aluminum case. Air-blast cleaning mechanism was capable of reducing clay/silt fouling on aluminum cases. The sensor tube of aluminum sensor experienced severe bio-fouling even with air-blast cleaning.

Only clay/silt fouling was found on polyethylene sensors. Air-blast cleaning mechanism was capable of reducing clay/silt fouling on sensors with polyethylene cases. Effect of bio-fouling seems to be insignificant on polyethylene cases. For field applications, polyethylene sensors with air-blast cleaning seem to be appropriate.

The current design of embedded air paths in polyethylene sensors was not effective to clean lenses at 45 and 90 degree. It is, however, rather effective to lenses at 0 and 180 degrees. Higher cleaning frequency and longer cleaning duration help improve the cleaning function

4.6 Acknowledgement

4.7 Reference

ATI. 2009. Highly Sensitive Turbidity Measurement, Unmatched Zero Stability: Model A15/76 Turbidity Monitor. Collegeville, PA: Analytical Technology, Inc. Available at: www.afcintl.com/water/pdf/L-A15-76.pdf. Accessed 22 March 2009.

Buttmann, Marc. 2001. Suspended solids measurement as reliable process control. In *ISA TECH EXPO Technology Update Conference Proceedings*, 413(1): 563-572. Houston, TX: Instrument Society of America.

Edgerton, G. A. 1977. Oceanographic sensor with in-situ cleaning and bio-fouling prevention system. U.S. Patent No. 4092858.

Flemming, H.C., A. Tamachkiarowa, J. Klahre, and J. Schmitt. 1998. Monitoring of Fouling and Biofouling in Technical Systems. *Water Science and Technology* 38(8-9): 291-298

FEI. 2009. YSI 6136 Turbidity Sensor. Alpha, OH: Fondriest Environmental, Inc. Available at: www.fondriest.com/products/ysi_6136.htm. Accessed 12 April 2009.

FTS. 2009. The DTS-12 Digital Turbidity Sensor from FTS. Victoria, BC, Canada: Forest Technology Systems Ltd. Available at: www.ftsinc.com/Sensors/dts-12_main.htm. Accessed 1 March 2009.

HEI. 2009. Technical White Paper. Loveland, CO: Hach Environmental Inc. Available at www.hachenvironmental.com/pdf/Technical_White_Paper-4-BeamTurbidity1.pdf. Accessed 6 June 2009.

Lillycrop, L. S., G. L. Howell. 1996. In-situ Long-term Deployment of Water Quality Sensors Adversely Affected by Biological Fouling. In *OCEANS 96 MTS/IEEE Prospects for the 21st Century Conference Proceedings* 2: 693-697.

Manov, D.V., G.C. Chang, and T. D. Dickey. 2004. Methods for reducing biofouling of moored optical sensors. *Journal of Atmospheric and Oceanic Technology* 21(6): 958-967.

Maxsonic Inc. 2006. Ultrasonic Cleaning. Maxsonic Inc. Available at www.maxsonic.cn/index5-1.htm. Accessed March 9, 2009

McLean, S., B. Schofield, G. Zibordi, M. Lewis, S. Hooker, and A.Weidemann. 1997. Field Evaluation of Anti-biofouling Compounds on Optical Instrumentation. In *Proc. SPIE* 2963: 708–713.

Postolache, O.A., P.M.B.S. Girao, J.M.D. Pereira, and H.M.G. Ramos. 2007. Multibeam optical system and neural processing for turbidity measurement. *IEEE Sensors Journal* 7(5): 677-684.

Ridd, P., and P. Larcombe. 1994. Biofouling control for optical backscatter suspended sediment sensors. *Marine Geology* 116(1994): 255-258.

RWT. 2009. Total Suspended Solids Systems. Wooloowin, AU: Royce Water Technologies. Available at: www.roycewater.com.au/uploads/file/Royce%20711-7011A%20Sus%20Solids.pdf. Accessed 1 March 2009.

WTW. 2009. Turbidity and Suspended Solids. Weilheim, Germany: WTW Wissenschaftlich-Technische. Available at: www.wtw.com/media/US_O_032_037_turb_web.pdf. Accessed 1 March 2009.

Zhang, N., Y. Zhang, G. Grimm, and C. Johnson. 2007. Preliminary Report on Real-time Sediment-Concentration Monitoring Before, During, and After the Construction Work. Unpublished Material. Final report submitted to Aberdeen Test Center. July 1, 2007.

CHAPTER 5 - AN OPTICAL SEDIMENT SENSOR INTEGRATED WITH FLOW VELOCITY MEASUREMENT

Abstract. Flow velocity measurement is usually conducted with SSC measurement to assess sediment mass transport at a given time and depth. However, flow velocity and sediment concentration measurements that were conducted by different sensors could result in time mismatch, and high cost for equipment. An optical sediment sensor integrated with flow velocity measurement based on cross-correlation principle was tested in this study. Two flow experiments were conducted in the laboratory to examine the sensor performance on velocity measurement using a closed circulation system, respectively. A solution of blue colorant, Brilliant Blue FCF, was used as an artificial absorbent to create signal variation pattern when water flow that carries the colorant passed through the sensor. Flow velocity was calculated based on the patterns using the cross-correlation principle. The results indicated that the cross-correlation-based velocity sensor was capable of measuring water flow velocity using the dye injection method.
Keywords. Cross-correlation, Flow velocity measurement, Brilliant Blue FCF, Optical sensor.

5.1 Literature Review

Flow velocity measurements have been conducted together with SSC measurement to determine sediment transportation in various field environments. Huntley and Hanes (1987) conducted SSC measurements from a backscattered sediment sensor with simultaneous velocity measurement from an electromagnetic flow meter. They employed five sediment sensors at five different heights above the seabed, and an electromagnetic current meter at only one height for velocity measurement. Downing et al. (1981) developed an instrumentation system to investigate sediment suspension process in shallow marine environment. This system consisted of an electromagnetic current meter for flow velocity measurement, and a five-element array of optical backscattered sensors for SSC measurement. The U. S. Army Corps of Engineers conducted research to estimate flux and direction of suspended material transport on the central California continental shelf during their harbor development projects. They used a vector-measuring current meter for velocity measurement paired with optical backscatterance sensor for SSC determination (Sherwood et al., 1989). Presto et al. (2006) studied the temporal and spatial

variability of the flow velocity and dispersal of suspended-sediment on a fringing reef flat, Molokai, Hawaii, using an electromagnetic current meter installed 20 cm above the bed, two optical backscatter sensors 20 and 50 cm above the bed, respectively, a pressure sensor 52 cm above the bed, and a transmissometer 70 cm above the bed (Presto et al., 2006). Holmes and Garcia (2002) used two acoustic Doppler velocimeters (ADV) and an optical backscatter sensor for velocity and sediment concentration measurement over bedforms in sand-bed rivers, respectively. They had to use a compass/tilt/roll sensor to determine orientation of the ADVs. However, flow velocity and sediment concentration measurements that were conducted by different data acquisition systems could result in time mismatch between the time series of the sediment and flow data. If these two measurements were done at multiple locations, high cost would be required for equipment/instrumentation setup.

Traditional flow measurement devices were designed based on various physical principles and each has its advantages and limitations. Anemometer and propeller meters use mechanical movement of anemometer cup wheels or propellers to sense flow velocity (Hooper et al., 2000; GPI, 2009). This type of flow meter does not sense direction of velocity (USBR, 1997). Electromagnetic meters use the principle of electromagnetic induction. When water flows through a magnetic field, a voltage is induced, from which the flow rate is inferred. This type of meter is directional (USBR, 1997). Doppler-type meters determine flow velocity by measuring the change in frequency of light or ultrasound waves reflected from moving sediment or air bubbles (Simpson, 2001; USBR, 1997). This type of meter requires the presence of suspended particles or air bubbles and is not suitable for clean waters (FWS, 2006). Optical strobe velocity meters use the strobe effect to determine surface velocity of streams. For this type of meter, no parts are immersed in the flowing stream (USBR, 1997). Changes in flow velocity can be converted to pressure changes by a pressure transducers attached to a standard wading rod. This type of meter does not produce good results in shallow waters or in slow-moving water flows (FWS, 2006). Transit-time flow meters measure the difference between transit times of a high-frequency ultrasonic wave in the upstream and downstream directions to calculate the flow velocity. These meters require clear water to operate properly (FWS, 2006).

Cross-correlation techniques have been widely used to determine the time delay between two or more signal series (Keech, 1991; Bendat and Piersol, 2000). Critten (1974) invented a flow meter based on cross-correlation principle. His invention consisted of a pair of acoustic-to-

electric transducers that were positioned apart in the flow direction to measure acoustic radiation generated by random fluctuations in a flowing fluid system. Keech (1991) invented a cross-correlation apparatus and method to measure traveling speed of a cable along a predetermined path. He conducted the measurement by detecting electrostatic charges induced on cable surface by two electrostatic charge sensors which were spaced in the direction of the cable. Wren et al. (2006) used the cross-correlation method to compare the timing and shape of dynamic electromyography (EMG) signals. Eam-O-Pas et al. (1994; 1997) developed a correlation-based flow velocity sensor to measure velocity of glass beads flowing through a pipe. A previously designed optical sediment concentration sensor that can measure SSC on real time has been developed in Instrumentation and Control Laboratory, Kansas State University. This device was applied to a long-term field experiment at low water stream crossings in Kansas and Georgia (Stoll, 2004; Zhang et al., 2006; Zhang, Y. et al., 2007). Zhang N. et al. (2007) proposed to add cross-correlation-based flow velocity measurement to the sediment sensors through a simple structure modification. The integrated sensor allows simultaneous measurement of sediment concentration and flow velocity using one data acquisition system, hence, guaranteeing time synchronization between the SSC and flow velocity measurements. The simple optical design would also provide an integrated SSC/flow velocity sensor at a very low cost.

5.2 Objective

The integrated SSC/flow velocity sensor was tested to evaluate its performance on flow velocity measurement based on the cross-correlation principle. The experiment was conducted using a closed circulation system in the laboratory. An injection system using pressurized air and the gravity principle was designed to inject colorant to the water flow as an artificial absorbent for cross-correlation calculation. Results of the flow velocity experiment were discussed and compared with a commercial flow meter.

5.3 Methodology

5.3.1 Sediment/velocity sensor design

The optical sediment sensor used in this study was developed from a previous design. It used three Light Emitting Diodes (LED) that emitted lights of different colors (blue-green, infrared, orange) as the light sources and nine phototransistors that were placed at 45º, 90º and

180° angles with respect to each LED (Stoll, 2004; Zhang et al., 2006). In order to avoid over-fitting in prediction models and allow a much simpler sensor design, the sediment sensor was then simplified over the previous design. The simplified design adopted a 2-ring structure (Figure 5.1a) that consisted of four phototransistors, BG90, IR45, ORA45 and ORA180, and three LEDs (Zhang et al., 2006). Zhang, N. et al. (2007) proposed to add a third ring for cross-correlation-based flow velocity measurement. In Figure 5.1b, the first two rings viewed from the far end were the original sediment sensor structure. The velocity measurement was enabled by using the "Orange LED 1" and two phototransistors (PT) on the first ring and the "Orange LED 2" and two PTs on the added third ring. Obviously, Orange LED 1 and its two PTs on the first ring were responsible for both SSC and water flow velocity measurement. The pin description of the sediment/velocity sensor was shown in Appendix L.

(a)   (b)
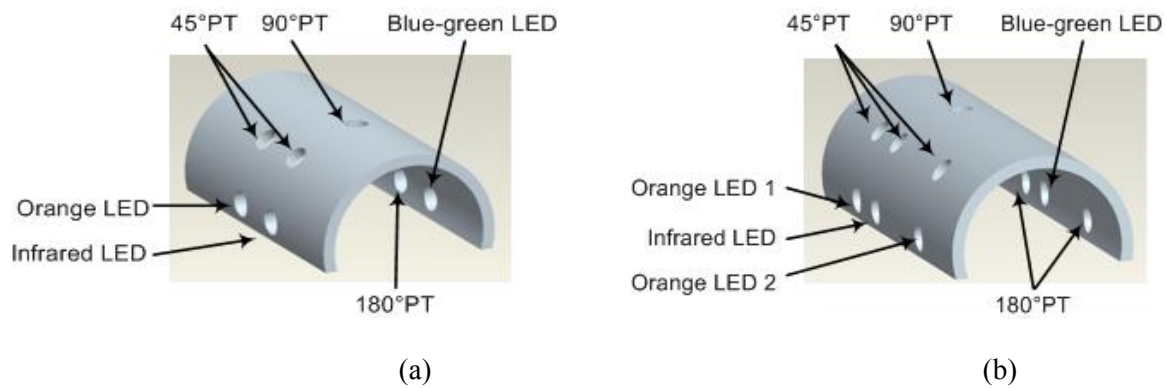
Figure 5.1 Flow-velocity measurement added to the SSC Sensor: (a) the two-ring SSC sensor, (b) the three-ring, integrated SSC/flow-velocity sensor (Zhang, N. et al., 2007). The first and added third rings are used for velocity measurement.

5.3.2 Cross-correlation principle

Cross-correlation is the correlation between two signals and is widely used for measurement of time delays or pattern shift in signal processing techniques (Bendat and Piersol, 2000; Beck and Plaskowski, 1987). Given two signal series that have identical shape but differ by a time delay along the time axis, calculation of cross-correlation coefficient can determine how much one signal has to shift along the time axis to coincide with the other signal. The cross-correlation coefficient has the maximum value of 1 when two signals, one measured at an

upstream location and the other downstream, exactly match (Bendat and Piersol, 2000; Bourke, 1996).

The working principle of the optical flow velocity sensor is shown in Figure 5.2. The "Orange LED 1" and two phototransistors (45º PT 1 and 180º PT 1) in ring 1 measure the upstream signal. The "Orange LED 2" and two phototransistors (45º PT 2 and 180º PT 2) located in ring 3 (Figure 5.2a) measure the downstream signal. The spacing between the two rings was 40 mm. For a stable flow, the upstream and downstream signals measured by two groups of PTs should be identical in shape because the PTs at the upstream and downstream locations were seeing the same water flow, with a time delay (Figure 5.2b).
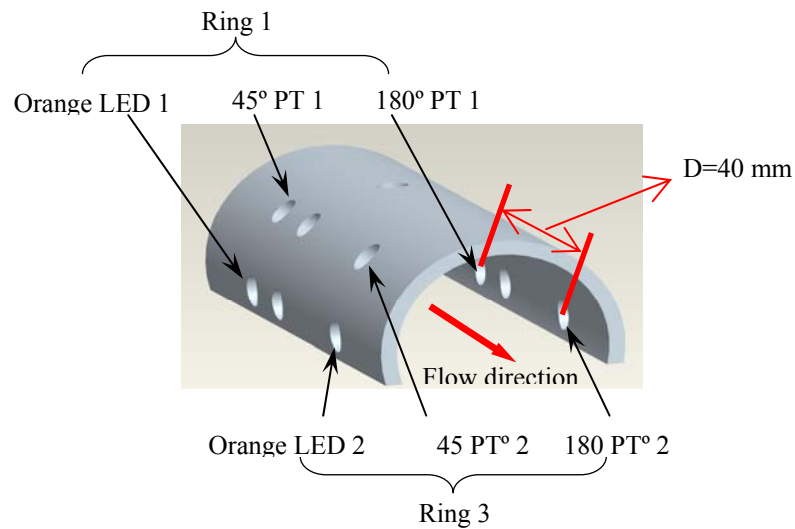
(a)
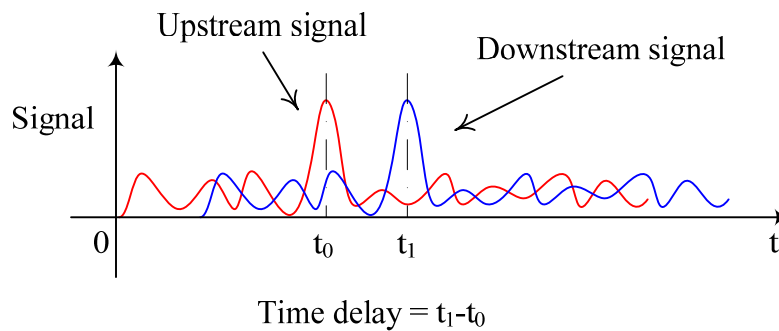
(b)

Figure 5.2 (a) 3-D view of the sensor structure for flow velocity measurement; (b) Identical signals measured at the upstream and downstream locations.

When sediment or air bubbles travel with a stream flow, identical variations in measured transmitted and backscattered light signals can be observed at both upstream and downstream with a time delay. This time delay can be identified as the time at which the cross-correlation coefficient of the upstream and downstream signals reaches the maximum value. By knowing the time delay and the distance between two rings, flow velocity can be determined by dividing the distance by the time delay:

$$V = \frac{D}{T_d} \qquad (5.1)$$

where

V = flow velocity (m/s);

D = distance between two rings (m);

T_d = Time delay between upstream and downstream signals (s).

Assume $X(t)$ and $Y(t)$ represent the upstream and downstream signals, respectively, cross-correlation coefficient ρ_{xy} can be calculated as (Eam-O-Pas et al., 1994):

$$\rho_{xy} = \frac{R_{xy}(\tau)}{\sqrt{R_{xx}(0)} \cdot \sqrt{R_{yy}(0)}} \qquad (5.2)$$

where

τ = time delay;

$R_{xy}(\tau)$ = cross-correlation function;

$R_{xx}(0)$ and $R_{yy}(0)$ = autocorrelation functions.

τ is a continuous variable. It can be calculated by discretization for discrete signals as follows:

$$\tau = ih \qquad (5.3)$$

where

i = number of data points shifting;

h = time interval between data points.

The cross-correlation coefficient for discrete signals is:

$$\rho_{xy} = \frac{\dfrac{1}{N-i}\sum\limits_{n=1}^{N-i}(X_n - \bar{X})(Y_{n+i} - \bar{Y})}{\sqrt{\dfrac{1}{N}\sum\limits_{n=1}^{N}(X_n - \bar{X})^2} \cdot \sqrt{\dfrac{1}{N}\sum\limits_{n=1}^{N}(Y_n - \bar{Y})^2}} \qquad (5.4)$$

where

X_n = data points in the upstream signal series;

Y_n = data points in the downstream signal series;

$\bar{X}$ = mean value of the upstream signal series;

$\bar{Y}$ = mean value of the downstream signal series;

N = number of data points recorded during time period T for each signal series.

Transit time T can be calculated by:

$$T = \frac{i_m}{S} \qquad (5.5)$$

where:

i_m = number of data shifting when the cross-correlation coefficient reached the maximum value;

S = Sampling frequency (Hz).

The cross-correlation coefficient lies between -1 and +1, with zero indicating no correlation between the two signals. Two signals with exactly the same shape have a cross-correlation coefficient of 1. A MATLAB program was developed to conduct the calculation of cross-correlation coefficient (Appendix M).

5.3.3 Preliminary color test

Since natural water flows do not always contain sufficient measurable sediment or air bubbles to generate useable signal patterns for cross-correlation analysis, flow measurement by injecting tagging markers into water flow has its advantages. Possible markers can be color markers, air bubbles, radioactive isotopes, temperature fluctuations, ions, etc. (Beck and Plaskowski, 1987). The injection of dye was selected for flow experiments in this study because various food colors are readily available and food dyes injected to water generally do not change

the density of water. A preliminary experiment was conducted to find the dye color that gives the greatest contrast in light signals generated by an orange LED. Six food dyes (Blue, Green, Pink, Purple, Yellow, Red) purchased from a grocery store were used for the experiment. For each food dye, the same amount of color was added to a fixed volume of water in a plastic container. A Labview program was developed to turn on orange LEDs in the velocity sensor and record sensor signals under each dye color for 5 seconds with a sampling frequency of 2000 Hz (Appendix N). The container and the sensor were fully cleaned after each test.

5.3.4 Flow velocity experiment

Indoor experiments were conducted to test the sensor performance on flow velocity measurement using a closed circulation system. A dye solution with a concentration of 3000 mg/L was used to create measurable signal variations for cross-correlation analysis.

The laboratory setup for flow velocity experiment (Figure 5.3) consisted of a velocity sensor, an F-1000-RB paddle flow rate meter (Blue-White Industries Ltd., Huntington Beach, CA), a compact, submersible centrifugal pump (Grainger, Inc., Chicago, IL) to circulate water, PVC pipes, a signal conditioning unit to convert light to electronic signals, and the dye injection system. The dye injection system consisted of a bottle with specially designed spray header and drop tube (R&D Sprayers, Opelousas, LA), a 12V normally closed solenoid valve (Aerocon Systems Co., San Jose, CA), a 12V air compressor equipped with a 3.5 liter air tank (Omega Research and development, Inc., Douglasville, GA), a pressure reducing valve (McMaster-Carr Supply Company, Robbinsville, NJ), a diaphragm check valve (Ark-Plas Products, Inc., Flippin, AR), two relay circuits to control the air compressor and the solenoid valve, respectively, a car battery as the power supply, and plastic tubing for air or dye.

The open-bottom sensor was modified by adding a rigid plastic tube as the bottom so that it could be connected to the circulation system. The sensor was mounted bottom up because: 1) the dye movement and LED status can be observed through the clear plastic bottom to check the system operations; 2) this orientation allowed most of dye to flow through LED/PT pairs. The flow meter was installed inline with the sensor, following installation directions, to measure the flow rate in Gallon per minute (GPM). A laboratory flow experiment with a total of 11 flow velocity settings and two repeats at each velocity setting was conducted. All GPM values were converted to meter per second (MPS) based on the inside diameter of the sensor tube.
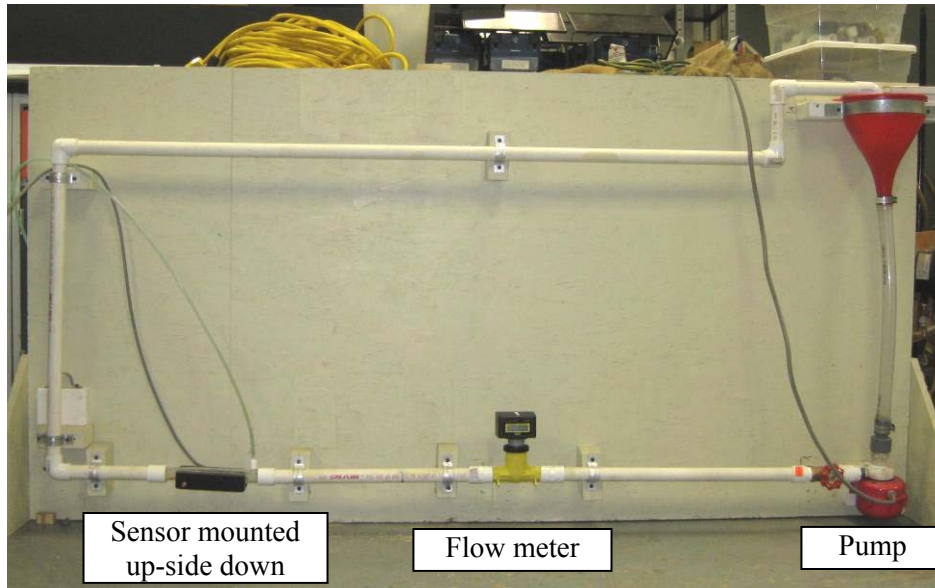
Figure 5.3 Flow velocity laboratory experiment setup using a closed circulation system.

The air compressor worked as the air source and its outlet pressure was regulated to 5psi through the pressure reducing valve. The diaphragm check valve with the cracking pressure of 1 psi was attached at the end of the plastic tubing through a hole on the sensor mounting bracket (Figure 5.4). This normally closed valve required a positive pressure that is higher than its cracking pressure to open. Once the positive pressure disappears, the diaphragm automatically returns back to its original position, closing the valve (SSL, 2009). Figure 5.4 also shows a metal plate attached to the bracket to direct the dye flow. A stretch out view showing the check valve position and the LED/PT pairs of the flow sensor is shown in Figure 5.5. A Labview program (Appendix N) was developed to control the LEDs and the dye flow, and acquire transmitted and backscattered signals using a NI6025E DAQ board (National Instruments Corporation, Austin, TX).
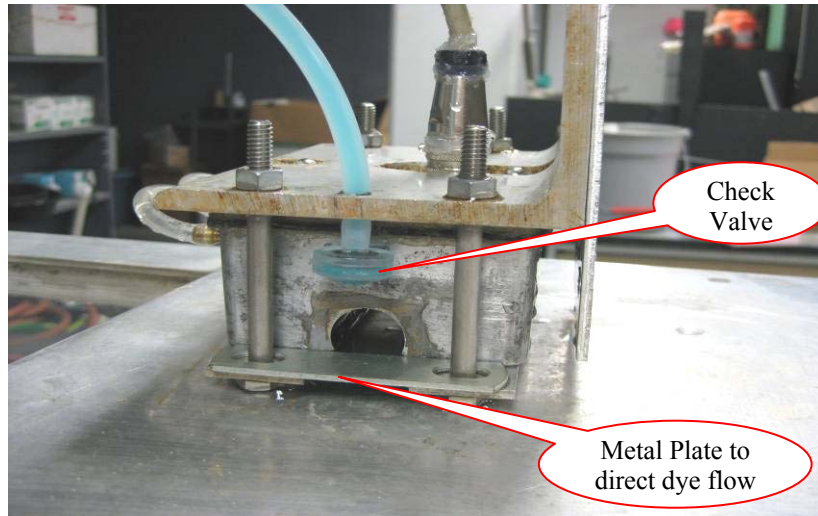
Figure 5.4 A metal piece used to direct the dye flow for velocity measurement.
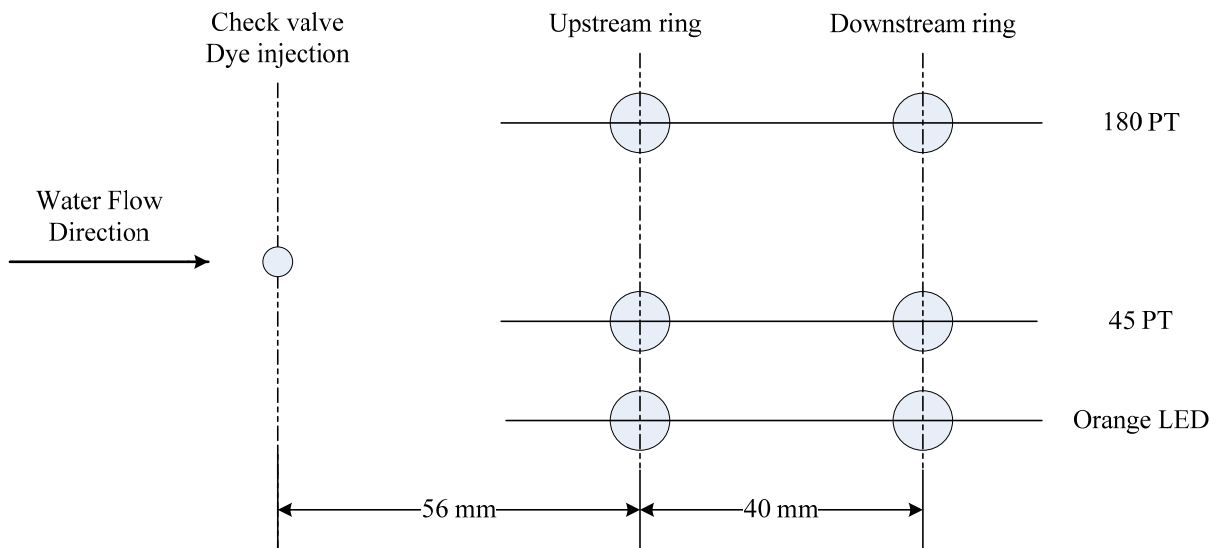
Figure 5.5 Stretch-out view of the flow velocity sensor.

In order to eliminate the air compressor from velocity measurement, the container of dye solution was mounted upside down so that dye can be injected by gravity (Figure 5.6). For this method, a hole was drilled at the bottom of the bottle to allow outside atmospheric pressure to act on dye solution in the bottle.
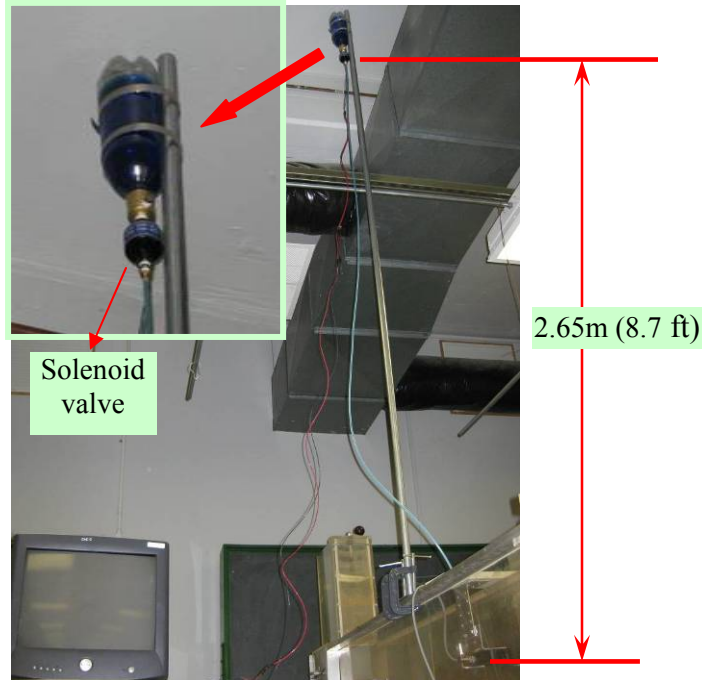
Figure 5.6 Flow velocity injection system using gravity principle.

Because the cracking pressure of the check valve is 1 psi, pressure on the upstream side of the air hose must be greater than 1 psi for the valve to open. The minimum head H, i.e. the hanging height of the dye bottle from the check valve, to achieve a 1 psi pressure, can be calculated as follows (Spellman, 2001).

$$H = \frac{P}{0.433} = \frac{1}{0.433} = 2.31 \,(\text{ft}) \tag{5.4}$$

where

P – cracking pressure of the check valve (psi).

In this study, the bottle was actually hung on the ceiling of the laboratory, which was 2.65m (8.7 feet) from the check valve. This gave 3.77 psi on the check valve when the solenoid valve is turned on.

5.4 Result

5.4.1 Preliminary color test

The preliminary color test showed a significant signal contrast between blue color and clean water (Figure 5.7), which indicated that blue colorant can absorb orange light emitted by the orange LEDs in the velocity sensor. Thus, a dye named Brilliant Blue FCF (CAS number 3844-45-9) was selected for the sensor. This dye is commonly used in foods, drugs and cosmetics. It is soluble in water, and the solution has a maximum absorption at 630 nm (O'Neil et al., 2001). The orange LED used in flow velocity measurement has a peak wavelength of 610 nm. When a drop of dye is flowing through the sensor, lights emitted from the orange LEDs on the upstream and downstream locations are absorbed by the dye, resulting in a significant signal drops for the PTs.
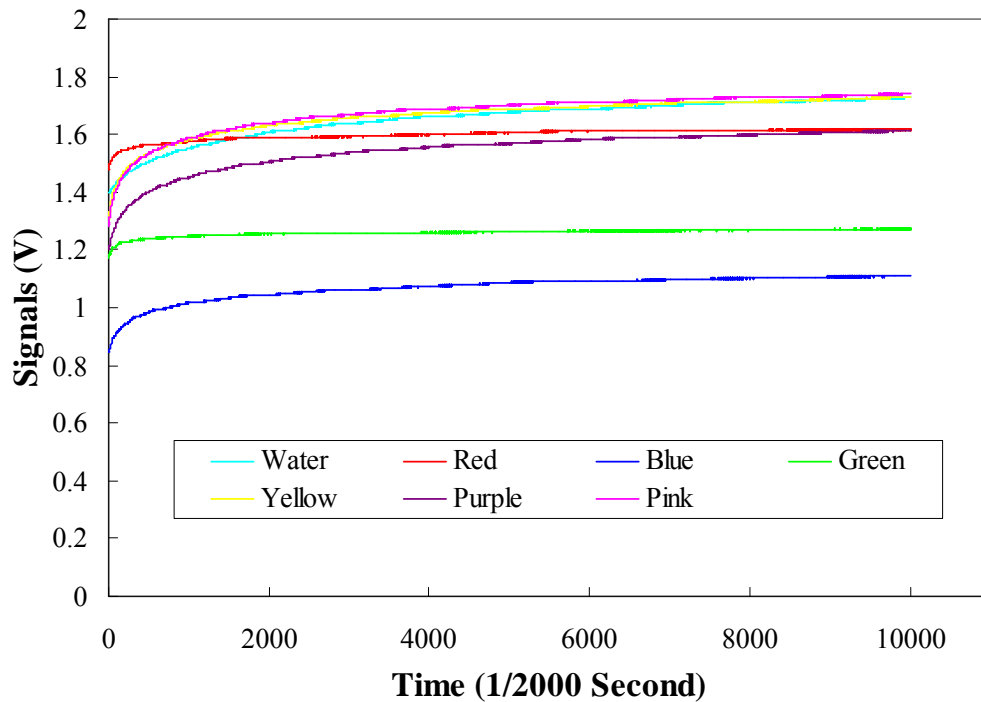
Figure 5.7 Sensor signal responses in different food colors.

5.4.2 *Comparison of velocity measurements using backscattered and transmitted signals*

Signals measured by PTs at 45º angle (ORA45) in the flow velocity sensor and the calculated cross-correlation coefficient are shown in Figure 5.8. The upstream and downstream signals have the same trend but with an obvious time delay. The calculated cross-correlation coefficient is plotted in Figure 5.8b. The time delay was determined when the cross-correlation coefficient reached its first peak.

Signals measured by PTs at 180º angle (ORA180) in the flow velocity sensor are shown in Figure 5.9. The signal fluctuated more than the ORA45 signals (Figure 5.8a). These results indicated that the transmitted light (ORA180) had high sensitivity to dye solution under clean water conditions, but the ORA45 signals were more stable in determination of cross-correlation coefficient for clean water situations. In addition, ORA180 signals tend to decrease and could become insensitive to dye at high sediment concentrations. However, the ORA45 signals will still respond to dye flow under high SSC conditions since it has an increasing trend when the SSC increases. ORA45 PTs are probably more useful than ORA180 PTs in flow velocity measurement.

(a)

Time Delay
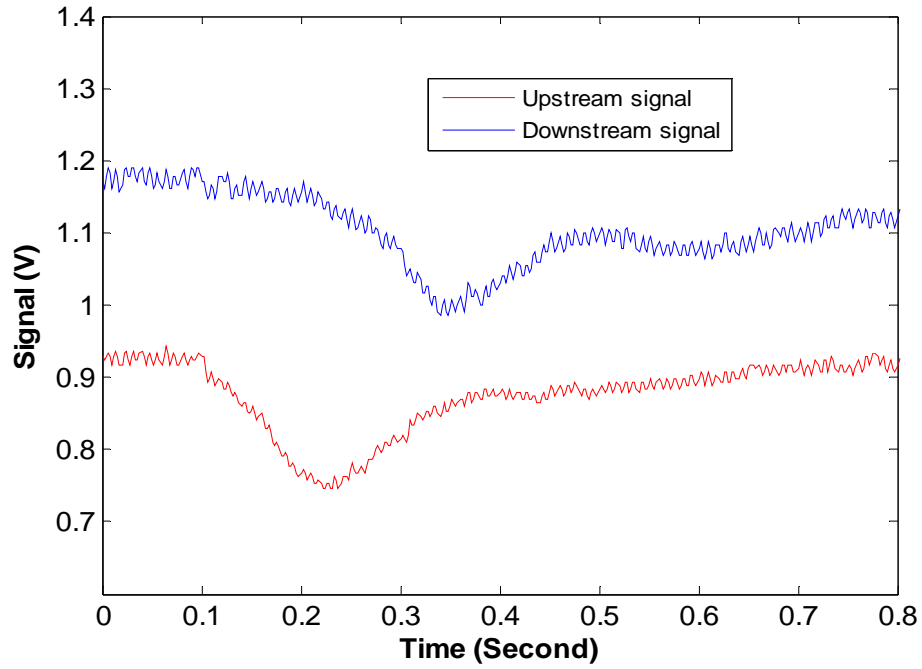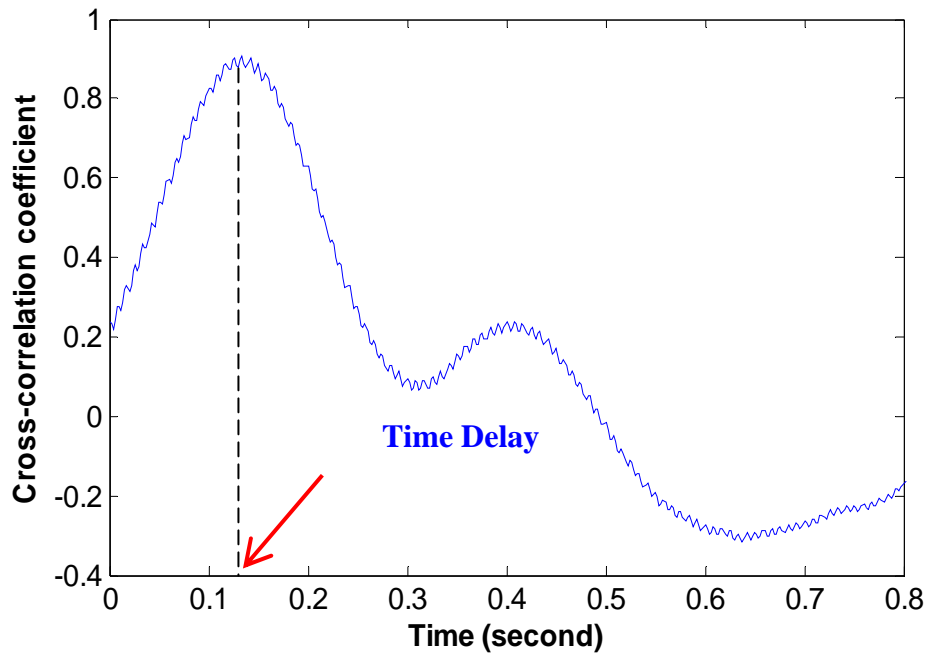
(b)

Figure 5.8 (a) Signals measured by ORA45 PTs in the flow velocity sensor; and (b) cross-correlation coefficient.
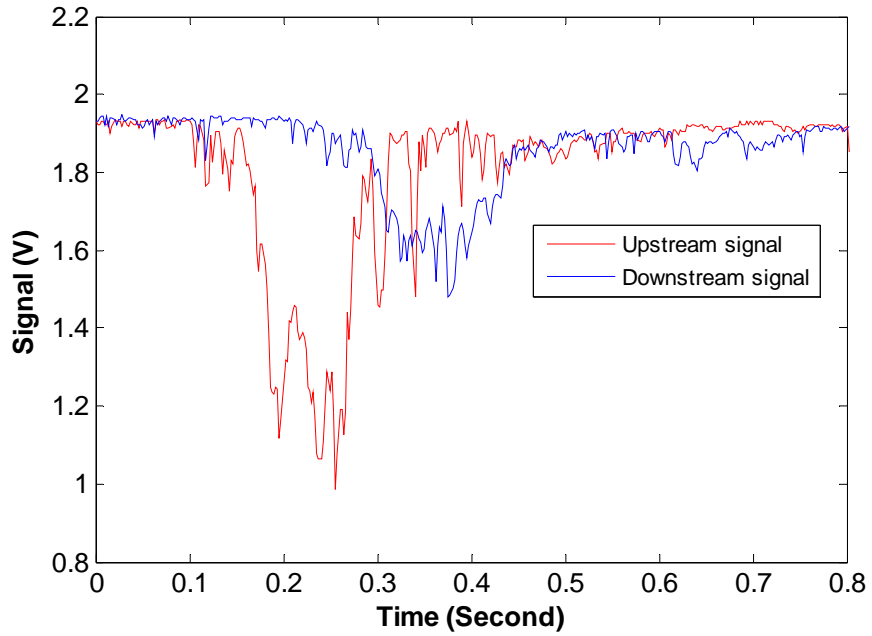
(a)
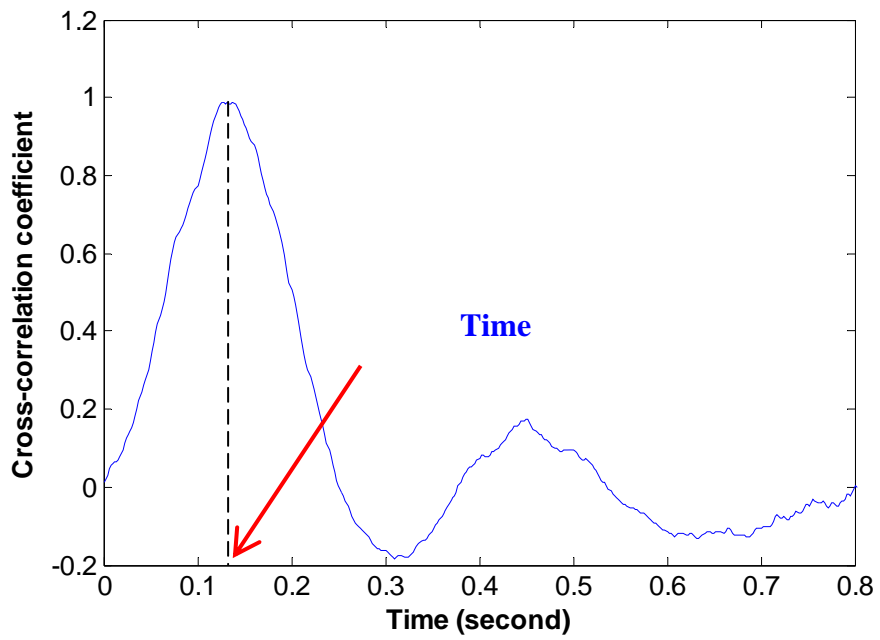
(b)

Figure 5.9 (a) Signals measured by ORA180 PTs in the flow velocity sensor; and (b) cross-correlation coefficient.

5.4.3 Flow velocity experiment

Results of 11 tests using a closed circulation system are shown in Table 5.1. The flow velocities were only calculated from the ORA45 signals. The results showed good agreement between flow velocities measured by the sensor and the flow meter except for measurements conducted at low velocity range (<0.24 m/s). This is because that the flow meter's working range is 3-30 GPM (BWI, 2009), which corresponds to a flow velocity range of 0.66 - 6.64 m/s for the pipe used in the experiment (0.75 inch inside diameter).

Table 5.1 Comparison between sensor measured velocity and flow meter measured velocity (2 repeats for each flow velocity setting).

Flow meter (GPM)	Flow meter (m/s)	Sensor measurement (m/s)
4.83	1.07	1.18
		1.18
4.53	1.00	0.95
		0.95
4.29	0.95	0.95
		0.95
3.78	0.84	0.80
		0.80
3.21	0.71	0.69
		0.69
2.53	0.56	0.61
		0.61
2.04	0.45	0.43
		0.43
1.49	0.33	0.34
		0.34
1.09	0.24	0.28
		0.30
0.49	0.11	0.25
		0.24
0.08	0.02	0.23
		0.22

Flow velocities measured by the sensor and the flow meter within the operating range of the flow meter are compared in Figure 5.10. Taking flow meter results as the true values, the R

120

Square value of the sensor was 0.9715. The Root Mean Square Error (RMSE) of the sensor measurement was 0.05m/s, and the average relative error was 2.89%.
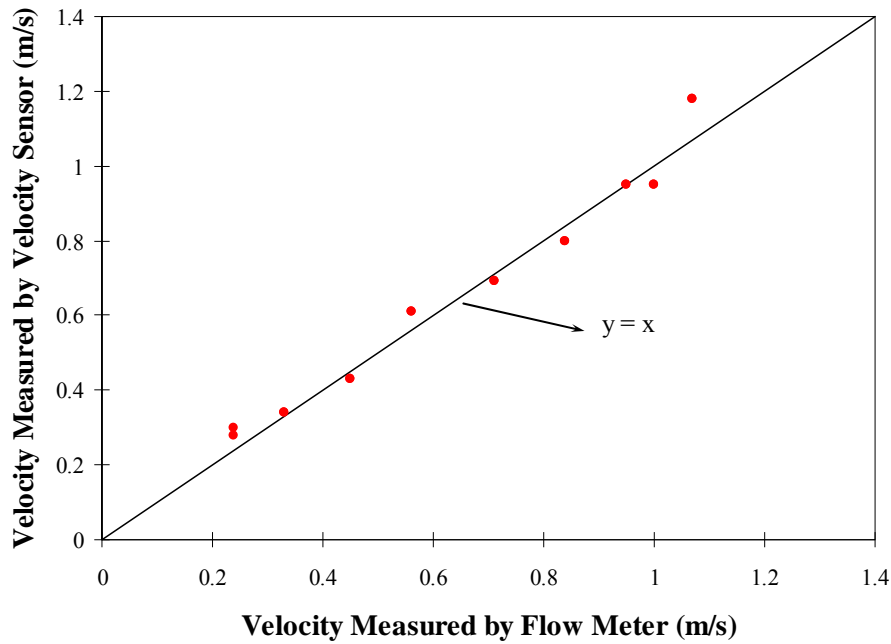
Figure 5.10 Comparison of flow velocities measured by the velocity sensor and the flow meter.

5.5 Conclusion

A cross-correlation-based flow velocity measurement function was added to a previously designed optical sediment sensor by adding a third LED/PT ring. This integrated design provides a low-cost solution for simultaneous measurements of sediment concentration and flow velocity.

A solution of Brilliant Blue FCF has a maximum absorption at 630 nm and can absorb orange light emitted by the orange LEDs which has a peak wavelength of 610nm. Thus, blue colorant Brilliant Blue FCF was selected for flow tests.

Indoor laboratory experiments were conducted to test the sensor performance on flow velocity measurement using a closed circulation system. Results showed good agreement between velocities measured by the sensor and a flow meter. Compared with the flow meter results, the root mean squre error (RMSE) for the measurement was 0.05m/s and the average relative error was 2.89%.

5.6 Acknowledgement

5.7 Reference

Beck, M.S., and A. Plaskowski. 1987. *Cross Correlation Flowmeters – Their Design and Application*. Bristol, England: IOP Publishing Ltd.

Bendat, J.S., and A.G. Piersol. 2000. *Random Data: Analysis and Measurement Procedures*, 3rd ed. New York, NY: John Wiley & Sons, Inc.

Bourke, P. 1996. Cross Correlation. Available at: local.wasp.uwa.edu.au/~pbourke/miscellaneous/correlate/. Accessed 10 April 2009

BWI. 2009. F-1000RB Flowmeter Information. Huntington Beach, CA: Blue-White Industries, Ltd. Available at: www.blue-white.com/Products/ElectronicFlow/F-1000RB/f1000_detail.asp?modelNumber=RB-750MI-GPM1. Accessed 20 April 2009.

Critten, D. L. 1974. Flow velocity measurement. U.S. Patent No. 3844170

Downing, John P.; Sternberg, R. W.; Lister, C. R. B. 1981. New instrumentation for the investigation of sediment suspension processes in the shallow marine environment. *Marine Geology* 42(1-4):19-34.

Eam-o-pas, K., N. Zhang, and M. Schrock. 1994. Monitoring the glass bead dispensing rate for highway striping vehicles. *Institute of Transportation Engineers Journal* 64(4):41-46

Eam-o-pas, K., N. Zhang, and M. Schrock. 1997. Parameter selection for correlation-based particle velocity sensors. *Transactions of the ASAE* 40(5):1501-1508

FWS. 2006. Water Measurement. Lakewood, CO: U.S. Fish and Wildlife Service Mountain-Prairie Region - Water Resources Division. Available at: www.r6.fws.gov/wtr/water_measure.htm. Accessed 1 March 2009.

GPI. 2009. GPI/Water Current Meters. Troy, NY: Gurley Precision Instruments. Available at: www.gpi-hydro.com/meters.htm#Gurley_Price_Meters. Accessed 1 March 2009.

Holmes, Robert R., and Marcelo H. Garcia. 2002. Velocity and Sediment Concentration Measurements over Bedform in Sand-bed Rivers. Available at: www.comm-tec.com/Library/Technical_Papers/USGS/RRHpaper.pdf. Accessed 20 March, 2009.

Hooper, F., and S. L. Kohler. 2000. Measurement of Stream Velocity and Discharge. Michigan Department of Natural Resources. Available at: www.michigandnr.com/PUBLICATIONS/PDFS/ifr/manual/SMII%20Chapter19.pdf. Accessed 1 March 2009.

Huntley, David A., and Daniel M. Hanes. 1987. Direct measurement of suspended sediment transport. In *Coastal Sediments'87, Proceedings of a Speciality Conference on Advances in Understanding of Coastal Sediment Processes*, 723-737. New York, NY: ASCE.

Keech, R. P. 1991. Cross-correlation apparatus and methods. U.S. Patent No. 5029481

O'Neil, M.J., A. Smith, P.E. Heckelman, J.R. Obenchain, J.A.R. Gallipeau, M.A. D'Arecca, and S. Budavari. 2001. *The Merck Index*, 13th ed. Whitehouse Station, NJ: Merch & Co., Inc.

Presto, M. K., A. S. Ogston, C. D. Storlazzi, and M. E. Field. 2006. Temporal and spatial variability in the flow and dispersal of suspended-sediment on a fringing reef flat, Molokai, Hawaii. *Estuarine, Coastal and shelf Science* 67(1): 67-81.

Sherwood, C.R., D. Coats, and B. Walls. 1989. Current and suspended sediment measurements on the central california continental shelf. In *OCEANS '89. Proceedings*, 320-325. New York, NY: IEEE.

Simpson, M.R. 2001. Discharge Measurements Using a Broad-Band Acoustic Doppler Current Profiler. United States Geological Survey Open-file Report 01-1:Sacrmento, California. Available at: pubs.usgs.gov/of/2001/ofr0101/text.pdf. Accessed 7 March 2009.

Spellman, F.R. 2001. Chapter 2: Intermediate waterworks math. In *The Handbook for Waterworks Operator Certification, Volume 2, Intermediate Level*, 15-49. Lancaster, PA: Technomic Publishing Company, Inc.

SSL. 2009. Check Valves. Blythewood, SC: Spirax-Sarco Limited. Available at:www.spiraxsarco.com/resources/steam-engineering-tutorials/pipeline-ancillaries/check-valves.asp. Accessed 10 April 2009.

Stoll, Q. M. 2004. Design of a real-time, optical sediment concentration sensor. MS thesis. Manhattan, Kansas: Kansas State University, Department of Biological and Agricultural Engineering.

USBR. 1997. Water Measurement Manual: A guide to effective water measurement practices for better water management, 3rd edition. Washington DC: US Department of the Interior, Bureau of Reclamation. Superintendent of Documents, Pittsburgh, PA. Available at: www.usbr.gov/pmts/hydraulics_lab/pubs/wmm/index.htm. Accessed 1 March 2009.

Wren, T.A.L., K.P. Do, S.A. Rethlefsen, and B. Healy. 2006. Cross-correlation as a method for comparing dynamic electromyography signals during gait. *Journal of Biomechanics* 39 (2006): 2714-2718.

Zhang, Y., N. Zhang, Q. Stoll, D. Oard, J. Steichen, P. Woodford, P. Barnes, and S. Hutchinson. 2006. Monitoring sediment concentration at a low-water stream crossing using an optical sediment sensor. ASABE Paper No. 063091. St. Joseph, Mich.: ASABE.

Zhang, N., K. Mankin, N. Wang, and S. Hutchinson. 2007. Wireless, continuous, watershed-scale monitoring of stream flow and sediment flux for quantifying BMP impact on reservoir sedimentation. A proposal submitted to USDA-NRI, "Water and Watershed" Program.

Zhang, Y., N. Zhang, G. M. Grimm, C. Johnson, D. Oard, J. Steichen. 2007. Long-term field test of an optical sediment-concentration sensor at low-water stream crossings. ASABE Paper No. 072137. St. Joseph, Mich.: ASABE.

CHAPTER 6 - CONCLUSIONS AND RECOMMENDED FUTURE WORK

6.1 Conclusions

Sediment concentration sensor developed in this study was designed to measure pure suspended sediment concentrations (SSC) in water. Overall statistics analysis indicated that soil texture played an important role in SSC measurement accuracy, whereas water type had a relatively small effect on the sensor performance. Multiple regression models developed for individual soil types all achieved R-square values of higher than 0.99, indicating almost complete elimination of the influence of water color on SSC measurement accuracy. When all five soil types were combined, the R-square value was reduced to 0.8802. Multiple regression models established for individual water types had R-square values of higher than 0.89, indicating that water color has relatively limited impact on SSC measurement accuracy.

Neural-network models were developed to predict SSC. R-square values of greater than 0.94 were achieved for the calibration and two validation datasets taken at all soil type and water type combinations, indicating that the neural-network models can further remove the influence of soil texture type on SSC measurement.

In order to avoid over-fitting in prediction models and allow a simpler sensor design, the optical sediment sensor was simplified from a "three-ring" design to a "two-ring" design based on a statistical "stepwise selection" analysis.

Results of an outdoor experiment indicated that a relative light index based on light modulation was capable of reducing the impact of ambient light on sensor measurement.

Long-term field experiments conducted in Kansas and Georgia indicated that the optical sediment sensor was capable of long-term, real-time SSC monitoring. The effect of temperature on SSC measurement was studied using grab samples taken within a seven-month period. R-square values of 0.9776 and 0.9773 were achieved for prediction models established without and with temperature compensation for SSC greater than 500mg/L, respectively. For SSC lower than 500mg/L, the R-square values were 0.9015 and 0.9057, respectively. An ANOVA analysis indicated that temperature had no significant effect on sensor signals at a 0.01 significance level.

Signals of the optical sediment sensor deteriorated from fouling during the long-term field experiments. Fouling on optical lenses caused the transmitted signal to decrease and the backscattered signal to increase. A signal correction algorithm was developed by determining the fouling trend through a regression analysis on peak signal values taken during no-rain periods. The field experiment at Fort Benning indicated that the open-bottom design of sensor case provided higher-quality signals than the closed-bottom design, mainly because of reduced clogging and fouling problems.

In order to reduce fouling problems, an air-blast cleaning mechanism was integrated into the optical sediment sensor. Laboratory experiments in manually created fouling environments were conducted to study the fouling on sensors with aluminum and polyethylene cases, and to evaluate the effectiveness of the air-blast cleaning. Two types of fouling, clay/silt fouling due to clay/silt accumulation on sensor lenses and bio-fouling due to bacterial contamination, were observed on sensors. Both forms of fouling caused transmitted signals to decrease and backscattered signals to increase. Results showed that air-blast cleaning was capable of removing clay/silt fouling on sensor signals. Aluminum sensors experienced severe bio-fouling even with air-blast cleaning. The effect of biofouling was not significant on sensors with polyethylene sensors. The current design of embedded air paths in polyethylene sensors needs to be modified to allow more effective cleaning. Higher cleaning frequency and longer cleaning duration would help enhance the cleaning power.

A cross-correlation-based flow velocity measurement function was added to the optical sediment sensor by adding a third LED/PT ring. This integrated design provided a low-cost solution for simultaneous measurement of sediment concentration and flow velocity. The solution of Brilliant Blue FCF was selected for flow experiments as artificial tagging markers. It has a maximum absorption at 630 nm and can absorb orange light emitted by the orange LEDs which has a peak wavelength of 610nm. Results of laboratory flow tests conducted in a closed circulation system showed good agreement between velocities measured using the sensor and a flow meter. The RMS errors of the measurement was 0.05m/s and the average relative error was 2.89% when compared with the flow meter.

6.2 Recommended Future Work

The indoor cleaning experiment has proved that the air-blast cleaning mechanism was capable of removing fouling on sensor lenses. However, the current air outlet design did not allow the pressurized air to be blasted directly onto the lenses. Redesign of the air passages is highly recommended.

Another problem is electric power supply for the cleaning mechanism for field deployment, especially when higher cleaning frequency and longer cleaning duration are needed. This is especially critical if an air-blast cleaning system has to be responsible for an array of sensors at the same installation site. A more efficient air pressure source that consumes less power consumption is recommended.

In this study, flow experiments were conducted within a limited velocity range. Future research work on flow velocity measurements using equipment with an expanded velocity range is highly recommended. If situation permits, hydraulic equipment that provides stable, laminar flow should be developed for the experiments. In addition, the laboratory flow experiments were only conducted with clean water. Future laboratory and field experiments on water flows with various sediment concentrations will need to be conducted to verify the sensor performance on simultaneous SSC and flow velocity measurement.

Appendix A - Schematics of Sensor Signal Conditioning Circuit

128
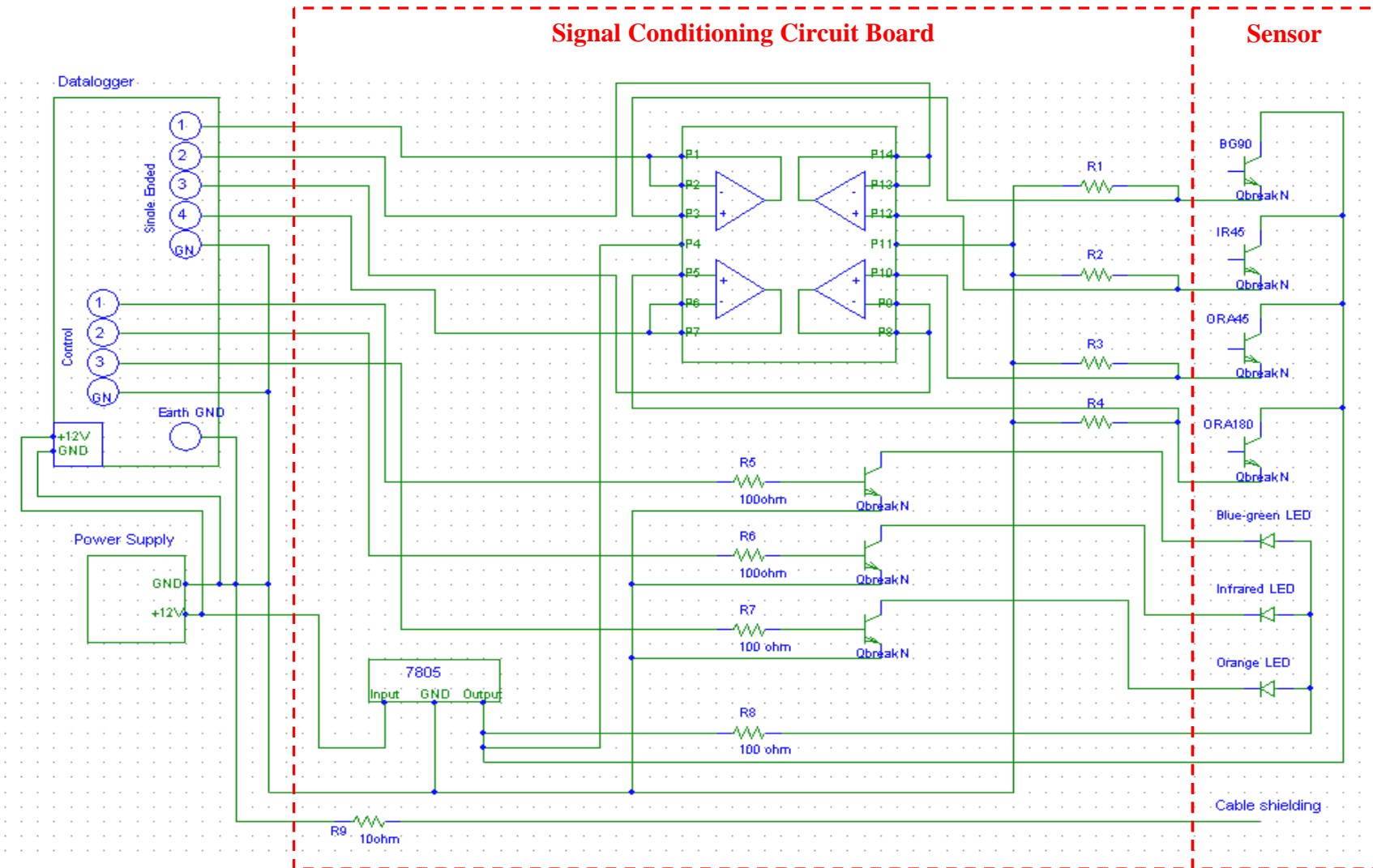
Appendix B - CR5000 Program for Laboratory Calibration

```
'CR5000
'Yali Zhang
'8/22/2004
'Suspended sediment sensor program

'//////////////////// Variable declarations ///////////////////
Dim photran(18)
Dim averag(18)
Dim i,j,k
Dim Trigger

'////////////////////// Data tables setup ///////////////////
DataTable(result,1,1000)
        DataInterval(0,0,0,0)
        Sample(18,photran(),FP2)
EndTable

DataTable(avresult,1,50)
        DataInterval (0,0,0,0)
        Sample(18,averag(),FP2)
EndTable

'/////////////// Main program and scanning setup ///////////////
BeginProg

For i=0 to 32 step 1

        do
                readio(Trigger,&B10000000)

                if Trigger=0 then
                        writeio(&B1000000,&B0000000)
                else
                        writeio(&B1000000,&B1000000)
                        exitdo
                endif

        loop

        For j = 0 To 499 Step 1          'loop for 30 seconds

                Scan(60,msec,2,1)

                        Portset(1,1)
                        VoltSE(photran(1),3,0,1,1,400,2000,1,0)
```

```
Portset(1,0)
VoltSE(photran(4),3,0,1,1,400,2000,1,0)

Portset(2,1)
VoltSE(photran(7),3,0,4,1,400,2000,1,0)

Portset(2,0)
VoltSE(photran(10),3,0,4,1,400,2000,1,0)

Portset(3,1)
VoltSE(photran(13),3,0,7,1,400,2000,1,0)

Portset(3,0)
VoltSE(photran(16),3,0,7,1,400,2000,1,0)

For k = 1 TO 18 step 1
        If photran(k)= NAN Then
                WriteIO(&B1000,&B1000)
        End If
Next k

Avgrun(averag,18,photran(),500)

CallTable result

    NextScan

Next j

CallTable avresult

Next i

writeio(&B01000000,&B0)

EndProg
```

Appendix C - Neural Network Program for Laboratory Experiment Analysis

```matlab
clear all;

%import data
data=xlsread('anndata.xls','a2:m1981');
BG=[data(1:1980,5)./-5500 data(1:1980,6)./-5500 data(1:1980,7)./-5500 data(1:1980,8)./-5500
data(1:1980,9)./-5500 data(1:1980,10)./-5500 data(1:1980,11)./-5500 data(1:1980,12)./-5500
data(1:1980,13)./-5500 data(1:1980,4)./5000];

%replication 2 as calibration set;
A=BG(661:1320,1:9)';
T=BG(661:1320,10)';
VA=BG(1:660,1:9)';
VT=BG(1:660,10)';
TA=BG(1321:1980,1:9)';
TT=BG(1321:1980,10)';

% %replication 1 as calibration set;
% A=BG(1:660,1:9)';
% T=BG(1:660,10)';
% VA=BG(661:1320,1:9)';
% VT=BG(661:1320,10)';
% TA=BG(1321:1980,1:9)';
% TT=BG(1321:1980,10)';

% %replication 3 as calibration set;
% A=BG(1321:1980,1:9)';
% T=BG(1321:1980,10)';
% VA=BG(661:1320,1:9)';
% VT=BG(661:1320,10)';
% TA=BG(1:660,1:9)';
% TT=BG(1:660,10)';

output=[];
result=[];
for n=3:9
%Training
net=newff(minmax(A),[n,1],{'tansig','tansig'},'trainlm');
net=init(net);

    for i=1:60
        net.trainParam.epochs=1; %Maximum number of epochs to train
        net.trainParam.show=5; %Epochs between showing progress
        net.trainParam.goal=0.0001; %Performance goal
```

```matlab
    net.trainParam.max_fail=5; %Maximum validation failures
    net.trainParam.mem_reduc=1; %Factor to use for memory/speed tradeoff
    net.trainParam.min_grad=1e-10; %Minimum performance gradient
    net.trainParam.mu=0.001; %Initial Mu
    net.trainParam.mu_dec=0.1; %Mu decrease factor
    net.trainParam.mu_inc=10; %Mu increase factor
    net.trainParam.mu_max=1e10; %Maximum Mu
    net.trainParam.time=inf; %Maximum time to train in second
    [net,tr]=train(net,A,T);

    %Simulation and calculation
    Y1=sim(net,A);
    rmse_a=sqrt(var(T-Y1).*559./555.*5000.*5000);
    rsq_a=corrcoef(T,Y1).*corrcoef(T,Y1);
    Y2=sim(net,VA);
    rmse_va=sqrt(var(VT-Y2).*559./555.*5000.*5000);
    rsq_va=corrcoef(VT,Y2).*corrcoef(VT,Y2);
    Y3=sim(net,TA);
    rmse_ta=sqrt(var(TT-Y3).*559./555.*5000.*5000);
    rsq_ta=corrcoef(TT,Y3).*corrcoef(TT,Y3);

    resultnew=[n i rmse_a rmse_va rmse_ta rsq_a(2,1) rsq_va(2,1) rsq_ta(2,1)];
    result=[result;resultnew];

  end;
  outputnew=[n Y1];
  output=[output;outputnew];
end;

%export files
xlswrite('result',result);
```

Appendix D - SAS Program for Laboratory Experiment Analysis

SAS Program:

```
*option ls=80;
proc import dbms=excel out=one replace
  datafile='c:\zhangyl\Dissertation\Statistics\March08\data.xls';
  getnames=yes;
run;
data yalidata;
set one (firstobs=2 rename=(replication=run Repeated=rep));
format concentration 6.2;
run;

Title 'BG45';
proc mixed data=yalidata ;
        class run water soil rep;
        model BG45= water soil water*soil concentration concentration*water concentration*soil
concentration*water*soil;
        *lsmeans water soil water*soil con con*water con*soil /pdiff cl ;
   *lsmeans con*soil/pdiff ;
     random rep(water*soil) run;
run;

Title 'BG90';
proc mixed data=yalidata ;
        class run water soil rep;
        model BG90= water soil water*soil concentration concentration*water concentration*soil
concentration*water*soil;
        *lsmeans water soil water*soil con con*water con*soil /pdiff cl ;
   *lsmeans con*soil/pdiff ;
     random rep(water*soil) run;
run;

Title 'BG180';
proc mixed data=yalidata ;
        class run water soil rep;
        model BG180= water soil water*soil concentration concentration*water concentration*soil
concentration*water*soil;
        *lsmeans water soil water*soil con con*water con*soil /pdiff cl ;
   *lsmeans con*soil/pdiff ;
     random rep(water*soil) run;
run;

Title 'IR45';
proc mixed data=yalidata ;
```

```
        class run water soil rep;
        model IR45= water soil water*soil concentration concentration*water concentration*soil
concentration*water*soil;
        *lsmeans water soil water*soil con con*water con*soil /pdiff cl ;
   * lsmeans con*soil/pdiff ;
     random rep(water*soil) run;
run;

Title 'IR90';
proc mixed data=yalidata ;
        class run water soil rep;
        model IR90= water soil water*soil concentration concentration*water concentration*soil
concentration*water*soil;
        *lsmeans water soil water*soil con con*water con*soil /pdiff cl ;
   * lsmeans con*soil/pdiff ;
     random rep(water*soil) run;
run;

Title 'IR180';
proc mixed data=yalidata ;
        class run water soil rep;
        model IR180= water soil water*soil concentration concentration*water concentration*soil
concentration*water*soil;
        *lsmeans water soil water*soil con con*water con*soil /pdiff cl ;
   *lsmeans con*soil/pdiff ;
     random rep(water*soil) run;
run;

Title 'ORA45';
proc mixed data=yalidata ;
        class run water soil rep;
        model ORA45= water soil water*soil concentration concentration*water concentration*soil
concentration*water*soil;
        *lsmeans water soil water*soil con con*water con*soil /pdiff cl ;
   * lsmeans con*soil/pdiff ;
     random rep(water*soil) run;
run;

Title 'ORA90';
proc mixed data=yalidata ;
        class run water soil rep;
        model ORA90= water soil water*soil concentration concentration*water concentration*soil
concentration*water*soil;
        *lsmeans water soil water*soil con con*water con*soil /pdiff cl ;
   *lsmeans con*soil/pdiff ;
     random rep(water*soil) run;
run;

Title 'ORA180';
proc mixed data=yalidata ;
        class run water soil rep;
```

```
        model ORA180= water soil water*soil concentration concentration*water concentration*soil
concentration*water*soil;
        *lsmeans water soil water*soil con con*water con*soil /pdiff cl ;
   *lsmeans con*soil/pdiff ;
    random rep(water*soil) run;
run;
```

SAS Output:

1. BG45

Effect	Num DF	Den DF	F Value	Pr > F
Water	3	40	1.85	0.1545
Soil	4	40	30.80	<.0001
Water*Soil	12	40	1.31	0.2533
Concentration	1	1898	25794.7	<.0001
Concentration*Water	3	1898	5.13	0.0016
Concentration*Soil	4	1898	820.53	<.0001
Concentra*Water*Soil	12	1898	3.00	0.0004

2. BG90

Effect	Num DF	Den DF	F Value	Pr > F
Water	3	40	12.18	<.0001
Soil	4	40	44.01	<.0001
Water*Soil	12	40	7.42	<.0001
Concentration	1	1898	879.30	<.0001
Concentration*Water	3	1898	2.01	0.1100
Concentration*Soil	4	1898	204.51	<.0001
Concentra*Water*Soil	12	1898	0.51	0.9108

3. BG180

Effect	Num DF	Den DF	F Value	Pr > F
Water	3	40	1.99	0.1303
Soil	4	40	65.97	<.0001
Water*Soil	12	40	0.23	0.9959
Concentration	1	1898	19462.4	<.0001
Concentration*Water	3	1898	0.15	0.9289
Concentration*Soil	4	1898	158.66	<.0001
Concentra*Water*Soil	12	1898	0.15	0.9996

4. IR45

Effect	Num DF	Den DF	F Value	Pr > F
Water	3	40	2.59	0.0663
Soil	4	40	20.17	<.0001
Water*Soil	12	40	0.69	0.7487
Concentration	1	1898	132113	<.0001
Concentration*Water	3	1898	3.54	0.0141
Concentration*Soil	4	1898	3084.04	<.0001
Concentra*Water*Soil	12	1898	4.21	<.0001

5. IR90

Effect	Num DF	Den DF	F Value	Pr > F
Water	3	40	12.53	<.0001
Soil	4	40	31.12	<.0001
Water*Soil	12	40	28.27	<.0001
Concentration	1	1898	19665.9	<.0001
Concentration*Water	3	1898	2.67	0.0459
Concentration*Soil	4	1898	354.07	<.0001
Concentra*Water*Soil	12	1898	3.24	0.0001

6. IR180

Effect	Num DF	Den DF	F Value	Pr > F
Water	3	40	2.55	0.0691
Soil	4	40	56.62	<.0001
Water*Soil	12	40	0.91	0.5467
Concentration	1	1898	80740.9	<.0001
Concentration*Water	3	1898	2.06	0.1034
Concentration*Soil	4	1898	1906.71	<.0001
Concentra*Water*Soil	12	1898	1.43	0.1439

7. ORA45

Effect	Num DF	Den DF	F Value	Pr > F
Water	3	40	0.29	0.8296
Soil	4	40	28.15	<.0001
Water*Soil	12	40	0.87	0.5817
Concentration	1	1898	112033	<.0001
Concentration*Water	3	1898	7.80	<.0001
Concentration*Soil	4	1898	4052.52	<.0001
Concentra*Water*Soil	12	1898	3.85	<.0001

8. ORA90

```
                                         Num    Den
        Effect                            DF     DF    F Value    Pr > F

        Water                              3     40      1.11     0.3560
        Soil                               4     40     66.69     <.0001
        Water*Soil                        12     40      3.23     0.0026
        Concentration                      1   1898   5846.22     <.0001
        Concentration*Water                3   1898      1.20     0.3077
        Concentration*Soil                 4   1898    193.19     <.0001
        Concentra*Water*Soil              12   1898      1.54     0.1038
```

9. ORA180

```
                                         Num    Den
        Effect                            DF     DF    F Value    Pr > F

        Water                              3     40      7.13     0.0006
        Soil                               4     40     69.21     <.0001
        Water*Soil                        12     40      4.03     0.0004
        Concentration                      1   1898   39528.3     <.0001
        Concentration*Water                3   1898      0.22     0.8802
        Concentration*Soil                 4   1898    621.92     <.0001
        Concentra*Water*Soil              12   1898      0.48     0.9288
```

Proc mixed summary

Signal	Pr > F						
	Water	**Soil**	**Water*Soil**	**Conc.**	**Water*Conc.**	**Soil*Conc.**	**Water*Soil*Conc.**
BG45	0.1545	<0.0001	0.2533	<0.0001	0.0016	<0.0001	0.0004
BG90	<0.0001	<0.0001	<0.0001	<0.0001	0.1100	<0.0001	0.9108
BG180	0.1303	<0.0001	0.9959	<0.0001	0.9289	<0.0001	0.9996
IR45	0.0663	<0.0001	0.7487	<0.0001	0.0141	<0.0001	<0.0001
IR90	<0.0001	<0.0001	<0.0001	<0.0001	0.0459	<0.0001	0.0001
IR180	0.0691	<0.0001	0.5467	<0.0001	0.1034	<0.0001	0.1439
ORA45	0.8296	<0.0001	0.5817	<0.0001	<0.0001	<0.0001	<0.0001
ORA90	0.3560	<0.0001	0.0026	<0.0001	0.3077	<0.0001	0.1038
ORA180	0.0006	<0.0001	0.0004	<0.0001	0.8802	<0.0001	0.9288

Appendix E - SAS Program for Stepwise Selection in Laboratory Experiment

SAS Program:

```
*option ls=80;
proc import dbms=excel out=one replace
datafile = 'c:\zhangyl\Dissertation\Statistics\data.xls';
getnames=yes;
run;

data yalidata;
set one (firstobs=2 rename=(replication=run Repeated=rep));
format concentration 6.2;
run;

Title 'Stepwise selection';
proc reg;
        model concentration = BG180 BG90 BG45 IR180 IR90  IR45 ORA180 ORA90  ORA45
/selection=stepwise;
run;

Title 'Residual plot for all 9 variables';
proc reg;
        model concentration = BG180 BG90 BG45 IR180 IR90  IR45 ORA180 ORA90  ORA45/r;
        plot r.*p.;
        output out=sun r=residual ;
run;

Title 'Residual plot for 4 selected variables';
proc reg;
        model concentration =BG90 IR45 ORA180 ORA45/r;
        plot r.*p.;
        output out=sun r=residual ;
run;

Title 'Residual plot for 3 variables with BG90 excluded';
proc reg;
        model concentration = IR45 ORA180 ORA45/r;
        plot r.*p.;
        output out=sun r=residual ;
run;
```

SAS Output:

```
                              Analysis of Variance

                                  Sum of          Mean
        Source                DF   Squares        Square   F Value   Pr > F

        Model                  8  3915357432    489419679   1540.29   <.0001
        Error               1971   626276460       317746
        Corrected Total     1979  4541633892
```

```
                              The REG Procedure
                               Model: MODEL1
                   Dependent Variable: Concentration Concentration

                           Stepwise Selection: Step 8

                           Parameter     Standard
            Variable        Estimate        Error    Type II SS   F Value  Pr > F

            Intercept    -4556.79382     611.39553     17650366     55.55  <.0001
            BG180            0.55182       0.20668      2265108      7.13   0.0076
            BG90            -1.50083       0.12654     44700375    140.68   <.0001
            BG45             0.49555       0.13794      4101081     12.91   0.0003
            IR90             0.45254       0.11009      5369250     16.90   <.0001
            IR45            -5.16949       0.24440    142155940    447.39   <.0001
            ORA180          -1.40801       0.19717     16203110     50.99   <.0001
            ORA90            1.79209       0.45890      4845770     15.25   <.0001
            ORA45            1.98601       0.22454     24858198     78.23   <.0001
```

```
                           Summary of Stepwise Selection

        Variable     Variable                Number  Partial   Model
   Step Entered      Removed       Label     Vars In R-Square R-Square   C(p)    F Value Pr > F

     1  IR45                       IR45          1    0.8258   0.8258  512.659 9379.64 <.0001
     2  ORA45                      ORA45         2    0.0094   0.8352  380.946  112.25 <.0001
     3  BG90                       BG90          3    0.0161   0.8513  153.535  213.27 <.0001
     4  ORA180                     ORA180        4    0.0090   0.8602   27.3269  126.78 <.0001
     5  BG45                       BG45          5    0.0003   0.8605   24.8292    4.46 0.0349
     6  IR90                       IR90          6    0.0004   0.8610   20.5263    6.26 0.0124
     7  ORA90                      ORA90         7    0.0006   0.8616   13.6483    8.85 0.0030
     8  BG180                      BG180         8    0.0005   0.8621    8.5214    7.13 0.0076
```

139

Appendix F - SAS Program for Outdoor Ambient Light Experiment

Correlation analysis between regulated signal and ambient light:

SAS Program:

```
*option ls=80;
proc import dbms=excel out=one replace
datafile = 'c:\zhangyl\Dissertation\Statistics\outdoor.xls';
getnames=yes;
run;

proc corr data=one;
var BG90ON_OFF IR45ON_OFF ORA45ON_OFF ORA180ON_OFF;
with Ambient_Light ;
run;

proc sort data=one out=eachtrial;
by trial;
run;
proc corr data=eachtrial;
var BG90ON_OFF IR45ON_OFF ORA45ON_OFF ORA180ON_OFF;
with Ambient_Light ;
by trial;
run;

proc sort data=one out=sorted;
        by concentration;
run;
proc corr data=sorted;
  var BG90ON_OFF IR45ON_OFF ORA45ON_OFF ORA180ON_OFF;
with Ambient_Light ;
by concentration;
run;
```

<u>SAS Output:</u>

1. Across all concentrations:

```
                    Pearson Correlation Coefficients, N = 216
                           Prob > |r| under HO: Rho=0


                        BG900N_        IR45ON_       ORA45ON_      ORA180ON_
                           OFF            OFF            OFF            OFF


        Ambient_Light    0.48823       -0.44514       -0.49495        0.50365
        Ambient_Light     <.0001         <.0001         <.0001         <.0001
```

2. At each trial:

Concentration level (mg/L)	Ambient light vs. BG90on-off		Ambient light vs. IR45on-off		Ambient light vs. ORA45on-off		Ambient light vs. ORA180on-off	
	Coefficient	P-valve	Coefficient	P-valve	Coefficient	P-valve	Coefficient	P-valve
Trial 1	0.45047	<.0001	-0.36189	0.0018	-0.37956	0.0010	0.41872	0.0003
Trial 2	0.55233	<.0001	-0.50833	<.0001	-0.57059	<.0001	0.55054	<.0001
Trial 3	0.47143	<.0001	-0.48787	<.0001	-0.56739	<.0001	0.56530	<.0001

3. At each concentration:

Concentration level (mg/L)	Ambient light vs. BG90on-off		Ambient light vs. IR45on-off		Ambient light vs. ORA45on-off		Ambient light vs. ORA180on-off	
	Coefficient	P-valve	Coefficient	P-valve	Coefficient	P-valve	Coefficient	P-valve
0	0.39466	0.1051	0.44924	0.0614	-0.09127	0.7187	-0.02347	0.9263
200	0.64922	0.0036	0.54048	0.0206	-0.15248	0.5458	0.02853	0.9105
400	0.71511	0.0009	0.32778	0.1842	-0.11634	0.6457	0.14325	0.5707
600	0.58927	0.0101	0.33433	0.175	-0.19447	0.4394	0.29669	0.2319
800	0.55244	0.0174	0.03021	0.9053	-0.31599	0.2015	0.33497	0.1742
1000	0.49683	0.0359	-0.20987	0.4037	-0.26824	0.2818	0.34721	0.1580
1200	0.55971	0.0157	-0.28277	0.2556	-0.19530	0.4374	0.37834	0.1216
1500	0.60123	0.0083	-0.16042	0.5249	-0.09917	0.6954	0.21623	0.3888
2000	0.34136	0.1656	0.60285	0.0081	0.36883	0.1320	-0.52883	0.0240
4000	-0.7732	0.0002	0.99989	<0.0001	0.53789	0.0213	-0.9541	<0.0001
6000	-0.90048	<0.0001	1.000	<0.0001	0.3049	0.2186	-0.93416	<0.0001
8000	-0.83569	<0.0001	1.000	<0.0001	-0.00989	0.9689	-0.85264	<0.0001

Appendix G - CR10X Program for Laboratory Calibration

;{CR10X}
;Yali Zhang
;4/29/2006
;Suspended Sediment Sensor Calibration Program

*Table 1 Program
01:0.0625   Execution Interval (seconds)

1: Read Ports (P25)
 1: 16   Mask (0..255)
 2: 1   Loc [trigger   ]

2: If (X<=>F) (P89)
 1: 1   X Loc [trigger   ]
 2: 1   =
 3: 16   F
 4: 30   Then Do

3: Beginning of Loop (P87)
 1: 1   Delay
 2: 80   Loop Count

4: Do (P86)
 1: 10   Set Output Flag High (Flag 0)

5: Real Time (P77)
 1: 221   Day,Hour/Minute,Seconds (midnight = 2400)

6: Set Port(s) (P20)
 1: 0000   C8,C7,C6,C5 Options
 2: 0001   C4..C1 = low/low/low/high

7: Volt (SE) (P1)
 1: 1   Reps
 2: 15   2500 mV Fast Range
 3: 1   SE Channel
 4: 2   Loc [bg90on   ]
 5: 1   Mult
 6: 0   Offset

8: Sample (P70)
 1: 1   Reps
 2: 2   Loc [bg90on   ]

9: Set Port(s) (P20)

143

1: 0000   C8..C5 = low/low/low/low
2: 0000   C4,C3,C2,C1 Options

10: Volt (SE) (P1)
1: 1   Reps
2: 15   2500 mV Fast Range
3: 1   SE Channel
4: 3   Loc [bg90off   ]
5: 1   Mult
6: 0   Offset

11: Sample (P70)
1: 1   Reps
2: 3   Loc [bg90off   ]

12: Set Port(s) (P20)
1: 0000   C8,C7,C6,C5 Options
2: 0010   C4..C1 = low/low/high/low

13: Volt (SE) (P1)
1: 1   Reps
2: 15   2500 mV Fast Range
3: 2   SE Channel
4: 4   Loc [ir45on   ]
5: 1   Mult
6: 0   Offset

14: Sample (P70)
1: 1   Reps
2: 4   Loc [ir45on   ]

15: Set Port(s) (P20)
1: 0000   C8,C7,C6,C5 Options
2: 0000   C4,C3,C2,C1 Options

16: Volt (SE) (P1)
1: 1   Reps
2: 15   2500 mV Fast Range
3: 2   SE Channel
4: 5   Loc [ir45off   ]
5: 1   Mult
6: 0   Offset

17: Sample (P70)
1: 1   Reps
2: 5   Loc [ir45off   ]

18: Set Port(s) (P20)
1: 0000   C8,C7,C6,C5 Options
2: 0100   C4..C1 = low/high/low/low

144

19: Volt (SE) (P1)
 1: 2   Reps
 2: 15   2500 mV Fast Range
 3: 3   SE Channel
 4: 6   Loc [orgon_1   ]
 5: 1   Mult
 6: 0   Offset

20: Sample (P70)
 1: 2   Reps
 2: 6   Loc [orgon_1   ]

21: Set Port(s) (P20)
 1: 0000   C8,C7,C6,C5 Options
 2: 0000   C4,C3,C2,C1 Options

22: Volt (SE) (P1)
 1: 2   Reps
 2: 15   2500 mV Fast Range
 3: 3   SE Channel
 4: 8   Loc [orgoff_1]
 5: 1   Mult
 6: 0   Offset

23: Sample (P70)
 1: 2   Reps
 2: 8   Loc [orgoff_1]

24: Internal Temperature (P17)
 1: 10   Loc [panel   ]

25: Thermocouple Temp (DIFF) (P14)
 1: 1   Reps
 2: 1   2.5 mV Slow Range
 3: 5   DIFF Channel
 4: 1   Type T (Copper-Constantan)
 5: 10   Ref Temp (Deg. C) Loc [panel   ]
 6: 11   Loc [temp   ]
 7: 1   Mult
 8: 0   Offset

26: Sample (P70)
 1: 1   Reps
 2: 11   Loc [temp   ]

27: End (P95)
28: End (P95)
*Table 2 Program
02:0.0000   Execution Interval (seconds)
*Table 3 Subroutines
End Program

Appendix H - CR10X Program for Field Experiment

```
;{CR10X}
;Yali Zhang
;8/20/2006
;Suspended Sediment Sensor Field Test Program

*Table 1 Program
01:1    Execution Interval (seconds)

1:  If time is (P92)
 1: 0     -- Minutes (Seconds --) into a
 2: 10    -- Interval (same units as above)
 3: 30       Then Do

2:  Do (P86)
 1: 10       Set Output Flag High (Flag 0)

3:  Real Time (P77)
 1: 221      Day,Hour/Minute,Seconds (midnight = 2400)

4:  Set Port(s) (P20)
 1: 0010     C8..C5 = low/low/high/low
 2: 0001     C4..C1 = low/low/low/high

5:  Volt (SE) (P1)
 1: 1        Reps
 2: 15        2500 mV Fast Range
 3: 1        SE Channel
 4: 2        Loc [ bg90on    ]
 5: 1        Mult
 6: 0        Offset

6:  Excitation with Delay (P22)
 1: 1        Ex Channel
 2: 0        Delay W/Ex (units = 0.01 sec)
 3: 100       Delay After Ex (units = 0.01 sec)
 4: 0        mV Excitation

7:  Sample (P70)
 1: 1        Reps
 2: 2        Loc [ bg90on    ]

8:  Set Port(s) (P20)
 1: 0100     C8..C5 = low/high/low/low
 2: 0000     C4,C3,C2,C1 Options
```

9: Volt (SE) (P1)
 1: 1   Reps
 2: 15   2500 mV Fast Range
 3: 1   SE Channel
 4: 3   Loc [bg90off   ]
 5: 1   Mult
 6: 0   Offset

10: Excitation with Delay (P22)
 1: 1   Ex Channel
 2: 0   Delay W/Ex (units = 0.01 sec)
 3: 100   Delay After Ex (units = 0.01 sec)
 4: 0   mV Excitation

11: Sample (P70)
 1: 1   Reps
 2: 3   Loc [bg90off   ]

12: Set Port(s) (P20)
 1: 0110   C8..C5 = low/high/high/low
 2: 0010   C4..C1 = low/low/high/low

13: Volt (SE) (P1)
 1: 1   Reps
 2: 15   2500 mV Fast Range
 3: 2   SE Channel
 4: 4   Loc [ir45on   ]
 5: 1   Mult
 6: 0   Offset

14: Excitation with Delay (P22)
 1: 1   Ex Channel
 2: 0   Delay W/Ex (units = 0.01 sec)
 3: 100   Delay After Ex (units = 0.01 sec)
 4: 0   mV Excitation

15: Sample (P70)
 1: 1   Reps
 2: 4   Loc [ir45on   ]

16: Set Port(s) (P20)
 1: 1000   C8..C5 = high/low/low/low
 2: 0000   C4,C3,C2,C1 Options

17: Volt (SE) (P1)
 1: 1   Reps
 2: 15   2500 mV Fast Range
 3: 2   SE Channel
 4: 5   Loc [ir45off   ]
 5: 1   Mult
 6: 0   Offset

18: Excitation with Delay (P22)
 1: 1   Ex Channel
 2: 0   Delay W/Ex (units = 0.01 sec)
 3: 100   Delay After Ex (units = 0.01 sec)
 4: 0   mV Excitation

19: Sample (P70)
 1: 1   Reps
 2: 5   Loc [ir45off   ]

20: Set Port(s) (P20)
 1: 1010   C8..C5 = high/low/high/low
 2: 0100   C4..C1 = low/high/low/low

21: Volt (SE) (P1)
 1: 2   Reps
 2: 15   2500 mV Fast Range
 3: 3   SE Channel
 4: 6   Loc [orgon_1   ]
 5: 1   Mult
 6: 0   Offset

22: Excitation with Delay (P22)
 1: 1   Ex Channel
 2: 0   Delay W/Ex (units = 0.01 sec)
 3: 100   Delay After Ex (units = 0.01 sec)
 4: 0   mV Excitation

23: Set Port(s) (P20)
 1: 1100   C8..C5 = high/high/low/low
 2: 0000   C4,C3,C2,C1 Options

24: Volt (SE) (P1)
 1: 2   Reps
 2: 15   2500 mV Fast Range
 3: 3   SE Channel
 4: 8   Loc [orgoff_1]
 5: 1   Mult
 6: 0   Offset

25: Excitation with Delay (P22)
 1: 1   Ex Channel
 2: 0   Delay W/Ex (units = 0.01 sec)
 3: 100   Delay After Ex (units = 0.01 sec)
 4: 0   mV Excitation

26: Sample (P70)
 1: 2   Reps
 2: 6   Loc [orgon_1   ]

27: Sample (P70)

1: 2   Reps
    2: 8   Loc [orgoff_1]

28: Internal Temperature (P17)
    1: 13   Loc [panelT   ]

29: Thermocouple Temp (DIFF) (P14)
    1: 1   Reps
    2: 1   2.5 mV Slow Range
    3: 3   DIFF Channel
    4: 1   Type T (Copper-Constantan)
    5: 13   Ref Temp (Deg. C) Loc [panelT   ]
    6: 14   Loc [T   ]
    7: 1.0   Mult
    8: 0.0   Offset

30: Sample (P70)
    1: 2   Reps
    2: 13   Loc [panelT   ]

31: Set Port(s) (P20)
    1: 0000   C8,C7,C6,C5 Options
    2: 0000   C4,C3,C2,C1 Options

32: Excitation with Delay (P22)
    1: 1   Ex Channel
    2: 0   Delay W/Ex (units = 0.01 sec)
    3: 300   Delay After Ex (units = 0.01 sec)
    4: 0   mV Excitation

33: End (P95)
34: Pulse (P3)
    1: 1   Reps
    2: 1   Pulse Channel 1
    3: 2   Switch Closure, All Counts
    4: 15   Loc [rain_mm   ]
    5: 0.254   Mult
    6: 0   Offset

35: If time is (P92)
    1: 0   Minutes (Seconds --) into a
    2: 5   Interval (same units as above)
    3: 10   Set Output Flag High (Flag 0)

36: Totalize (P72)
    1: 1   Reps
    2: 15   Loc [rain_mm   ]
*Table 2 Program
02:0.0000   Execution Interval (seconds)
*Table 3 Subroutines
End Program

Appendix I - Program for Fouling/Clogging Correction Algorithm

```matlab
% Written for For Benning Data Correction;
% Naiqian Zhang;
% January 28, 2007;

clear all;

filename = 'Juneasybottom';
ora180_m=xlsread(filename,'g2:g65535');
%ora180_n=xlsread(filename,'g2:g65535');
time=xlsread(filename,'d2:d65535');
weather=xlsread(filename,'c2:c65535');
precipitation=xlsread(filename,'h2:h65535');
L=length(time);
%L = 20500;
Sclear=ora180_m(L+1);


threshold = 0;
ripple = 0;
minilift = 10;
contrast = 4;
mean_upslope = 0;
mean_downslope = 0;
seg = L;
width_t = 5;
width_s = 11;
width_f = 21;


ora180_t=ora180_m(1:L);

for i = (width_t+1)/2:L-(width_t-1)/2
    if(width_t ~= 1)
        ora180_t(i) = mean(ora180_m(i-(width_t-1)/2:1:i+(width_t-1)/2));
    end;
end;

ora180_f = ora180_t(1:L);

for i = (width_f+1)/2:L-(width_f-1)/2
    if(width_f ~= 1)
        ora180_f(i) = mean(ora180_m(i-(width_f-1)/2:1:i+(width_f-1)/2));
    end;
end;
```

```
cv_t=std(ora180_t)/mean(ora180_t)
cv_f=std(ora180_f)/mean(ora180_f)

% cutoff = 0.1;
% [b,a] = ellip(6,5,50,cutoff);
% ora180_f(1:L) = filter(b,a,ora180_m(1:L));
% ora180_t(1:L) = filter(b,a,ora180_m(1:L));

figure
plot(time(1:L),ora180_m(1:L),'c-',time(1:L),ora180_t(1:L),'r-
',time(1:L),ora180_f(1:L),'b',time(1:L),weather(1:L)*2000,'g')
xlabel('Time (minute)');
ylabel('Signal (mV)');
axis([0 L -500 2500]);
title ([filename, 'Filter width = ', num2str(width_t)]);
legend('Measured Signal','ora180_t Filtered Signal','ora180_f Filtered Signal');
grid on;

for i=1:L-1
    slope(i)=ora180_f(i+1)-ora180_f(i);
end;
slope(L) = 0;

for i = (width_s+1)/2:L-(width_s-1)/2
    if(width_s ~= 1)
        slope(i) = mean(slope(i-(width_s-1)/2:1:i+(width_s-1)/2));
    end;
end;

for i = 1:(width_s-1)/2
    slope(i) = 0;
end;

for i = L-(width_s-1)/2: L
    slope(i) = 0;
end;
%slopet = slope';

% for i=1:L-1
%     slope(i)=ora180_f(i+1)-ora180_f(i);
% end;
% slope(L) = 0;
% slopet = slope';

figure
plot(time(1:L),slope(1:L),'b-',time(1:L), ora180_f(1:L)/50,'r-')
xlabel('Time (minute)');
ylabel('Slope(mV/min)');
axis([0 L 0 40]);
title ([filename, 'Slope filter width = ', num2str(width_s)]);
legend('Slope', 'Filtered signal/50');
```

```matlab
grid on;

% converge = 0;
% limit = 3;
% iteration = 0;
% while (converge ~= 1)

%t0 = 1;
    %converge = 1;
    %converge1 = converge;
    %iteration = iteration + 1;

peak = 1;
valley = 1;
peak_all=[];
valley_all=[];

for i=1:seg-1
    if slope(i) < ripple
        if(slope(i+1)) >= 0
            valley = i+1;
            mean_downslope = mean(slope(peak:valley-1));
        end;
    else
        if slope(i+1) < 0
            peak = i+1;
            mean_upslope = mean(slope(valley:peak-1));
            lift = ora180_f(peak) - ora180_f(valley);
            if(mean_upslope >= threshold && mean_upslope>contrast*abs(mean_downslope) &&
lift>minilift)
%               i = i
%               mean_upslope = mean_upslope
%               mean_downslope = mean_downslope
%               lift = lift

                Pstart=ora180_f(1);
                Pend=ora180_f(valley);

                Sini0=ora180_f(1);
                Sini1=ora180_f(peak);

                if (valley ~= 1)
                    [a1, a0] = coeffcom(1,valley,Pstart,Pend,Sini0,Sini1);
                    %Correction;
                    for j=1:valley
                        E(j)=a1*time(j)+a0;
                        ora180_t(j)=ora180_t(j)-E(j);
                    end;
                else
                    ora180_t(valley) = ora180_t(peak);
                end;
```

```matlab
        for j = valley+1:peak-1
            ora180_t(j) = ora180_t(peak);
        end;

        peak_all=[peak_all;peak];
        valley_all=[valley_all;valley];

        figure;
        plot(time(1:seg), precipitation(1:seg)*1500,'g-',time(1:seg), ora180_f(1:seg),'b-', time(1:seg),
ora180_t(1:seg),'r-')
        xlabel('Time (minute)');
        ylabel('Signal (mV)');
        axis([0 seg 0 3000]);
        title ([filename, ', Filter width=',num2str(width_t),', Slope filter width=',num2str(width_s),',
Minilift=',num2str(minilift), ', Contrast=',num2str(contrast), ', Time=', num2str(i)]);
        legend('Percipitation', 'ora180_f Filtered signal', 'ora180_t clogging-corrected signal');
        grid on;
        hold on;
        plot(valley, ora180_t(valley), 'x', peak, ora180_t(peak), 'o');

    end;
    end;
    end;
end;
ora180_tt = [ora180_f slope'];

figure
plot(time(1:L),ora180_t(1:L),'-');
grid on;
hold on;

%peak=[peak_all ora180_f(peak_all(:,1))];
peak=fpeak(time(1:L),ora180_t(1:L),200,[0,45000,400,5000]);
plot(peak(:,1),peak(:,2),'o');
title('Peak Detection');

peak=[1 ora180_t(1);peak];
New_peak = [];
Num_peak = length(peak(:,1))
for i = 1:Num_peak
    if weather(peak(i,1)) == 0
        New_peak = [New_peak; peak(i,1) peak(i,2)];
    end;
end;

Num_new_peak = length(New_peak(:,1));
ora180_n=ora180_t;
for i=1:Num_new_peak-1
    [a1, a0] = coeffcom(New_peak(i,1),New_peak(i+1,1),New_peak(i,2),New_peak(i+1,2),Sclear,Sclear);
    %Correction;
```

```matlab
    for j=New_peak(i,1):1:New_peak(i+1,1)
        E(j)=a1*time(j)+a0;
        ora180_n(j)=ora180_t(j)-E(j);
    end;
end;

ora180_t=ora180_t(1:New_peak(Num_new_peak));
ora180_n=ora180_n(1:New_peak(Num_new_peak));
L_new=length(ora180_t);

figure
plot(time(1:L_new),ora180_t,'b-',time(1:L_new),ora180_n,'r-')
xlabel('Time (minute)');
ylabel('Signal (mV)');
%axis([0 50000 -500 2500]);
title ([filename, ', Fouling Correction']);
legend('Measured Signal','Corrected Signal');
grid on;

% figure
% plot(time(1:L), precipitation(1:L)*1500,'g-',time(1:L), ora180_f(1:L),'b-', time(1:L), ora180_n(1:L),'r-')
% xlabel('Time (minute)');
% ylabel('Signal (mV)');
% axis([0 L 0 1500]);
% title ([filename, ', Filter width=',num2str(width_t),', Step threshold=',num2str(threshold)]);
% legend('Percipitation', 'Filtered signal', 'clogging/fouling-corrected signal');
% grid on;

% Part IV: Calculating accumulated concentration using integral;

% Read slope rate and intercept of the concentration regression;
ora180_slope=xlsread(filename,1,'I2');
ora180_intercept=xlsread(filename,1,'J2');

% Calculating concentration;
for i = 1:L_new
    conc_ora180(i)=ora180_n(i)*ora180_slope+ora180_intercept;
    if(conc_ora180(i) < 0)
        conc_ora180(i) = 0;
    end;
end;

% Initialize parameters;
% sednew - cummulative area
% sed -
sednew=0;
precinew=0;
sed=[];
preci=[];

%Calculate integral;
```

```matlab
for i=1:L_new-1
    if precipitation(i) ~= 0
        sednew=sednew+conc_ora180(i);
        if precipitation(i+1) == 0
            sed=[sed;sednew];
            preci=[preci;precipitation(i)];
            sednew=0;
        end;
    end;
end;

% Accumulated sediment concentration vs. precipitation linear regression;
% The first value is the slope rate of the linear line;
sediment=polyfit(preci,sed,1);

figure
plot(time(1:L_new), precipitation(1:L_new)*5000,'g-',time(1:L_new), conc_ora180(1:L_new),'b-')
title([filename,', width_t=',num2str(width_t),', width_f=',num2str(width_f),',
Contrast=',num2str(contrast),', Slop=',num2str(sediment(1)/100000)]);
xlabel('Time (minute)');
ylabel('Predicted Concentration(mg/L)');
axis([0 seg 0 15000]);
legend('Precipitation*5000','concentration');
%axis([0 50000 -500 2500]);
grid on;

figure
plot(preci, sed, 'o', preci,polyval(sediment,preci), '-')
title([filename,', Accumulated Concentration vs. Precipitation']);
xlabel('precipitation (inch)');
ylabel('Accumulated Concentration (mg)');
legend('Concentration','Regressing Line');
%axis([0 50000 -500 2500]);
grid on;
```

Appendix J - SAS Program for the Analysis of Temperature Effect

SAS Program:

DATA;
INPUT ActualSSC Temperature PredicedSSC;
CARDS;
………………
………………
………………
;

*/PROC ANOVA;
        */CLASS ActualSSC Temperature;
proc glm;
        MODEL PredicedSSC = ActualSSC Temperature ActualSSC*Temperature;
RUN;
*/proc glm;
*/   MODEL PredicedSSC = ActualSSC Temperature;
        */RUN;

SAS Output:

```
                              The GLM Procedure

                      Number of Observations Read        258


Dependent Variable: PredicedSSC

                                    Sum of
     Source                    DF       Squares    Mean Square   F Value   Pr > F

     Model                      3   88040554.16   29346851.39   10750.8   <.0001

     Error                    254     693355.81       2729.75

     Corrected Total          257   88733909.97


              R-Square     Coeff Var     Root MSE     PredicedSSC Mean

              0.992186      23.52136     52.24698            222.1257



     Source                    DF      Type I SS    Mean Square   F Value   Pr > F


     ActualSSC                  1   88014237.23   88014237.23   32242.6   <.0001

     Temperature                1         59.25         59.25      0.02   0.8830
```

Source	DF	Type III SS	Mean Square	F Value	Pr > F
ActualSSC*Temperatur	1	26257.68	26257.68	9.62	0.0021

Source	DF	Type III SS	Mean Square	F Value	Pr > F
ActualSSC	1	151742.8277	151742.8277	55.59	<.0001
Temperature	1	120.6735	120.6735	0.04	**0.8336**
ActualSSC*Temperatur	1	26257.6813	26257.6813	9.62	**0.0021**

Parameter	Estimate	Standard Error	t Value	Pr > |t|
Intercept	-1.456453881	10.96869349	-0.13	0.8945
ActualSSC	1.698362876	0.22779156	7.46	<.0001
Temperature	-0.126107736	0.59978690	-0.21	0.8336
ActualSSC*Temperatur	-0.031957056	0.01030386	-3.10	0.0021

Appendix K - Program for Sediment Sensor Laboratory Cleaning Experiment

```
;{CR10X}
;Yali Zhang
;7/10/2008
;Suspended Sediment Sensor Air-blast Cleaning Test Program; Air-blast Cleaning Mechanism is
activated every 12 hours for 2 seconds.

*Table 1 Program
01:1    Execution Interval (seconds)

1:  Do (P86)
 1: 10      Set Output Flag High (Flag 0)

2:  Real Time (P77)
 1: 221     Day,Hour/Minute,Seconds (midnight = 2400)

3:  Set Port(s) (P20)
 1: 0000    C8,C7,C6,C5 Options
 2: 0001    C4..C1 = low/low/low/high

4:  Volt (SE) (P1)
 1: 2       Reps
 2: 15       2500 mV Fast Range
 3: 1       SE Channel
 4: 1       Loc [ bg90on_1  ]
 5: 1       Mult
 6: 0       Offset

5:  Set Port(s) (P20)
 1: 0000    C8,C7,C6,C5 Options
 2: 0000    C4,C3,C2,C1 Options

6:  Volt (SE) (P1)
 1: 2       Reps
 2: 15       2500 mV Fast Range
 3: 1       SE Channel
 4: 3       Loc [ bg90off_1 ]
 5: 1       Mult
 6: 0       Offset

7:  Set Port(s) (P20)
 1: 0000    C8,C7,C6,C5 Options
```

2: 0010   C4..C1 = low/low/high/low

8: Volt (SE) (P1)
 1: 2   Reps
 2: 15   2500 mV Fast Range
 3: 3   SE Channel
 4: 5   Loc [ir45on_1]
 5: 1   Mult
 6: 0   Offset

9: Set Port(s) (P20)
 1: 0000   C8,C7,C6,C5 Options
 2: 0000   C4,C3,C2,C1 Options

10: Volt (SE) (P1)
 1: 2   Reps
 2: 15   2500 mV Fast Range
 3: 3   SE Channel
 4: 7   Loc [ir45off_1]
 5: 1   Mult
 6: 0   Offset

11: Set Port(s) (P20)
 1: 0000   C8,C7,C6,C5 Options
 2: 0100   C4..C1 = low/high/low/low

12: Volt (SE) (P1)
 1: 4   Reps
 2: 15   2500 mV Fast Range
 3: 5   SE Channel
 4: 9   Loc [oraon_1   ]
 5: 1   Mult
 6: 0   Offset

13: Set Port(s) (P20)
 1: 0000   C8,C7,C6,C5 Options
 2: 0000   C4,C3,C2,C1 Options

14: Volt (SE) (P1)
 1: 4   Reps
 2: 15   2500 mV Fast Range
 3: 5   SE Channel
 4: 13   Loc [oraoff_1]
 5: 1   Mult
 6: 0   Offset

15: Sample (P70)
 1: 12   Reps
 2: 5   Loc [ir45on_1]

16: If time is (P92)

1: 660   Minutes (Seconds --) into a
2: 1440   Interval (same units as above)
3: 30   Then Do

17: Set Port(s) (P20)
1: 1000   C8..C5 = high/low/low/low
2: 0000   C4..C1 = low/low/low/low

18: Excitation with Delay (P22)
1: 1   Ex Channel
2: 100   Delay W/Ex (units = 0.01 sec)
3: 100   Delay After Ex (units = 0.01 sec)
4: 1   mV Excitation

19: Set Port(s) (P20)
1: 0000   C8,C7,C6,C5 Options
2: 0000   C4,C3,C2,C1 Options

20: End (P95)

21: If time is (P92)
1: 1320   Minutes (Seconds --) into a
2: 1440   Interval (same units as above)
3: 30   Then Do

22: Set Port(s) (P20)
1: 1000   C8..C5 = high/low/low/low
2: 0000   C4..C1 = low/low/low/low

23: Excitation with Delay (P22)
1: 1   Ex Channel
2: 100   Delay W/Ex (units = 0.01 sec)
3: 100   Delay After Ex (units = 0.01 sec)
4: 1   mV Excitation

24: Set Port(s) (P20)
1: 0000   C8,C7,C6,C5 Options
2: 0000   C4,C3,C2,C1 Options
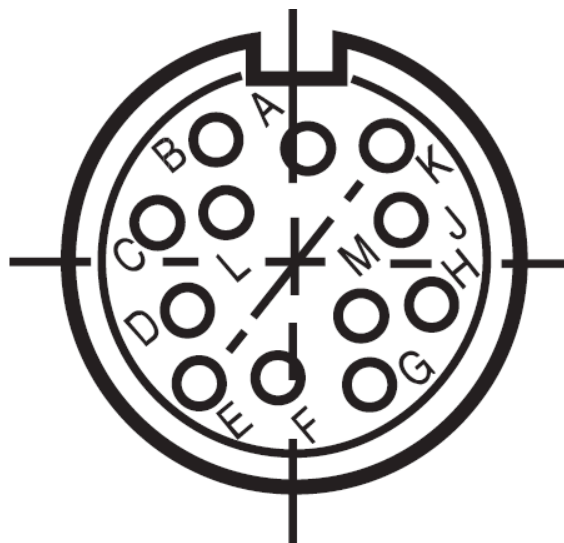
25: End (P95)

*Table 2 Program
02:0.0000   Execution Interval (seconds)

*Table 3 Subroutines

End Program

Appendix L - Pin Description of Sediment/velocity Sensor

C091 31N012 2002: Socket, panel, 12 contacts (View on termination side of contact insert):

Pin number	Description
A	BG90 PT emitter
B	IR45 PT emitter
C	ORA45_1 PT emitter, Upstream
D	ORA180_1 PT emitter, Upstream
E	ORA45_2 PT emitter, Downstream
F	ORA180_2 PT emitter, Downstream
G	BG LED cathode
H	IR LED cathode
J	ORA LED_1 cathode, Upstream
K	ORA LED_2 cathode, Downstream
M	Anodes of all 4 LEDs
L	Collectors of all 6 PTs

Note:

PT stands for phototransistor

Appendix M - MATLAB Program of Cross-Correlation Analysis

```matlab
%Computes and plot cross-correlation coefficients of up- and down-stream signals
% Yali Zhang
% Aug. 5, 2008

clear all;

%read upstream signal
X=xlsread('33.xls',1,'a1:a500');
%read downstream signal
Y=xlsread('33.xls',1,'c1:c500');
%data points
N=length(X);
%sampling frequency
S=500;
%total measuring time
time=0:1/S:(N-1)*1/S;

%calculate autocorrelation functions
sse_x=0;
sse_y=0;
for j=1:N
    sse_x_new=(X(j)-mean(X))^2;
    sse_x=sse_x+sse_x_new;
    sse_y_new=(Y(j)-mean(Y))^2;
    sse_y=sse_y+sse_y_new;
end;
Rxx_zero=sse_x/N;
Ryy_zero=sse_y/N;

%compute cross-correlation coefficient array
sse_xy=0;
Rxy=[];

for i=0:N-1
    for j=1:N-i
        %mean value of X and Y
        Xs=X(1:N-i);
        Ys=Y(i+1:N);
        Xbar=sum(Xs)/(N-i);
        Ybar=sum(Ys)/(N-i);

        sse_xy_new=(X(j)-Xbar)*(Y(j+i)-Ybar);
        sse_xy=sse_xy+sse_xy_new;
    end;
```

```
    Rxy_new=[sse_xy/(N-i) i];
    Rxy=[Rxy;Rxy_new];
    sse_xy=0;
end;

Xcorr=[Rxy(:,1)/sqrt(Rxx_zero*Ryy_zero) Rxy(:,2)];

%plot original signals in time domain
figure
plot(time,X,'r',time,Y,'b')
grid on;
%axis([0 1.4 2.6 4]);
title('Original Upstream and Downstream ORA45 signals');
xlabel('Time (Second)');
ylabel('Signal (V)');
legend('Upstream signal','Downstream signal');

%plot cross-correlation coefficient in time domain
figure
plot(time',Xcorr(:,1))
grid on;
%axis([0 1.4 -0.8 1.2]);
title('ORA45 Signals Cross-correlation Coefficient vs Time');
xlabel('Time (second)')
ylabel('Cross-correlation coefficient')

%find the maximum cross-correlation coefficient
im=find(Xcorr(:,1)==max(Xcorr(:,1)));

%compute velocity
Tm=(im-1)/S
V=0.04/Tm
```
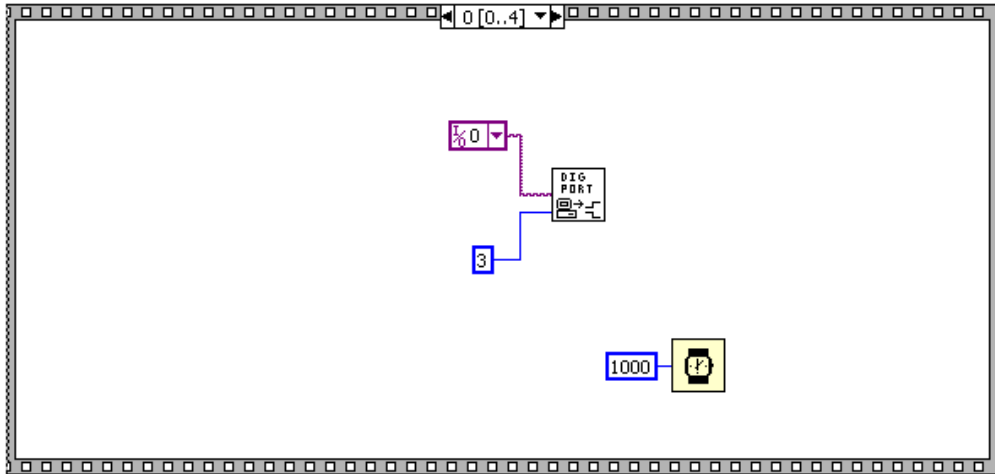
Appendix N - LABVIEW Program for Flow Velocity Experiment
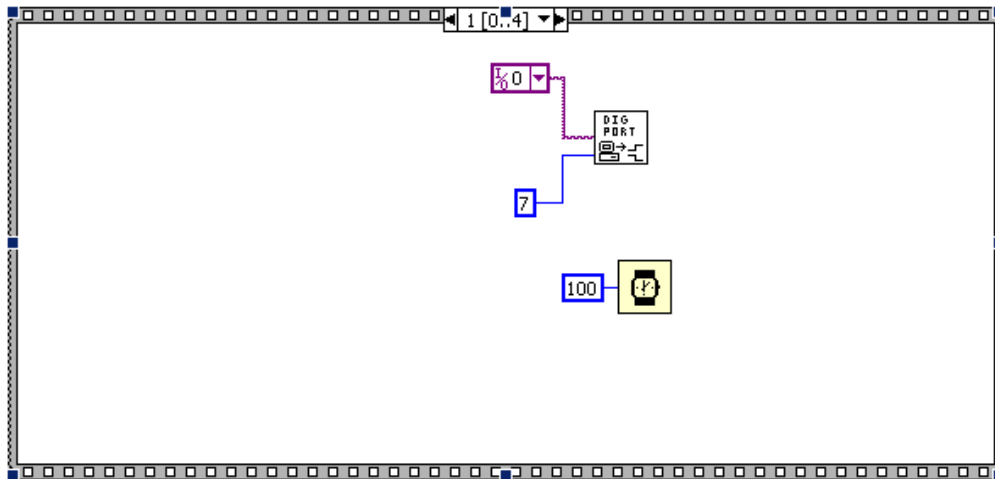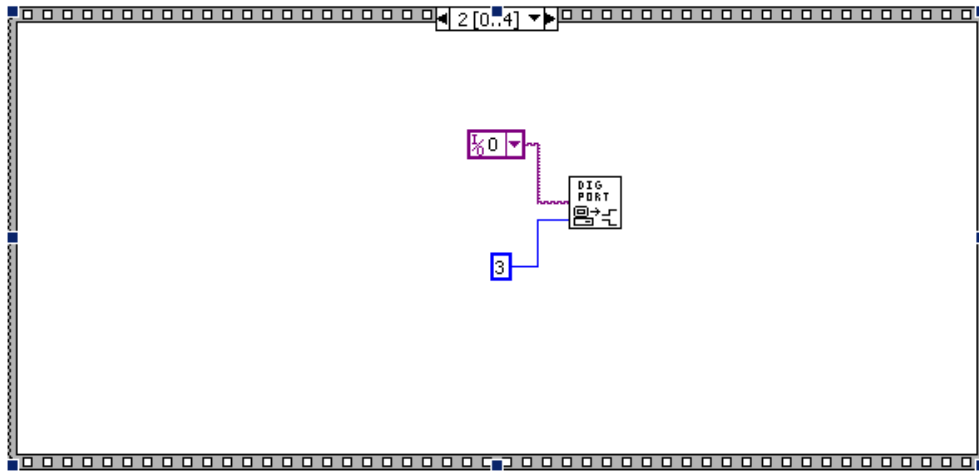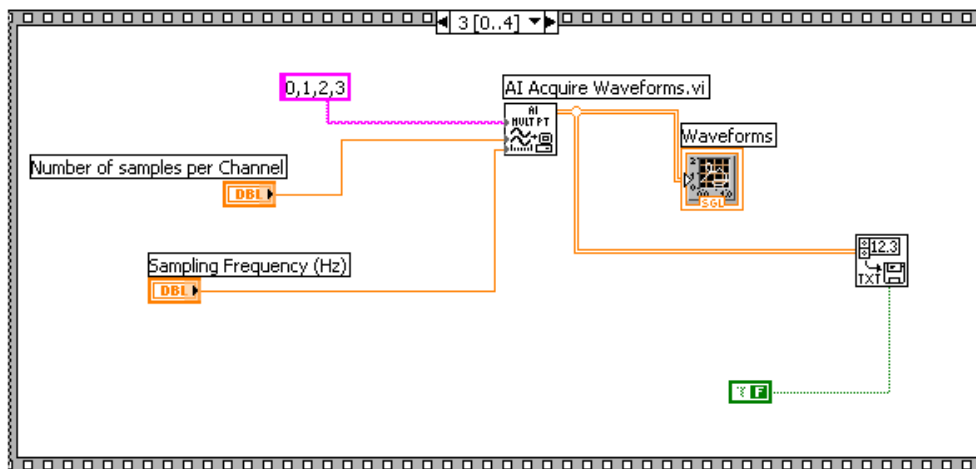
Front Panel:
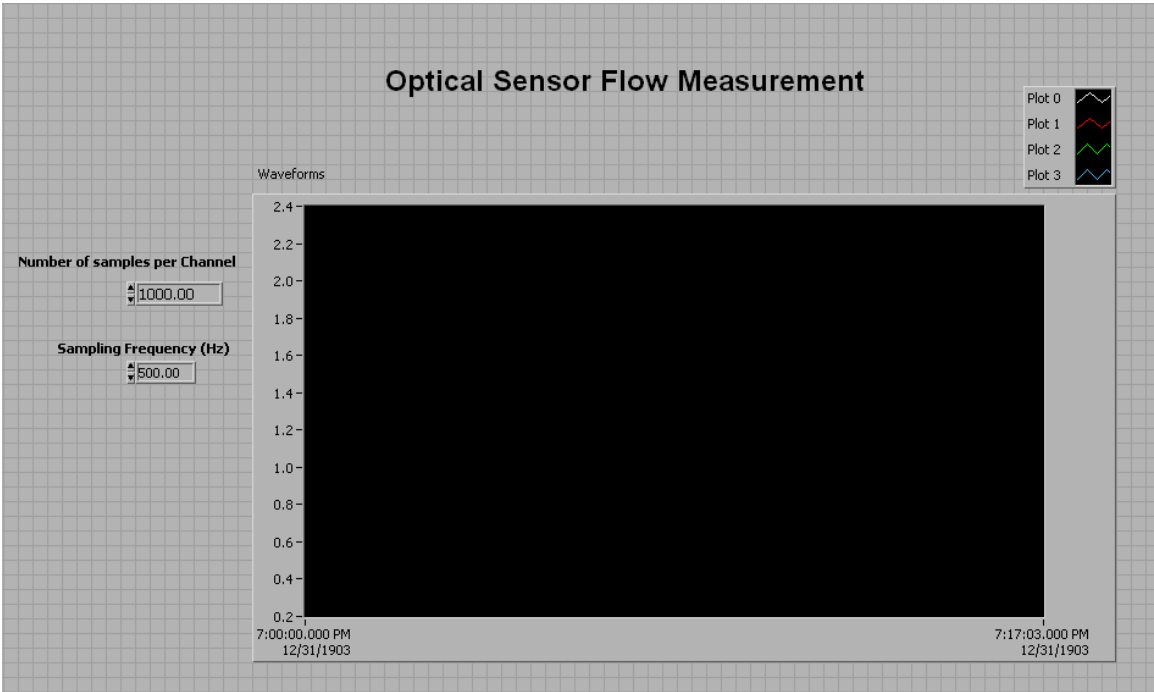
Block Diagram:

Sequence 1:

Sequence 2:

Sequence 3:

Sequence4:

Sequence 5: